1

PM-1 3½"x4" PHOTOGRAPHIC MICROCOPY TARGET
NBS 1010a ANSI/ISO #2 EQUIVALENT

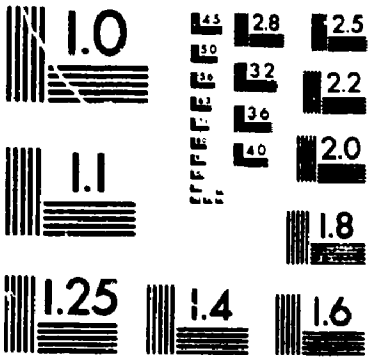

PRECISION℠ RESOLUTION TARGETS

ICE LENS FORMATION AND FROST HEAVE FROM A THERMODYNAMIC RHEOLOGIC PERSPECTIVE

by

SHARON LEE SMITH, B.Sc., M.Sc.

A thesis submitted to

the Faculty of Graduate Studies and Research

in partial fulfilment of

the requirements for the degree of

Doctor of Philosophy

Department of Earth Sciences

Carleton University

Ottawa, Ontario

July, 1992

ISBN 0-315-79874-2

The undersigned hereby recommend to

the Faculty of Graduate Studies and Research

acceptance of the thesis,

ICE LENS FORMATION AND FROST HEAVE FROM A THERMODYNAMIC RHEOLOGIC PERSPECTIVE

submitted by

SHARON LEE SMITH, B.Sc., M.Sc.

in partial fulfilment of the requirements

for the degree of Doctor of Philosophy

Chair, Department of Earth Sciences

Thesis Supervisor

External Examiner

Carleton University

ABSTRACT

An experimental approach has been used to examine the formation of ice lenses in freezing soils. Special attention has been given to the rheologic conditions. These are important because ice can only continue to accumulate within the heaving soil if the resistance of the frozen soil can be overcome.

Small-scale laboratory experiments were carried out to examine the importance of creep of ice and frozen soil in determining the pressures which develop in the frozen soil and the amount of heave. Results from ice sandwich experiments indicated that ice deforms slowly in response to stress arising during freezing of water and it is proposed that ice in a soil pore behaves in a similar way. Experimental results show that the pressures which develop in the frozen soil are influenced by the thermodynamic conditions and the creep properties of the frozen soil. Pressures may change over time as stress relaxation occurs. This relates to the time-dependence of the frost heave process.

The results of experiments in a controlled environment facility were used to examine ice lens orientation and distribution around a chilled buried pipe at a field scale. The ice lens pattern is clearly influenced by the thermal regime but this is not the only factor. The ice lens pattern also appears to be related to the mechanical

conditions as well. Changes in soil density and soil texture also influence the ice lens pattern. A complex pattern of heave is suggested by the ice lens orientation and stresses and displacements have vertical and horizontal components.

The experimental results suggest that the rate of frost penetration and nature of ice accumulation depend on a complex interaction between the thermal and rheologic properties of the frozen soil. The thermal properties depend on the mechanical behaviour of the soil and are time-dependent.

ACKNOWLEDGEMENTS

I wish to thank my thesis supervisor, Dr. P.J. Williams for his support and encouragement. I would also like to thank Dr. M.W. Smith for his advice.

The Canada-France Pipeline Ground Freezing study is being carried out in the controlled environment facility of the Centre de Géomorphologie, Caen France under the auspices of Centre National de la Recherche Scientifique, Laboratoire Central des Ponts et Chaussées and Energy Mines and Resources Canada. The advice provided by B. Van Vliet-Lanoe is greatly appreciated. A. Dupas, B. Dumoulin, O. Jean and T.L. White provided much help with the excavations and sample retrieval. Laboratory experiments were carried out at the Geotechnical Science Laboratories. L. Boyle and A. Pendlington provided help with the equipment.

I would like to thank Diane, Heather, David, Joyce, Quentin, Jeanne, Elizabeth, Awegechew, Fons, Steve and the staff and faculty of the Geography Department for making my stay at Carleton an enjoyable one. Thanks also go to Fiona for the weekly tennis and squash games and to Barb for her friendship and support. I wish to thank the members of my baseball team for the friendship and good times they have provided over the last five years. Lastly, I would like to thank Mom, Dad, Cindy and Wendy for their love and support.

This thesis is dedicated to Poppy who I wish could be here to share this accomplishment with me.

TABLE OF CONTENTS

LIST OF FIGURES

LIST OF TABLES

NOTATION

Thermal and hydrologic equations

C_{vT} = apparent volumetric heat capacity at temperature T

C_s, C_i, C_w = volumetric heat capacity of soil minerals, ice and water

ΔG = Gibbs free energy

h = hydraulic head

J_m, J_q = mass and heat flow rates

K = hydraulic conductivity

k_T = thermal conductivity at temperature T

k_w, k_i, k_s = thermal conductivity of water, ice and soil minerals

L = latent heat of fusion

L_m, L_q = Isometric mass and isobaric heat transfer coefficients

L_{mq}, L_{qm} = cross coefficients for coupled transport

n = porosity

P = pressure

Q = internal heat generation term

q = water flow

r = radius

S_{iw} = surface tension for ice-water interface

T = temperature

t = time

V_w = specific volume of water

X_s, X_i, X_w = volume fractions of soil minerals, ice and water

z = distance

θ_w = gravimetric unfrozen water content

α = thermal diffusivity

ρ_d = dry bulk density

ρ_i, ρ_w = density of ice and water

Creep equations

b = Burgers vector

d = average grain size

D = coefficient of diffusion

G = shear modulus

k = Boltzmann constant

R = universal gas constant

U = activation energy

$\dot{\epsilon}$ = strain rate

σ = stress

GLOSSARY

These definitions are based on those given in "Glossary of Permafrost and Related Ground Ice Terms" (Prepared by S.A. Harris, H.M. French, J.A. Heginbottom, G.H. Johnston, B. Ladanyi, D.C. Sego and R.O. van Everdingen 1988. Permafrost Subcommittee, Associate Committee on Geotechnical Research, National Research Council of Canada Technical Memorandum No. 142).

Continuing heave - Heave (ice lens formation) which takes place in the frozen soil behind the warmest ice lens.

Excess ice - Volume of ice in ground which exceeds the total pore volume that the ground would have under natural unfrozen conditions.

Freezing front - Advancing boundary between frozen or partially frozen ground and unfrozen ground.

Frost-susceptible soil - Soil in which segregated ice will form (causing frost heave) under the required conditions of moisture supply and temperature.

Frozen fringe - The zone in a freezing, frost-susceptible soil between the warmest isotherm at which pore ice exists and the isotherm at which the warmest ice lens is growing.

Ice content - amount of ice contained in frozen or partially frozen soil or rock.

Ice lens - Lens-shaped body of ice which may range in thickness from hair line to more than 10 m. This term is commonly used for layers of segregated ice that are more or

less parallel to the ground surface but in this thesis the term will refer to segregated ice of a preferred orientation (which may or may not be parallel to the ground surface).

Ice vein - Ice occupying cracks or fissures in frozen ground. They may occur in various forms including, horizontal layers, tabular sheets, wedges and reticulate nets.

Pore ice (also interstitial ice) - Ice occurring in pores of soils and rocks. On melting pore ice does not yield water in excess of the pore volume of the same soil when unfrozen.

Reticulate ice veins - A network of horizontal and vertical ice veins usually forming a three dimensional, rectangular or square lattice. Reticulate ice veins often grow in shrinkage cracks with much of the water coming from the adjacent material in a semi-closed freezing system rather than from migration of water in an open system.

Segregated ice - Ice formed by the migration of pore water to the frozen fringe where it forms into discrete layers or lenses.

CHAPTER ONE

INTRODUCTION

1.1 General

As soils cool below a temperature of 0°C, water freezes over a range of temperatures, so that a frozen soil may contain a significant amount of unfrozen water. Gradients of thermodynamic and hydraulic potential develop during freezing which tend to cause water to move toward the colder part of the soil where it freezes and accumulates in the form of ice lenses (figure 1.1). The accumulation of ice results in an expansion of the soil volume and an uplift of the soil surface or frost heave.

The frost heave process is responsible for the formation of such landscape features as hummocky topography and patterned ground and is probably responsible for the accumulation of large bodies of ground ice in permafrost areas. Frost heave must be considered when designing structures such as chilled gas pipelines, buildings and roads for cold climates.

1.2 Previous Research

The potential gradients which develop in a freezing soil are thermodynamic in origin and the formation of segregated ice lenses involves both heat and moisture transport. Several attempts have been made to model frost heave numerically and these have been reviewed by Berg

FIGURE 1.1. Typical ice lenses in frozen Caen silt.

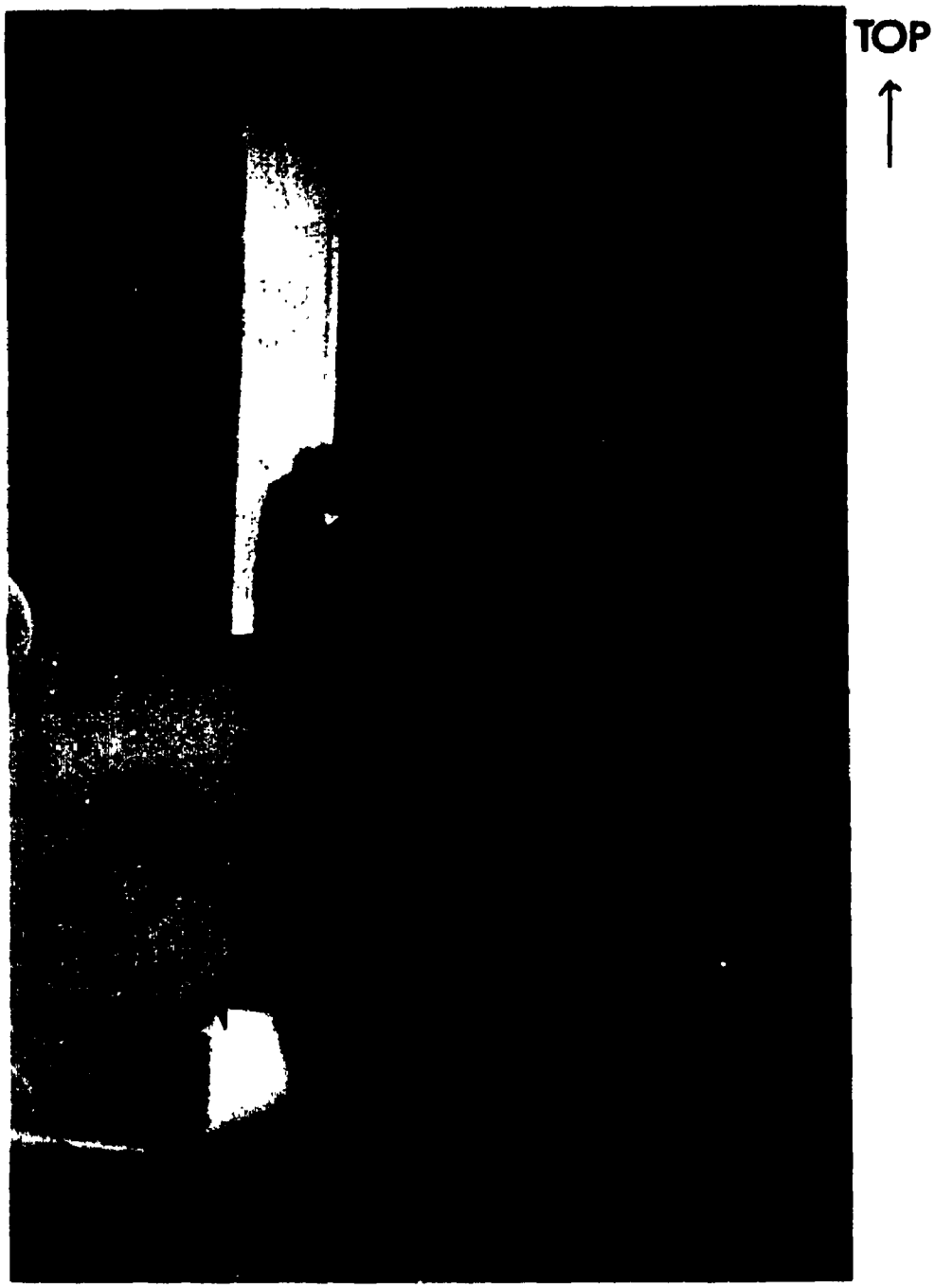

(1983), Hopke (1980), Kay and Perfect (1988), Lundin (1989), O'Neill (1983), Williams and Smith (1989) and Wood (1985).

Models (eg. Harlan 1973) have been developed which couple the heat and moisture flow. These models consider the pore ice to be immobile and mass transport takes place only in the form of liquid flow and the driving force is directly proportional to the temperature gradient. The thermal gradient is analogous to the water pressure gradient in unsaturated unfrozen soil. Other similar hydraulic models have been developed by Cary (1987), Guymon and Luthin (1974), Kinosita (1975), Konrad and Morgenstern (1980) and Ryokai (1985).

Models have also been developed which consider the mobility of the ice phase (eg. Holden 1973, 1983, Holden et al. 1985, Miller 1977, 1978 and O'Neill and Miller 1985). These rigid-ice models assume that pore ice is rigidly connected and moves as a rigid body. The ice moves by the process of regelation. This type of model is complex and requires parameters that are difficult to estimate. Black and Miller (1985) apply a continuum approach in an attempt to simplify the rigid ice model.

Observations of continuing heave (Smith and Patterson 1989) imply that the amount and rate of heave depend on the rheological properties of the frozen soil. Ice lenses can only continue to grow if they can overcome the resistance provided by the surrounding frozen soil. The amount of

heave and the rate of heave will depend on the deformation properties of the frozen soil. Little work has been done in this area. Studies by Wood and Williams (1985a), Williams and Wood (1985) and Smith and Patterson (1989) suggest that ice pressure and heave are governed by the creep properties of the frozen soil. Wood (1990) and Lundin (1989) consider the rheological properties of the frozen soil and propose a thermodynamic-rheologic model of frost heave.

The distribution and orientation of ice lenses will depend on both the thermal and rheologic conditions of the material. There has been little work done on the links between soil rheology and ice lens orientation and distribution. Many studies on ice lens growth (eg. Penner 1986 and Penner and Goodrich 1980) have been conducted in which the heat flow direction is upward and ice lenses are oriented parallel to the unrestricted soil surface. Few studies have considered situations where ice lenses do not form parallel to the ground surface. This is the case in the present experiment where heat flow is modified by the presence of the pipe and the soil stress state is complicated. Such studies are useful in determining the relative importance of the heat flow direction and the stress system in the ground in influencing the distribution and orientation of ice lenses. While the process of ice lens formation and the associated stresses and displacements are of basic importance, there has been little work done in

this latter area.

1.3 Research Objectives

The research in this thesis was undertaken to examine the role of rheology and thermodynamics in ice lens formation. This objective was achieved by carrying out the following experiments:

1. Ice sandwich experiments which examine thermally induced regelation and the importance of the creep properties of ice in the frost heave process.
2. Experiments with a silt in a frost pressure cell in which ice pressures over short freeze-thaw cycles were observed to examine the importance of rheology in determining ice pressure.
3. Observations of the character of ice lenses around a large chilled pipe in order to determine the factors influencing their distribution and orientation.

Experiments 1 and 2 allow consideration of the processes occurring in a single soil pore and also of the stress distribution in a small body of freezing soil. The results of these experiments were used in the analysis of the observations of ice lens orientation and distribution in the field scale experiment (experiment 3). The experimental results have been used to further develop the conceptual model which describes the importance of the interaction of the rheologic and thermodynamic conditions in the formation of ice lenses.

CHAPTER TWO

THE FROST HEAVE PROCESS

2.1 Unfrozen Water in Freezing Soils

As the temperature of a wet porous material such as soil falls below 0°C, water freezes over a range of temperature. There is a reduction of free energy which results in a progressive depression of the freezing point. This is a consequence of a combination of factors (Harlan 1973, Hoekstra 1966, Konrad and Morgenstern 1983, Oliphant et al. 1983, Perfect and Williams 1980, Williams 1967 and 1977, Williams and Smith 1989 and Wood 1985):

1. Adsorptive forces originating in the double layer associated with mineral surfaces.
2. Free solutes in the soil solution.
3. Capillary effects produced by the confining nature of the soil pores.

The free energy of the ice-water system is related to the freezing point depression by a fundamental thermodynamic equation (Perfect and Williams 1980 and Williams 1977):

$$\Delta G = \frac{\Delta T L}{T} \tag{2.1}$$

ΔG = Gibbs free energy

L = latent heat of fusion of water

ΔT = freezing point depression

T = normal freezing point of water at 1 atm. pressure (273.15 K)

Ice and water coexist at temperatures below 0°C if there is a difference in pressure across the ice-water interface and the water pressure must be less than that of the ice. This pressure difference is similar to that across an air-water interface in a capillary, the cause of suction in unfrozen soils. The difference in pressure can be equated with the free energy and one form of the Clausius-Clapeyron equation may be written (Groenvelt and Kay 1977, Hopke 1980, Koopmans and Miller 1966, Oliphant et al. 1983, Penner and Goodrich 1980, Smith 1985, Takagi 1978 and 1980 and Williams 1967, 1982 and 1986):

$$T-T_o = \frac{(P_w V_w - P_i V_i)T}{L} \qquad (2.2)$$

P_i = ice pressure

P_w = water pressure

L = latent heat of fusion of water

T = absolute temperature

T_o = normal freezing point of water (273.15 K)

V_w, V_i = specific volume of water and ice

The difference in pressure across the ice-water interface can also be expressed in terms of surface tension and the radius of the interface in a manner similar to the application of the Kelvin equation to unfrozen soils (Anderson and Morgenstern 1973, Hopke 1980, Loch and Kay

1978, Outcalt 1969, Washburn 1979):

$$P_i - P_w = \frac{2S_{iw}}{r} \qquad (2.3)$$

S_{iw} = surface tension for ice-water interface

r = radius of ice-water interface

It can be seen from equations 2.2 and 2.3 that as the temperature decreases, ice forms in smaller pores and the unfrozen water content decreases. There is a relationship between (P_i-P_w) and unfrozen water content analogous to the suction-moisture content relationships for unfrozen soil. The pressure difference is related to temperature according to the Clausius-Clapeyron equation. Thus, the relationship between temperature and unfrozen moisture content (figure 2.1) can be obtained as was done by Koopmans and Miller (1966).

2.2 Water Migration in Freezing Soils

Frozen soils will have a permeability since continuous liquid water films exist. Horiguchi and Miller (1983), Perfect and Williams (1980) and Williams and Burt (1974) determined the hydraulic conductivity of frozen soil and found that it decreases as temperature decreases and liquid films become thinner (figure 2.2). Coarse-grained material such as sand has a lower hydraulic conductivity when frozen at a given temperature than silt because of its lower surface area and lower unfrozen water content.

As the soil freezes, there is an increasing difference in pressure between the ice and the water (P_i-P_w) as shown

FIGURE 2.1. Relationship between unfrozen water content and temperature for Caen silt (density = 1.420 gcm^{-3}). Unfrozen water contents were determined using time domain reflectometry by Patterson (personal communication 1988).

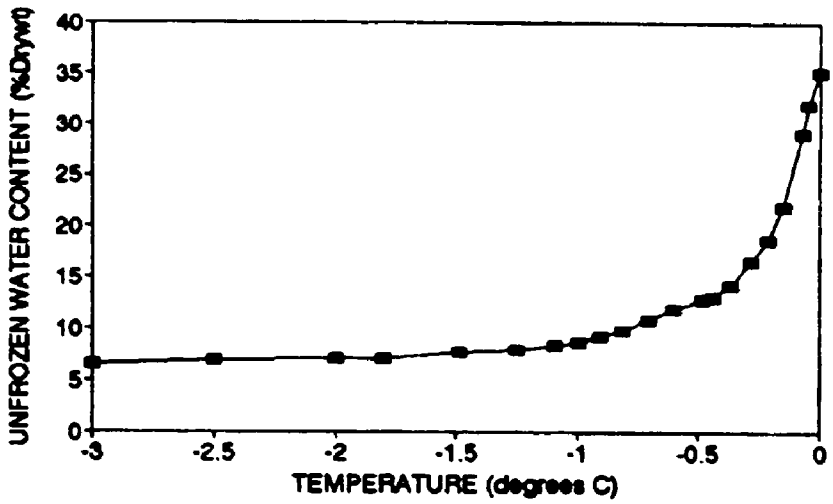

FIGURE 2.2. Hydraulic conductivity of frozen soil (from Williams and Burt 1974 and Williams 1982).

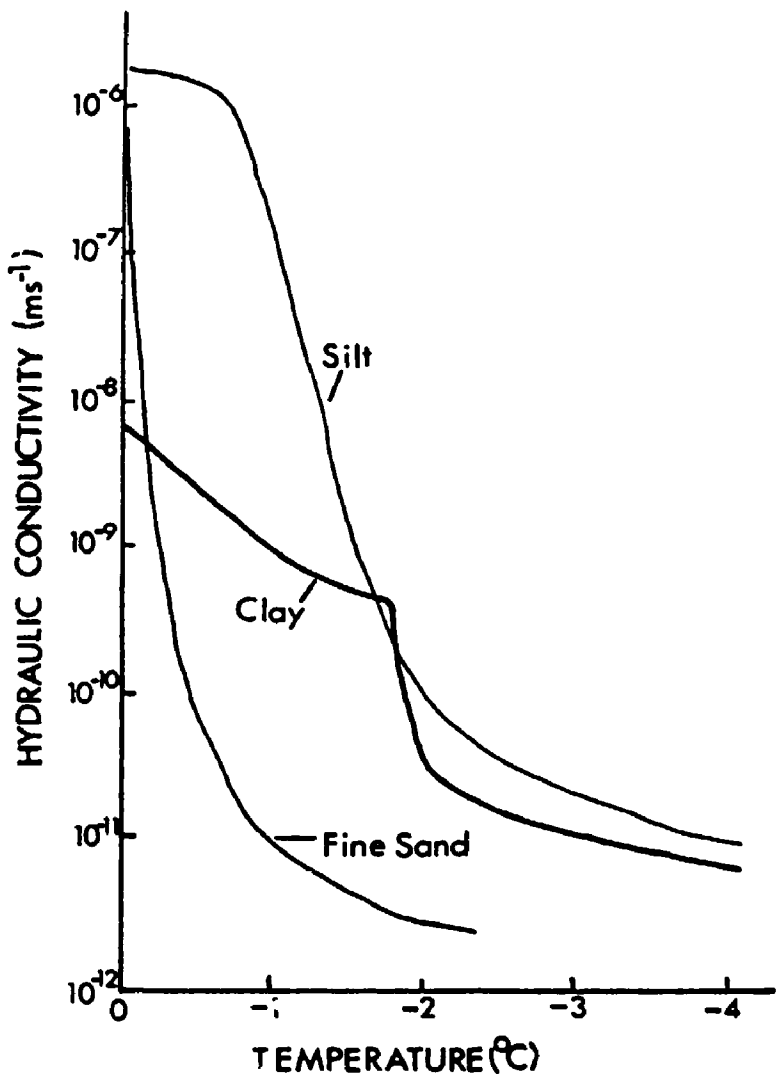

by equations 2.2 and 2.3. Cryosuction (Williams and Smith 1989) refers to the fall in water pressure which may cause the migration of water from the warmer part of the soil to the area where freezing is taking place. The rate of water migration will depend on the size of the pressure gradient (and therefore the temperature gradient) and the hydraulic conductivity. This relationship is similar to that in unfrozen soils and can be described by Darcy's law:

$$q = K \frac{dh}{dz} A \tag{2.4}$$

q = flow of water ($m^{-3}s^{-1}$)

K = hydraulic conductivity (ms^{-1})

h = head (metres of water)

z = distance

dh/dz = hydraulic gradient (m H_2O/m -- analogous to pressure gradient)

A = cross-sectional area of flow (m^2)

Darcy's law and the Clausius-Clapeyron equation may be combined to describe the flux of water across the frozen fringe (a zone containing pore ice and unfrozen water between the warmest ice lens and the unfrozen soil), once the freezing front stops advancing, if it is assumed that no water accumulates within the frozen fringe (Loch and Kay 1978):

$$q = K\left[\frac{V_i}{V_w}\frac{(P_{i2} - P_{i1})}{l} - \frac{L}{V_w T_o}\left(\frac{dT}{dz}\right)\right] \tag{2.5}$$

P_{i2} and P_{i1} = ice pressure at base of ice lens and freezing front respectively

K = overall hydraulic conductivity of frozen fringe

l = length of frozen fringe

dT/dz = temperature gradient

Other variables as defined earlier.

However, the relationship between hydraulic conductivity and temperature is non-linear and there is a rapid decrease in conductivity as temperature decreases. Water will therefore, flow toward the freezing zone and accumulate where the hydraulic conductivity becomes small and water flow rates are small. This water freezes and accumulates in the form of ice lenses (Hoekstra 1966 and Perfect and Williams 1980).

2.3 Ice Lens Formation and Frost Heave

Konrad and Morgenstern (1980) present a mechanistic model of frost heave based on the coupled heat and mass flow model of Harlan (1973), which describes the formation of ice lenses. As the frost front penetrates the ground, water is drawn to an accumulation zone (figure 2.3) (where permeability decreases rapidly with decreasing temperature). The thermodynamic equilibrium will be upset as the water film thickness increases and causes a change in the free energy. Some of the water will freeze to restore the equilibrium and maintain a constant film thickness at a given temperature. As water freezes, latent heat is

FIGURE 2.3. Model of ice lens formation (from Konrad and Morgenstern 1980 and Wood 1985).

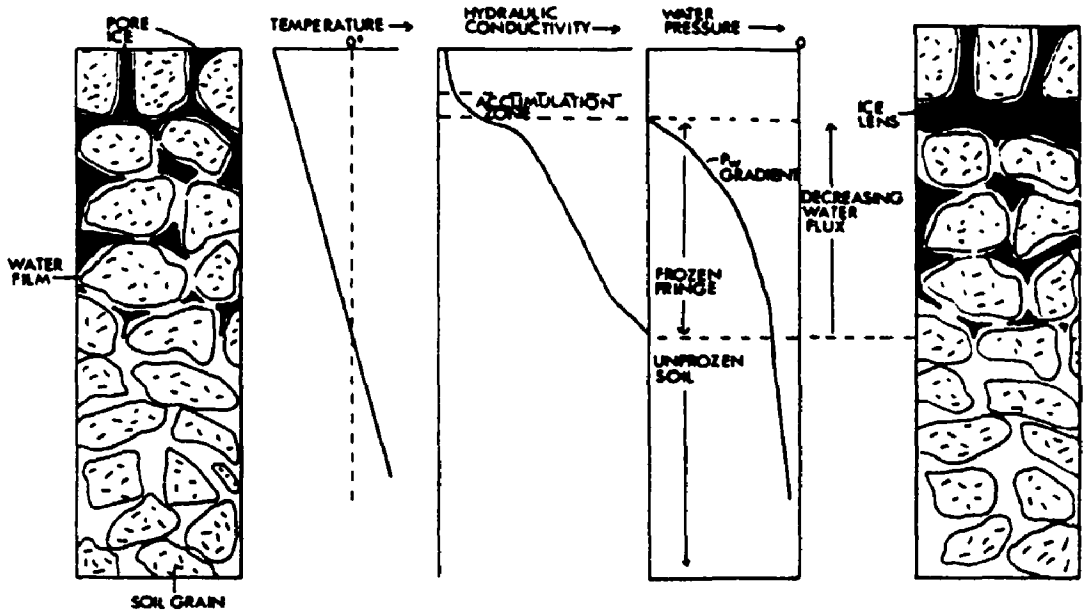

released which offsets the cooling of the ground. As ice segregates and lenses continue to grow, the moisture content in the soil below will fall if the flow of water is insufficient to replenish it. Thermal imbalance occurs, the soil cools and the ice lens stops growing because (P_i-P_w) is too great for the temperature. The freezing front advances to a new position and a new ice lens forms. This process is repeated until steady-state conditions are reached and the freezing front stops penetrating.

The size and distribution of ice lenses depends on the temperature gradient (although other factors may modify the effects). Small closely spaced ice lenses are found where the temperature gradient is steep because the rate of cooling is high and water can not migrate at a rate sufficient to create a large continuous lens. The rate of cooling therefore, will be much greater than the rate of release of latent heat by the freezing of water which migrates to the freezing front and the frost front will penetrate rapidly. Under these conditions, the rate of heave may be large but the total heave within a given soil layer is small (Williams and Smith 1989). Deeper in the ground, the temperature gradient is small and the rate of cooling is slower. Large ice lenses that are spaced farther apart are able to grow because there is sufficient time for water to migrate to the freezing front. The rate of heave will be smaller but the total heave within a given soil

layer will be greater than it is when subjected to a large temperature gradient (Williams and Smith 1989).

2.4 Mechanical Properties of Frozen Soil

2.4.1 *Introduction*

Models of the type proposed by Konrad and Morgenstern (1980) do not consider the role of the rheologic properties of the frozen soil in the frost heave process to be important. The frozen material surrounding a growing ice lens must yield to allow the ice lens to expand. This will only occur if the ice pressure exceeds the resistance of the frozen material. The mechanical behaviour of the frozen material therefore is an important factor in the frost heave process.

Since frozen soil consists of soil grains, unfrozen water, ice (pore ice and segregated ice lenses) and air within ice, the response of the frozen soil to an applied stress will be determined by the combined reaction of the individual components and their interaction with each other (Sayles 1988 and Tsytovich 1975). The strength of frozen soils is determined by the same factors as determine the resistance of unfrozen soil but frozen soils are usually stronger and display time-dependent creep similar to ice (Sayles 1988 and Williams and Smith 1989).

The strength of frozen soils is determined by a combination of interparticle and intraparticle bonds. There are three types of bonds for frozen soil (Andersland et al.

1978, Johnston et al. 1981 and Vialov 1965):

1. Molecular cohesion forces which depend on molecular attraction between solid particles separated by water films.
2. Structural cohesion which reflects the influence of physicochemical, mechanical and other processes which originate in soil as a result of its geological formation.
3. Cementing by ice as a result of bonds between ice crystals and mineral particles separated by a film of unfrozen water.

The rheological behaviour and strength of the frozen soil changes as the relative amounts of unfrozen water and ice change with temperature and when stress is applied to the soil (Sayles 1988, Vialov 1965 and Williams and Smith 1989). Since the presence of ice in frozen soils has a strong influence on rheological behaviour, it is useful to discuss the mechanical behaviour of ice before examining the behaviour of frozen soil.

2.4.2 *Mechanical behaviour of ice*

The crystal structure of ice consists of crinkled sheets of hexagonal rings which are stacked (Fletcher 1970, Jumikis 1979 and Williams and Smith 1989). Plastic deformation occurs principally through glide of these sheets over each other and is referred to as basal glide.

A variety of deformation mechanisms occur in ice and most of them exhibit some degree of time-dependence (Williams and Smith 1989). Plastic deformation may occur

through the migration of defects or dislocations which cause the crystal to weaken (Fletcher 1970, Glen 1987, Langdon 1973, Michel 1978 and Vyalov 1986). Deformation may also occur through grain boundary sliding along basal planes when a shear stress acts in that plane (Gold 1963, Langdon 1973 and Michel 1978). Reorganisation of the crystal structure may take place in individual grains of ice due to stress (Williams and Smith 1989). Melting and recrystallization may produce an orientation favourable for easy glide (Glen 1963 and Williams and Smith 1989).

Ice behaves perfectly elastically up to a limit but once this elastic limit is exceeded, irreversible deformation takes place. Under long-term stress, ice will behave as a viscous liquid (Gold 1978, Haefeli 1965 and Jumikis 1966). The rheological behaviour has been classified as visco-elastic (Haefeli 1965) and visco-plastic (Gold 1978 and Michel 1978).

Budd and Jacka (1989) outlined the general features of creep curves for polycrystalline ice. The initial response to an applied stress is an instantaneous elastic impulse strain which is fully recoverable. This strain increases approximately linearly with stress and shows little dependence on temperature. The second stage is a period of decreasing strain rate or primary creep. Deformation is anelastic and is time-dependent recoverable if the load is removed. Beyond 1% strain, irreversible viscous strain is

dominant. As strain progresses, the crystal structure changes as crystals rotate. The third stage occurs when strain is greater than 10% and steady-state tertiary flow may develop with strengthening of fabrics but also increased effects of rotation occurring. A balance may be reached where deformation and rotation are balanced by crystal growth and change. Typical creep curves for ice are shown in figure 2.4.

Strain rate is related to applied shear stress by a power law (Glen 1963):

$$\dot{\epsilon} = k\sigma^n \tag{2.6}$$

$\dot{\epsilon}$ = strain rate

σ = shear stress

n = constant = approximately 1.5 for ice

Langdon (1973) gives a generalized creep equation for all types of deformation mechanisms. At high temperature, ice will have a secondary steady-state axial creep rate $\dot{\epsilon}$:

$$\dot{\epsilon} = \frac{ADGb}{kT}\left(\frac{b}{d}\right)^m\left(\frac{\sigma}{G}\right)^n \tag{2.7}$$

A = constant

D = coefficient of diffusion $D=D_o \exp(-U_d/kT)$

D_o = frequency factor

U_d = activation energy for diffusion

k = Boltzman constant

T = temperature (K)

G = shear modulus

b = Burgers vector (4.523×10^{-8} cm for ice)

FIGURE 2.4. Creep curves for ice at (a) constant load σ (where $\sigma_3>\sigma_2>\sigma_1$) and (b) constant strain rate $\dot{\epsilon}$ (where $\dot{\epsilon}_4>\dot{\epsilon}_3>\dot{\epsilon}_2>\dot{\epsilon}_1$) (from Michel 1978).

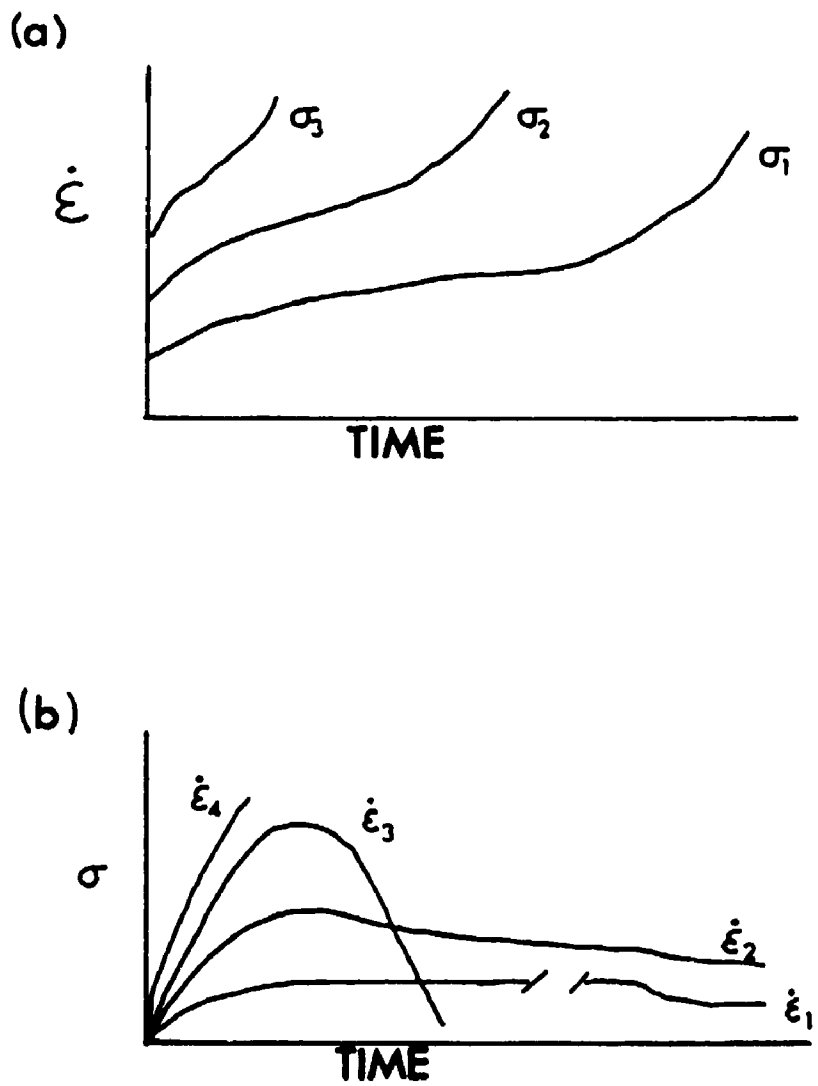

d = average grain size

σ = applied stress

m = constant = $-[\partial(\ln\epsilon)/\partial(\ln d)]_{\sigma,T}$

n = constant = $[\partial(\ln\epsilon)/\partial(\ln\sigma)]_{d,T}$

Similar equations illustrating the power relationship between applied stress and strain rate are given by Gold (1973 and 1978) and Weertman (1973).

The constant A is usually not well defined but contains factors such as the density of mobile dislocations and the effective width of the grain boundary. The exponents n and m indicate the importance of stress and grain size in determining the creep rate and their values depend on the creep mechanism.

At temperatures close to the melting point and at stresses less than 175 kPa, ice exhibits plasto-viscous behaviour. Point defect mechanisms dominate and the strain rate is linearly related to stress (steady-state creep) and n is equal to one. Nabarro-Herring creep is dominant and this involves diffusion of vacancies between grain boundaries (Gold 1973, Langdon 1973 and Wood 1990).

The creep rate depends on a variety of factors such as ice temperature, grain size and shape and orientation of crystals. Mellor and Testa (1969) found that creep of polycrystalline ice was strongly dependent on temperature as the ice temperature rises above -10°C. An abrupt increase in deformability was observed at ice temperatures between

0°C and -1.2°C which was probably a result of pressure melting and recrystallization.

Grain size is important when point defect and grain boundary shear mechanisms dominate because they depend on the surface area of grain boundaries. Cole (1987) proposed that fine-grained ice is more susceptible to softening effects of recrystallization because it has more potential nucleation sites than coarse-grained ice.

The deformation of polycrystalline ice depends on the shape and orientation of individual crystals. A preferred orientation for easy glide is one in which all optical axes (C-axis) are parallel (Glen 1963, Jumikis 1979 and Williams and Smith 1989). Slip occurs more easily if a shear stress is oriented in the same direction as the basal plane (Gold 1963, Michel 1978). Ice which has a more random crystal orientation will have a different rheological behaviour and will have a creep curve in which the creep rate falls off with time. At high stress, ice may recrystallize in an orientation which is more suitable for the flow that is proceeding (Glen 1963).

2.4.3 *Creep of frozen soils*

Generally stresses in nature do not build suddenly and frozen soil deforms in a ductile manner with slow continuous deformation throughout the material (Andersland et al. 1978 and Williams and Smith 1989). There are four components to the time-dependent deformation curve. The initial response

is an elastic instantaneous deformation which is reversible if the load is removed quickly. If the load is not removed, deformation will continue at a decreasing rate and the soil will exhibit primary creep. This stage includes both structurally reversible and irreversible components and plastic deformation. The strain rate will reach a minimum value if the deformation process is undamped. Creep will then enter the secondary stage in which creep occurs at a constant rate. This is a period of plastic viscous flow which is not completely reversible. As strain increases, deformation enters the tertiary creep stage during which the creep rate accelerates and results in brittle or viscous fracture. Tertiary creep should be divided into two stages with the first including the development of plastic deformations which do not cause failure and the second relating to the appearance of cracks or the rapid growth of deformation (Andersland et al. 1978, Hoeve and Smith 1988, Johnston et al. 1981, Sayles 1988, Vialov 1965, Williams and Smith 1989 and Williams and Wood 1985). All three stages of creep develop in frozen soil with the second and third stage becoming more important as plasticity and ice content of the soil increase. Frozen soil is considered as an elasto-plasto-viscous body because all three types of deformation may develop depending on the magnitude of stress and its time factor (Vialov 1965).

Several factors influence the rheological behaviour of

frozen soil. Temperature, grain size and ice content will determine the creep stages that will develop and their duration.

The influence of temperature is especially important at temperatures near the freezing point (0° to -2°C) where the relative amounts of unfrozen water and ice and therefore, the strength characteristics can change greatly with small changes in temperature (Williams and Smith 1989). Generally, a decrease in temperature results in a decrease in creep strain rate and an increase in strength as the strength of the ice bonds and those of unfrozen water increase (Johnston et al. 1981 and Jumikis 1979). Temperature is also important because thermal activation is involved in the deformation process and is related to the rate of deformation by the Arrhenius equation (Andersland et al. 1978, Sayles 1988 and Williams and Smith 1989):

$$\dot{\epsilon} = A\exp(-L/T) \qquad (2.8)$$

L = (U/R) where U is the activation energy and R is the universal gas constant

A = constant

T = absolute temperature

Grain size is an important influence on rheological behaviour because the unfrozen water content at a given temperature depends on grain size. Frozen sands generally exhibit brittle failure because they contain almost no unfrozen water, even at temperatures close to 0°C. Lower

ice contents than in sand and a thin layer of unfrozen water on soil particles contributes to a plastic type failure in frozen clays and silts which tend to behave in a ductile manner and exhibit creep (Andersland et al. 1978, Sayles 1988 and Williams and Smith 1989).

The mechanical behaviour of frozen soil will be greatly influenced by the amount of ice it contains. Frozen soils of low density and high ice content (eg. where massive ice beds exist) will generally display deformation behaviour similar to that of ice as outlined earlier (Johnston 1981, Williams and Smith 1989 and Yuanlin and Carbee 1987).

Generally, for sand-ice or silt-ice mixtures, strength increases with ice content to a point. At this point there exists the optimum combination of ice-cement cohesion, intergranular friction and dilatancy (Johnston et al. 1981). The optimum ice content corresponds to the complete filling in of pores with ice. At ice contents lower than this, the load is still carried by the mineral particles and the cohesive resistance supplied by the ice as well as the frictional resistance between particles combine to provide strength for the frozen material. The cohesive strength will therefore increase with ice content until the ice completely fills the pores and mineral particles are no longer in contact (Williams and Smith 1989). At ice contents greater than the optimum value, strength decreases with increasing ice content due to the lack of intergranular

contacts (Johnston et al. 1981).

2.4.4 *Application to frost heave*

The resistance of the frozen soil must be overcome for an ice lens to continue to grow. The rigid ice model of Miller (1978) and O'Neill and Miller (1985) uses a stress partition factor which describes the distribution of the pore constituent pressures. When the combined pore stress or neutral stress rises above the overburden pressure the pore contents alone will support the load. The effective stress will fall to zero and the soil particles will no longer be held together and an ice lens forms (O'Neill 1983 and Williams and Smith 1989). As the ice lens grows and the water pressure in the soil below falls, the ice pressure must also fall to maintain the pressure difference according to equation 2.2. When the ice pressure is less than the overburden pressure the ice lens cannot displace the overlying soil and the ice lens stops growing (Williams and Smith 1989). This model however, does not consider the cohesive strength due to the presence of ice which also must be overcome for heaving to occur. The ice pressure would have to be higher than that assumed by this model for heave to occur (Williams and Smith 1989). Nixon (1991) includes a separation pressure in his model which is the pressure required to separate the soil skeleton. This model however, does not take the time-dependent rheologic behaviour of the soil into account.

Creep behaviour of frozen soils is time-dependent and examples for Caen silt are shown in figure 2.5. The applied stress in this case is an external load, but similar rheologic behaviour would be expected to occur in response to a stress generated within the frozen soil during ice lens growth. Williams and Wood (1985) measured ice pressures of 200 kPa during frost heave experiments on Caen silt. These pressures were of the same magnitude as the applied load used to produce the creep curve in figure 2.5. Williams and Wood (1985) concluded from their observations that the resistance to ice lens growth is probably determined by creep in the frozen soil.

Shen and Ladanyi (1987) present a theoretical model which considers the stress field and the creep properties of the frozen soil which is able to predict the amount of ice accumulation behind the freezing front but not the position of discrete ice lenses. This model does not consider the continuing heave (ice accumulation in frozen soil behind the warmest ice lens) observed by Smith and Patterson (1989) which also illustrates the importance of the creep properties of the frozen soil.

The rheological behaviour of the frozen soil and the factors which control it therefore, are important in determining the amount and rate of heave that occurs.

FIGURE 2.5. Creep curves for Caen silt at various applied stresses at a temperature of -2°C. The applied stress (kPa) is in the brackets (from Ladanyi and Lauzon 1985 as presented in Wood 1985).

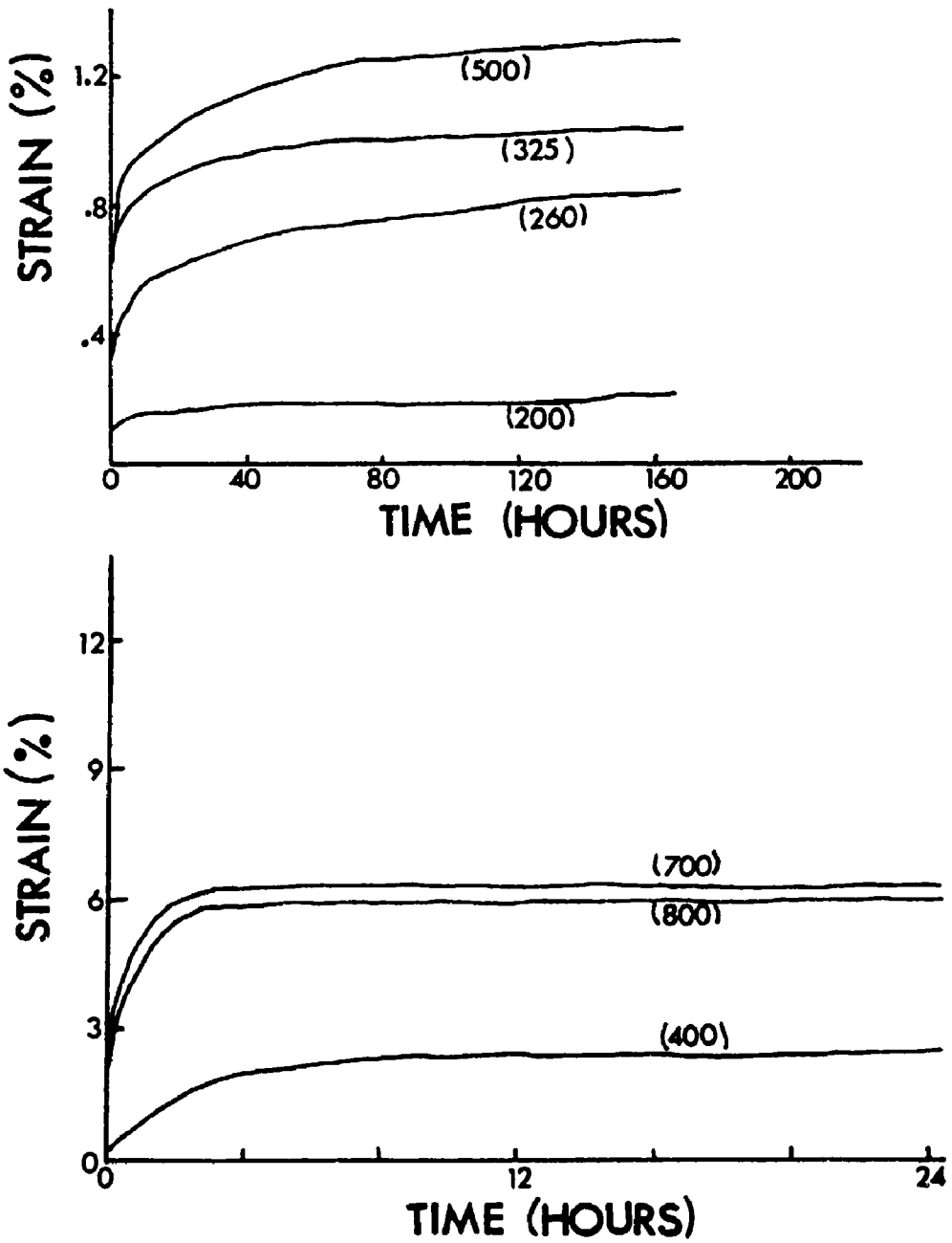

CHAPTER THREE

THERMALLY INDUCED REGELATION IN PURE ICE

3.1 Historical Review of Earlier Experiments

Regelation refers to the melting and refreezing of ice and water due to pressure changes. The sliding of ice around bumps on a rough rock surface may be attributed to this process (Nye 1973, Walden 1986). Melting occurs on the upstream side due to the higher pressure and freezing occurs on the downstream side due to lower pressure. For large objects however this process alone is not sufficient and plastic deformation of ice is also essential (Nye 1973).

It has been suggested that a significant portion of the total mass transport in freezing soils is due to ice movement as the result of regelation of pore ice (Horiguchi and Miller 1980, Kay and Perfect 1988, Miller 1983, Ohrai and Yamamoto 1985, Philip 1980 and Wood and Williams 1985b).

Ice sandwich experiments conducted by Miller (1970), Horiguchi and Miller (1980) and Wood and Williams (1985b) illustrate the regelation process that may occur in a single soil pore. A layer of ice was sandwiched between two reservoirs of supercooled water with semi-permeable membranes placed between the reservoir and the ice. An elevated water pressure was applied to one end of the ice sandwich and water was observed to flow into the reservoir at the opposite end. The flow rate may be described by a

linear transport equation similar to Darcy's law (Wood and Williams 1985b):

$$J = -Ldh/dz \tag{3.1}$$

J = Flow velocity (ms^{-1})

L = Transport coefficient (ms^{-1})

dh/dx = hydraulic gradient (mH_2O/m)

Lower flow rates were observed at lower temperature as the transport coefficient decreased with temperature. The transport coefficient may also change with time as changes in the ice occur due to aging and recrystallization.

The results can be explained using the Clausius-Clapeyron equation (Wood and Williams 1985 and Miller et al. 1975). According to equation 2.2, as water pressure is increased at one side of the ice, the equilibrium freezing temperature rises above the ambient temperature. Water then flows through the membrane and freezes onto the ice and the ice pressure rises. The increase in ice pressure is transmitted to the other end possibly by creep (Wood and Williams 1985) where the water pressure remains unchanged. At this end, the equilibrium freezing temperature falls below ambient and some of the ice melts and flows into the reservoir. Latent heat will be released at the high pressure side as freezing occurs causing a rise in temperature at the water-ice interface. At the low pressure end, the temperature will drop as melting occurs. A

temperature gradient will be produced which will cause heat flow in the same direction as mass flow.

Miller et al. (1975) describes the mass flow in the ice sandwich as a translational movement of ice and pure series transport. The ice behaves as a rigid body and can be thought of as moving as a plug. Wood and Williams (1985) suggest that the ice exhibits creep and therefore is not behaving as a rigid body. They suggest that flow rates decrease with temperature because creep effects of ice are less at lower temperature. According to Miller et al. (1975), flow rates decrease with temperature due to an increase in sliding friction of the ice plug along the walls of the frost cell and this is consistent with an increase in ice pressure as temperature decreases. There is some controversy therefore, as to whether the ice behaves as a rigid body or exhibits creep behaviour.

The regelation process observed in the ice sandwich has also been observed in frozen soils. Burt (1974) found that if a hydraulic gradient was applied to a frozen soil sample which contained a layer of ice, outflow was still observed at the low pressure end. Ice lenses do not form a barrier to moisture migration in frozen soils and mass flow may occur through regelation in frozen soils.

3.2 Earlier Evidence of Thermally Induced Regelation

It has also been suggested that a temperature gradient induces the movement of ice and soil grains with respect to

each other through the process of thermally induced regelation (Hoekstra and Miller 1967, Kay and Perfect 1988, Miller 1983 and Romkens and Miller 1973). Isolated grains embedded in ice migrate up the temperature gradient by this process. If ice fills the space between a mass of grains that cannot move, the ice will move down gradient, if feasible, causing frost heave (Miller 1983). Miller (1983) and Hoekstra and Miller (1967) offer the following explanation for thermally induced regelation around a grain embedded in ice. When a temperature gradient exists across the grain, a thick film of water will exist on the warm side of the particle. This condition is compatible with that of thermal equilibrium but incompatible with conditions of mechanical equilibrium since the film is asymmetrical. The grain will move relative to the rigid ice to restore symmetry and mechanical equilibrium. This however, disturbs the thermal equilibrium and melting occurs on the warm side of the grain and water flows around to the cold side of the grain and refreezes in order to maintain equilibrium. The grain will move in the direction of warmer temperatures as the system attempts to maintain thermal and mechanical equilibrium.

Hoekstra and Miller (1967) and Romkens and Miller (1973) conducted experiments with glass beads embedded in ice and observed the migration of the beads towards the warm end of the ice. Their experiments were conducted with a

temperature gradient of 0.8°C cm^{-1} or 80°C m^{-1} (temperature at one end was -0.04°C) and rates of particle movement ranged from 1 μmh^{-1} to 7 μmh^{-1} as the bead approached the warm end. Very small migration rates were observed under very large temperature gradients in these experiments. The importance of this process in freezing soils in nature where temperature gradients are much smaller may be minimal.

Ohrai and Yamamoto (1985) also suggest that regelation allows water to migrate through frozen soil. They propose that as an ice lens grows, water migrating through unfrozen soil should freeze on the high temperature side of the lens and melting should occur on the low temperature side. The water would then migrate through the frozen soil and freeze on the high temperature side of the next lens. Ohrai and Yamamoto (1985) consider this migration of water between ice lenses to be due to regelation.

3.3 Objective of Present Experiments on Thermally Induced Regelation

The present experiments were conducted to illustrate that thermally induced regelation occurs when a temperature gradient, instead of a hydraulic gradient as in the experiment of Horiguchi and Miller (1980) and Wood and Williams (1985b), is applied to the ice sandwich. The thermal gradient should induce a pressure gradient across the ice because according to the Clausius-Clapeyron equation (equation 2.2) and with uniform water pressures, different

ice pressures will exist at the two water-ice interfaces. Pressures measured within the ice should indicate whether or not the ice can sustain a pressure gradient. This information can be used to make inferences about the rheological behaviour of the ice i.e. whether it behaves as a rigid body or exhibits creep. The experimental situation is different than that which would occur in nature, where the pore water would be at a lower pressure (less than atmospheric) than the water in the reservoirs.

3.4 Description of Experiment

3.4.1 *Apparatus*

Experiments were carried out using the frost pressure cell developed by Wood (1985). The cell (figure 3.1) consisted of a cylindrical perspex sample holder 3.5 cm long with an internal diameter of 5.4 cm and walls 1.90 cm thick. The total volume of the sample was 78.42 cm^3. The sample was confined by aluminum cooling plates at both ends.

Two Kulite VQS-250 pressure transducers were located 1.20 cm apart and 1.15 cm from each end of the sample. These were activated by 1 V d.c. and provided a resolution of 0.01 kPa. The transducers were connected to copper tubes which extended into the sample. These were covered by rubber bladders approximately 2 cm long and 0.35 cm in diameter which were filled with Dow Corning 200 dimethyl silicone oil. A Canlab 285 chart recorder was used to provide a continuous record of pressure.

FIGURE 3.1. Exploded view of the frost pressure cell used in ice sandwich and frost heave experiments (from Wood 1985).

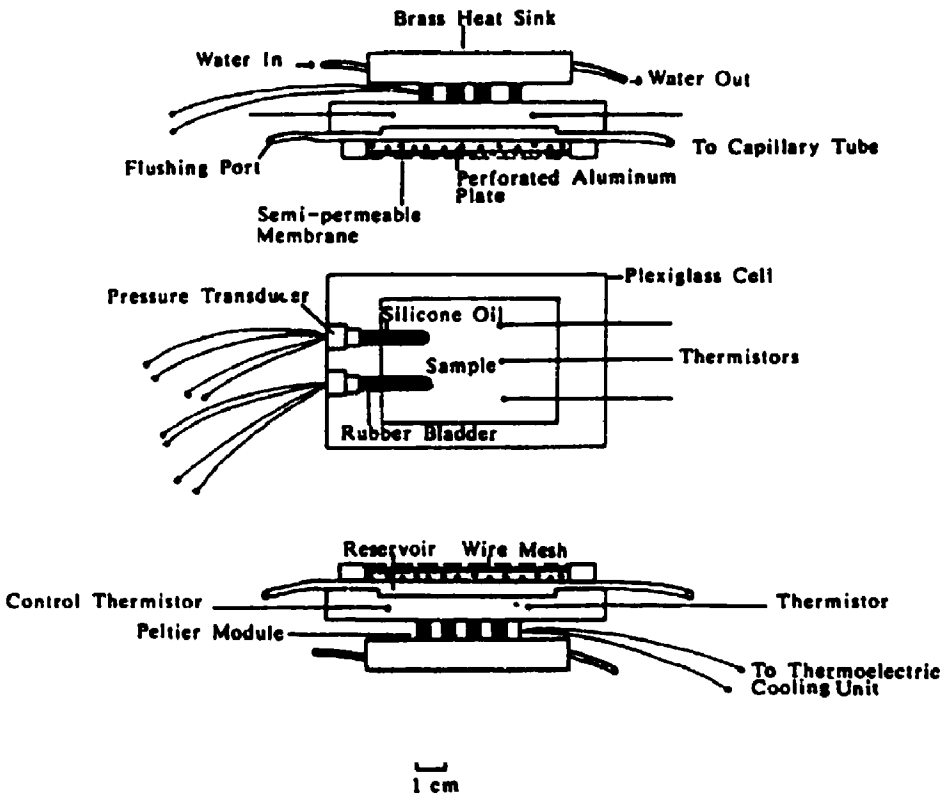

The temperature of the sample was controlled by Peltier modules located on each aluminum cooling plate and connected to a thermoelectric cooling unit. It was possible to maintain a cooling plate temperature within 0.0025°C of the desired temperature using this equipment. Sample temperature was determined with three YSI 3kΩ thermistors with a precision of ±0.0025°C. These were placed in copper tubes containing heat conducting grease spaced 1.25 cm apart and located 0.5 cm from the ends of the sample. A Keithly multimeter was used to monitor the sample temperature. To reduce heat transfer between the sample and its surroundings, the cell was wrapped in foam rubber insulation approximately 15 cm thick and placed in an incubator set at 0°C. Fans in the incubator provided good circulation of air.

Two small reservoirs (volume 5.5 cm^3) containing distilled water were located at each end of the sample. Cellulose acetate membranes separated the ice from the reservoir water which was supercooled and prevented ice crystals from growing in the reservoir. Capillaries with an internal diameter of 0.184 cm were connected to the reservoir and mounted on a graduated scale to allow the recording of inflow and outflow of water from the sample.

3.4.2 *Sample preparation*

Ice for the experiment should be bubble free and this was achieved by freezing de-aired, distilled water slowly. Water was frozen unidirectionally on a thermoelectric cooling plate within the frost pressure cell. After freezing, the cell was placed in a freezer (temperature approximately -20°C) for about 24 hours. Prior to assembly of the cell the ends of the ice sample were scraped until they were flush with the ends of the sample container. The ice was allowed to warm to about -5°C before placing the membranes on the ends of the sample. The aluminum cooling plates were then attached to the cell and the reservoirs were filled with distilled de-aired water. The cell was then wrapped in insulation and a clamp was placed on it before placing it in the incubator.

3.4.3 *Data Collection*

After the cell was placed in the incubator the temperature at both ends of the sample was set to the same temperature (between -0.05° and -0.08°C) and the sample was allowed to equilibrate for 24 to 48 hours. The temperature at one end was then lowered slowly in steps to no more than -0.2°C (to avoid freezing in the reservoir).

During the experiment internal pressures were recorded by the chart recorder. The position of the meniscus in the capillaries was recorded every two or three hours during the day for the duration of the experiment. These readings were

later converted to a volume of water inflow or outflow. Temperature readings were taken periodically also.

A total of twelve experiments were carried out. The duration of individual experiments was 2 to 4 weeks. During most experiments the direction of the temperature gradient was kept constant but in some cases it was reversed during the experiment.

3.5 Results

3.5.1 *Water flow*

Water flow data for experiments 14 and 17 are presented graphically (figures 3.2 and 3.3) as cumulative flow (cm^3) versus time. A negative slope on the water flow curve indicates an inflow of water into the sample and a positive slope indicates an outflow of water from the sample. Data for other experiments are presented in Appendix 1.

After some initial perturbations at the beginning of the experiment, steady state conditions were reached after a temperature gradient was established. Water was generally observed to flow into the cold end of the sample and flow out of the warm end. Thus water appears to flow from the cold end of the ice to the warm end. Rates of inflow and outflow vary between experiments and during experiments but were found to range from 0.002 cm^3h^{-1} to 0.047 cm^3h^{-1}. The rate of flow increased with time in some experiments, reached a maximum and then declined in the latter part of the experiment.

FIGURE 3.2. Cumulative water flow over time during ice sandwich experiment 14. Positive slope for water flow indicates an outflow of water from the sample and a negative slope indicates an inflow of water to the sample.

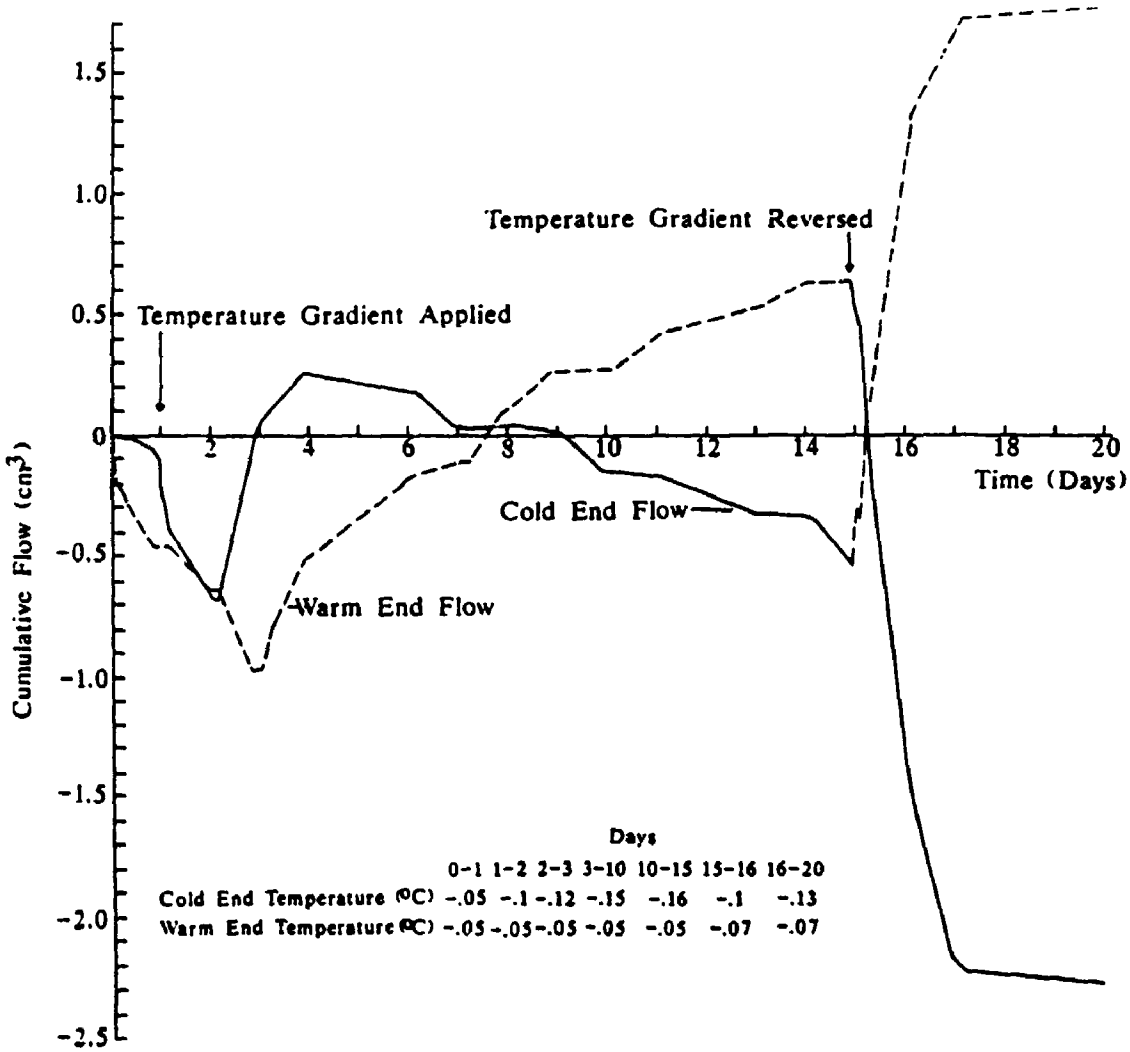

FIGURE 3.3. Cumulative water flow and pressure over time during ice sandwich experiment 17. Positive slope for water flow indicates an outflow of water from the sample and a negative slope indicates an inflow of water to the sample.

COOLING PLATE TEMPERATURE (°C)

Days	0-1	1-2	3-14	14-15	15-17
Cold end	-.07	-.11	-.13	-.10	-.13
Warm end	-.07	-.08	-.08	-.08	-.08

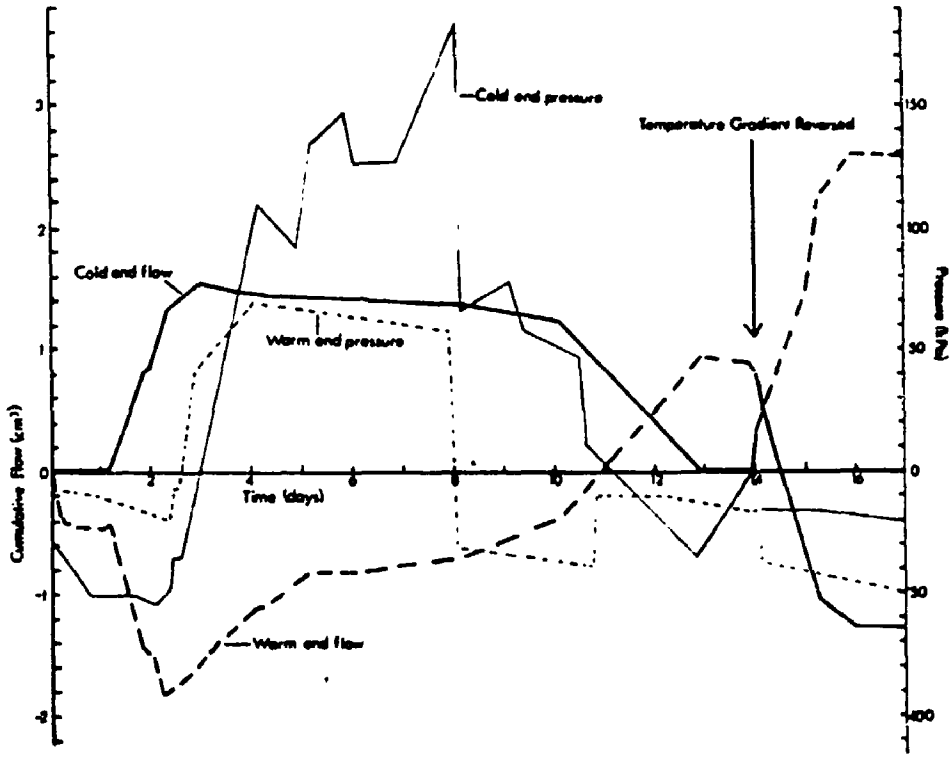

In some experiments the temperature gradient was reversed (figures 3.2 and 3.3). The direction of water flow was also observed to reverse and water appeared to flow from the cold end to the warm end. Immediately after the change in the thermal regime of the system there was a rapid inflow of water into the new cold end and rapid outflow from the new warm end of the sample. Flow rates were found to vary from 0.066 cm^3h^{-1} to 0.079 cm^3h^{-1} at this stage of the experiment which are larger than those observed during the earlier stages. Flow rates then decline to values similar to those observed during the earlier part of the experiment.

In summary, water flow data indicates that water flows from the reservoir through the membrane and freezes onto the cold end of the ice. At the warm end of the sample, ice melts and water flows into the reservoir.

3.5.2 *Pressure*

Ice pressures for experiment 17 are plotted in figure 3.3. Data for other experiments are presented in Appendix 1. In some experiments (eg. expt 14) the pressure did not vary significantly from atmospheric. In most experiments, pressure increased with time as the temperature at the cold end was lowered, reached a peak (when the cold end temperature was constant) and then declined (figure 3.3). A pressure gradient was generally observed with higher pressures occurring at the cold end of the sample and the pressure difference decreasing over time. The difference in

pressure between the two transducers was found to be as large as 180 kPa in one experiment. In two experiments, the pressure at both transducers increased as the temperature at the cold end decreased but there was little difference in pressure between them, indicating a uniform pressure throughout the ice body.

The peak pressure at the colder transducer is close to that predicted (using the Clausius Clapeyron equation) for the ice-water interface at the colder end of the sample. The observed pressure also drops over time even though the temperature at the cold end does not increase. During the later stages of the experiment, therefore, the observed pressure may become lower than the predicted pressure.

The pressure data suggest that a linear pressure gradient is not necessarily present across the ice body. The results also suggest that the magnitude of the pressure gradient changes through time with pressures becoming more uniform as time passes.

3.5.3 *Relationship between water flow, pressure and temperature*

The rate of water flow to and from the sample has been plotted against the average ice temperature (figure 3.4). There is a large amount of scatter but higher flow rates appear to occur at higher temperature.

Flow rate has been plotted against the observed pressure difference between warm and cold transducers

FIGURE 3.4. Relationship between water flow rates and average ice temperature for experiments 14 and 15. Cold end flow refers to inflow at cold end and warm end flow refers to outflow at warm end.

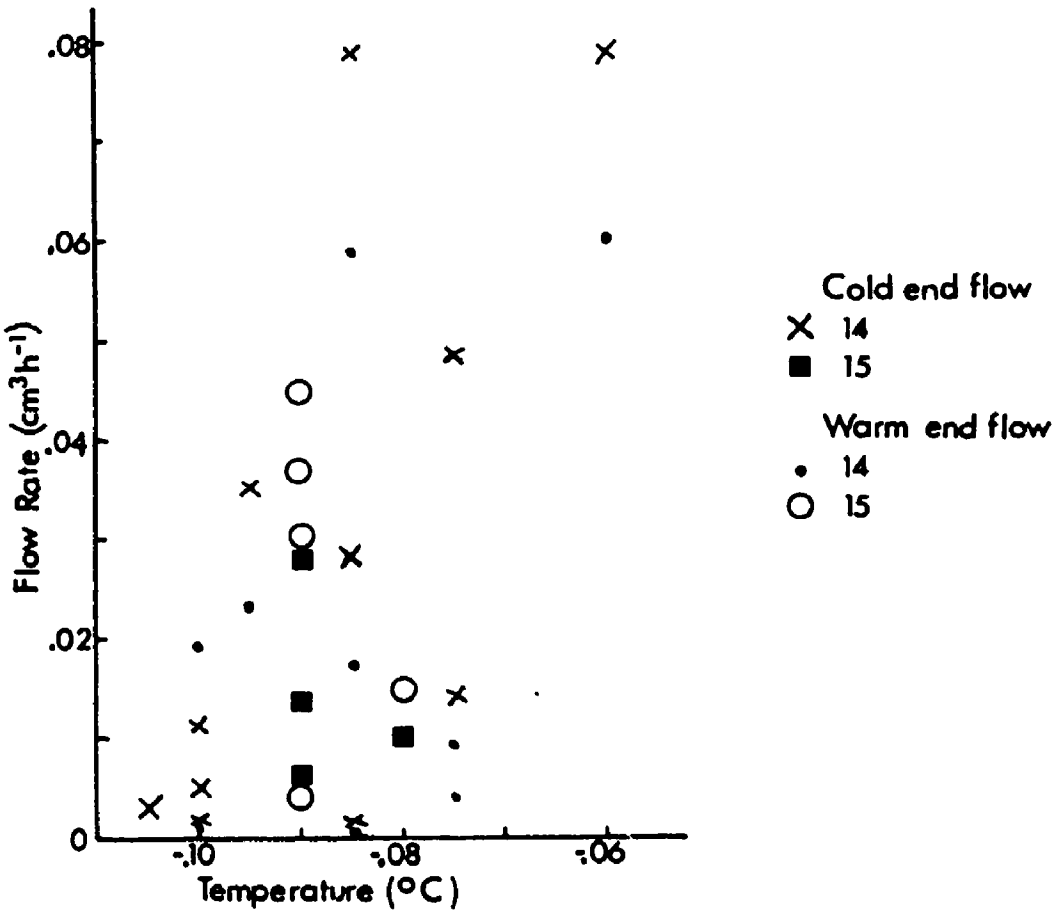

(figure 3.5). Flow rates appear to be higher when pressure gradients are smaller. The relationship varies between experiments and is non-linear.

3.6 Interpretation of Results

The experimental results illustrate the process of thermally induced regelation in an ice-water system. Observations may be explained using the Clausius-Clapeyron equation (equation 2.2) as was proposed by Wood (1990). A drop in temperature at the cold end of the sample results in an increase in ice pressure. This induces a pressure gradient and ice creeps toward the warm (low pressure) end causing an increase in ice pressure there. The equilibrium freezing temperature at the warm end drops accordingly and ice melts and flows into the reservoir. The ice pressure at the cold end remains lower than the equilibrium value due to creep of the ice and water will freeze onto the ice to raise the pressure back to equilibrium and maintain the pressure difference between the warm and the cold ends of the sample. Mass flow therefore, will be in the opposite direction to heat flow.

A secondary thermal gradient would also be produced in the same direction of mass flow as a result of latent heat released at the cold end and absorption at the warm end. This secondary gradient would cause some reduction in the size of the primary gradient and conductive heat flow. The amount of latent heat released or absorbed plays a part in

FIGURE 3.5. Relationship between water flow rates and difference in warm end and cold end ice pressure. Cold end flow refers to inflow at cold end and warm end flow refers to outflow at warm end.

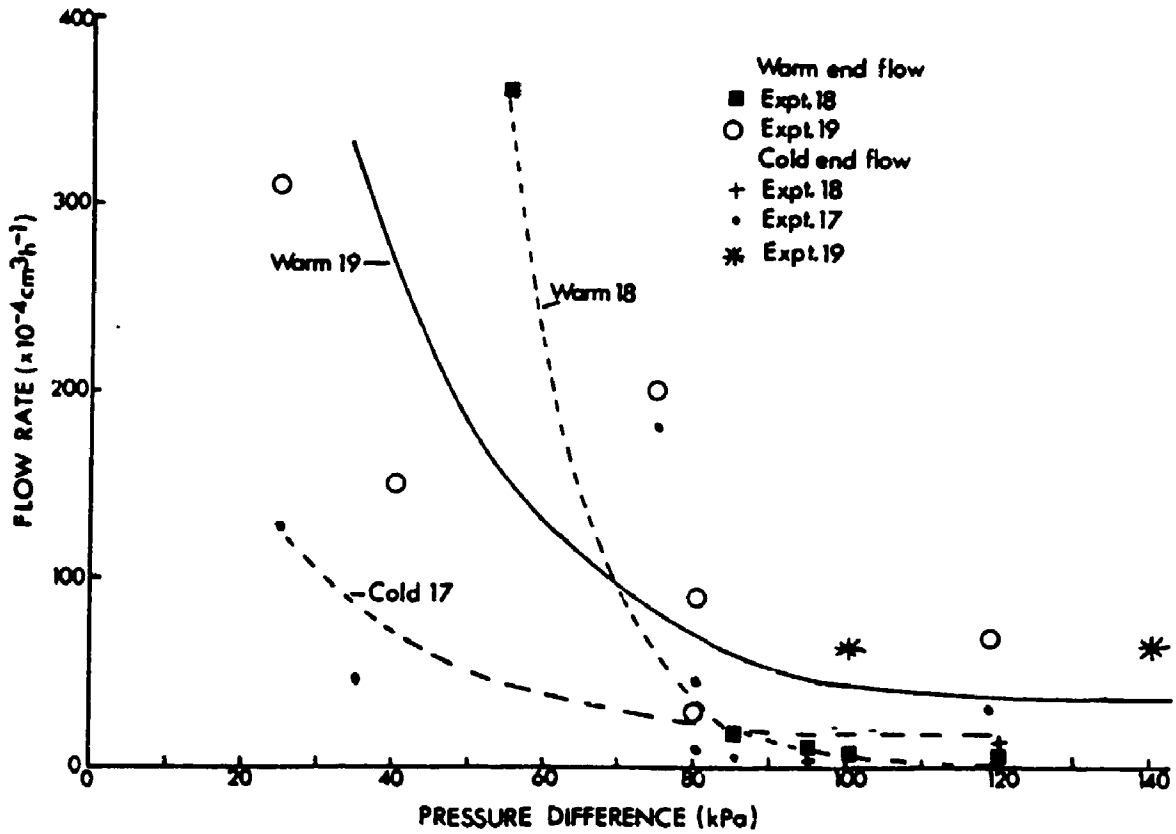

the maintenance of equilibrium at the cold and warm ends of the ice. Latent heat is absorbed as melting occurs at the warm end and would cause cooling. The temperature would approach the new, lower equilibrium temperature and reduce the amount of melting necessary to establish equilibrium. When freezing occurs at the cold end, latent heat will be released and result in an increase in temperature toward the new equilibrium value and a lower equilibrium ice pressure. A reduced rate of freezing is required therefore, to establish equilibrium at the cold end.

The Clausius-Clapeyron equation predicts a pressure gradient across the ice and the experimental results support this but the gradient may not necessarily be linear. The size of the pressure gradient also changes through time and uniform pressures may also be observed. This suggests that thermodynamic considerations alone cannot explain the experimental results. The rheological properties of the ice must also be considered.

Following Wood (1985, 1990), it is useful to consider the stress distribution in an ideal rigid solid and a viscous fluid. A rigid solid is able to sustain a stress gradient when a stress is applied to one end. If a stress is suddenly applied to one end of such a material, a linear distribution of stress should be observed (figure 3.6). Such a material would have a high resistance to deformation and would tend to move as a plug. A viscous fluid deforms

FIGURE 3.6. Stress distribution in an ideal rigid solid and viscous fluid (from Wood 1985).

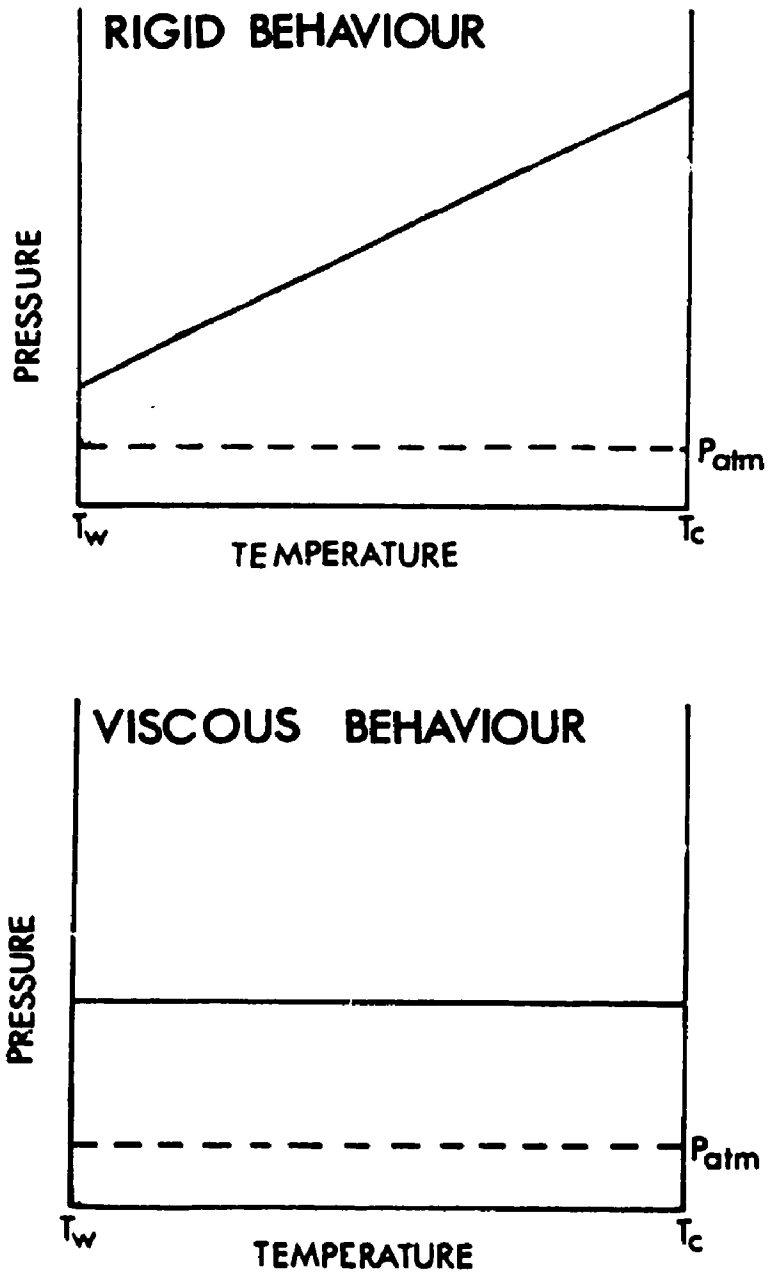

when any magnitude of stress is applied and it is unable to sustain a stress gradient. A uniform distribution of stress would be expected in a viscous fluid when a stress is applied.

Pressure gradients were observed in some of the experiments suggesting rigid behaviour, while in others pressures were uniform, indicating viscous behaviour. Pressure gradients were also found to decrease over time, suggesting a transition between rigid and viscous behaviour. The results show that at temperatures close to the melting point, ice exhibits the characteristics of a rigid solid or a viscous fluid and that over time there is a transition from rigid to viscous behaviour as reorganisation of the crystal structure occurs. Ice may exhibit plug displacement initially when stress is applied and over time begin to flow or creep as a viscous fluid would.

The relationship between pressure gradient and water flow (figure 3.5) also suggests that the type of rheological behaviour exhibited by the ice varies through time and between ice samples due to variations in grain size and crystal orientation. Lower water flow was observed when measured pressure gradients were high. This indicates that when a large ice pressure gradient exists, less deformation occurs. Higher water flows occurred when pressure gradients were small or when ice pressure was uniform, indicating greater deformation of the ice body. In other words greater

deformation (creep) occurs when ice behaves like a viscous fluid, than a rigid body. The amount of deformation (water flow) is also related to ice temperature. Less deformation occurs at lower temperatures because the resistance to deformation is greater.

3.7 Thermodynamic-Rheological Link

A generalized flow law for steady state creep at temperatures close to the melting point (as was presented in chapter 2) may be written as:

$$\dot{\epsilon} = \frac{A_o Dbo}{kT} \qquad (3.2)$$

σ = shear stress

$\dot{\epsilon}$ = strain rate

T = absolute temperature

$A_o = A\ (b/d)^m$

A = constant

d = grain size

m = constant

D = diffusion constant

b = Burger's vector

k = Boltzmann's constant

This equation expresses the strain rate in terms of an applied stress and the rheological behaviour of the ice. In the case of the ice sandwich experiment a stress (pressure) developed at the cold end of the sample when the temperature there was lowered. The response to this stress is

deformation or creep of the ice and an inflow of water at the cold end and outflow at the warm end (regelation). The observed water flow therefore represents deformation or strain. The water flow rate or strain rate therefore, will be a function of the rheological properties as well as the thermodynamic characteristics of the system.

Ice pressures are related to the thermal conditions (temperature) of the ice body by the Clausius-Clapeyron equation. Strain or flow rate is related to stress (ice pressure) by the creep equation. Wood (1990) suggests that the transport coefficient for regelation (see equation 3.1) can be expressed as a function of the rheological properties of the ice. This suggests that the thermodynamic (equation 2.2) and creep equations (equation 3.2) can be combined and that the strain rate may be expressed in terms of the thermodynamic conditions:

$$\dot{\epsilon} = \frac{A_o Db}{kT} \frac{L(T-T_o)}{V_w T_o} \qquad (3.3)$$

It should be noted that equation 3.3 is a simplification and requires some adaptation to be used for practical problems. In the case of the ice sandwich the water pressure is assumed to be atmospheric and the temperature (T) in equation 3.3 refers to the temperature at the cold end of the ice body.

CHAPTER FOUR

FROST HEAVE AND CREEP IN CAEN SILT

4.1 Introduction

The frost pressure cell was used by Wood (1985) to observe ice pressures in Caen silt and Snec sand. Lundin (1989) conducted similar experiments using sand and manipulated the temperatures at the sample ends to study the time response of the system. The temperature at one end of the sample in these experiments was always kept below 0°C. Lundin (1989) and Wood (1985) found that the Clausius-Clapeyron equation (thermodynamic conditions) alone could not fully explain the results and suggested that the rheologic properties of the frozen material are important in determining the pressures which develop.

The experiments that will be described here are similar to those carried out by Wood (1985) and Lundin (1989). Caen silt was used and the temperature was manipulated at the colder end of the sample to produce short freeze-thaw cycles. An attempt was then made to relate the observed pressures to the thermodynamic and rheologic conditions.

4.2 Method

The frost pressure cell (described by Wood 1985) used for the ice sandwich experiments was used in these experiments (figure 3.1). A lactose solution was placed in the reservoir at the cold end in these experiments to avoid

freezing of water in the reservoir.

Caen silt was saturated with distilled water and placed in a vacuum chamber for 20 to 30 minutes to remove air from the soil pores. The vacuum was broken periodically to release entrapped air. The moist soil was placed in the partially assembled cell which had a semipermeable membrane on the bottom. After the soil was placed in the cell, it was left for 24 hours to consolidate under its own weight. Excess water on the top of the sample was removed using a syringe and additional soil was added until the cell was full. A semipermeable membrane was placed on top of the soil and the cooling plate was fastened on. Both reservoirs were filled with de-aired, distilled water. The cell was wrapped in foam insulation and placed in an incubator set at 0°C.

The temperature of both cooling plates was set to 0.1°C and the sample was allowed to equilibrate for 24 hours. The temperature at one end of sample (cold end) was then lowered to approximately -1.0°C and the cell was given a sharp blow to initiate nucleation. The temperature at the cold end of the soil increased and there was a rapid outflow of water from the warm end as freezing occurred. After nucleation was initiated the temperature at the cold end was increased quickly to -0.5°C. The lactose solution was not added to the reservoir at the cold end until approximately 24 hours after freezing was initiated. This was done to prevent

lactose from moving into the unfrozen soil at the cold end. Lactose molecules diffuse slowly through the membrane and cause some melting of the soil at the cold end of the sample. An exact concentration of lactose was used to prevent freezing in the reservoir and lower the chemical potential of water in the reservoir and eliminate osmotic gradients between the reservoir and the soil (see Wood 1985). The lactose concentration required had a freezing point depression that was equal to the temperature at the cold end (-0.5°C).

Three experiments, 16 to 36 days in duration were conducted. Once or twice during the experiment the temperature at the cold end was increased from -0.5°C to between 0.03 and 0.13°C for a period of 1 to 2 hours. The temperature was then lowered slowly to -0.5°C, 1 to 4 hours later. During the experiments, water flow into and out of the sample and pressure within the sample were monitored as they were in the ice sandwich experiment. At the end of the experiment the position and thickness of ice lenses were recorded and the moisture content of the sample was determined.

4.3 Results

4.3.1 *General observations*

Water was expelled from the warm end of the sample when nucleation was initiated (figure 4.1). Inflow of water at the warm end began approximately 24 hours after freezing was

FIGURE 4.1. Cumulative water flow and pressure over time during Caen silt experiment 21. Positive slope for water flow indicates an outflow of water from the sample and a negative slope indicates an inflow of water to the sample. The cold end temperature was initially -0.5°C. The cold end temperature was increased to 0.13°C on day 17 for a period of 20 minutes, the temperature was then lowered to -0.5°C. During day 25 the cold end temperature was increased to .04°C for a period of 75 minutes and then lowered to -0.5°C. The warm end temperature during the experiment was 0.1°C.

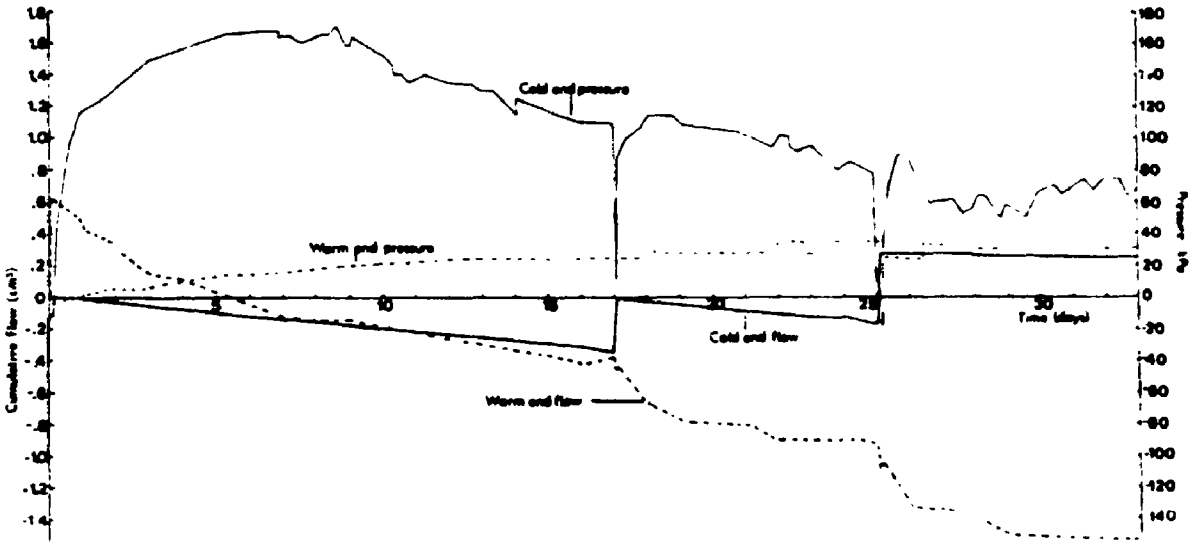

initiated and the rate of water flow into the warm end decreased with time. Water generally flowed into the cold end of the sample also.

The pressure at the cold end increased sharply 1 to 3 hours after the temperature at the cold end was lowered. After approximately 24 hours, the pressure at the cold end increased at a decreasing rate until it reached a maximum value (approximately 170 kPa). The pressure at the cold end then slowly declined after reaching the peak. The pressure at the warm end increased slowly and then levelled off at approximately 30 kPa.

4.3.2 *Observations during temperature change*

a. *pressure*

The temperature at the cold end was increased to a temperature above 0°C during the experiment for various lengths of time (figures 4.1, 4.2 and 4.3). Detailed diagrams showing soil temperature, water flow and pressure during the period of temperature change can be found in Appendix 2. The initial response of the pressure at the cold end to the temperature increase was a sharp drop in pressure. After the initial pressure drop, the pressure declined at a decreasing rate. Similar observations were made by Wood (1985) but the temperature remained below 0°C at the cold end and the pressure drop observed was smaller than that in the present experiments. The pressure at the cold end continued to decrease for a short time after the

FIGURE 4.2. Cumulative water flow and pressure over time during Caen silt experiment 20. Positive slope for water flow indicates an outflow of water from the sample and a negative slope indicates an inflow of water to the sample. The cold end temperature was initially -0.5°C. The cold end temperature was increased to .08°C on day 11 for a period of 40 minutes, the temperature was then lowered to -0.5°C. The warm end temperature during the experiment was 0.1°C.

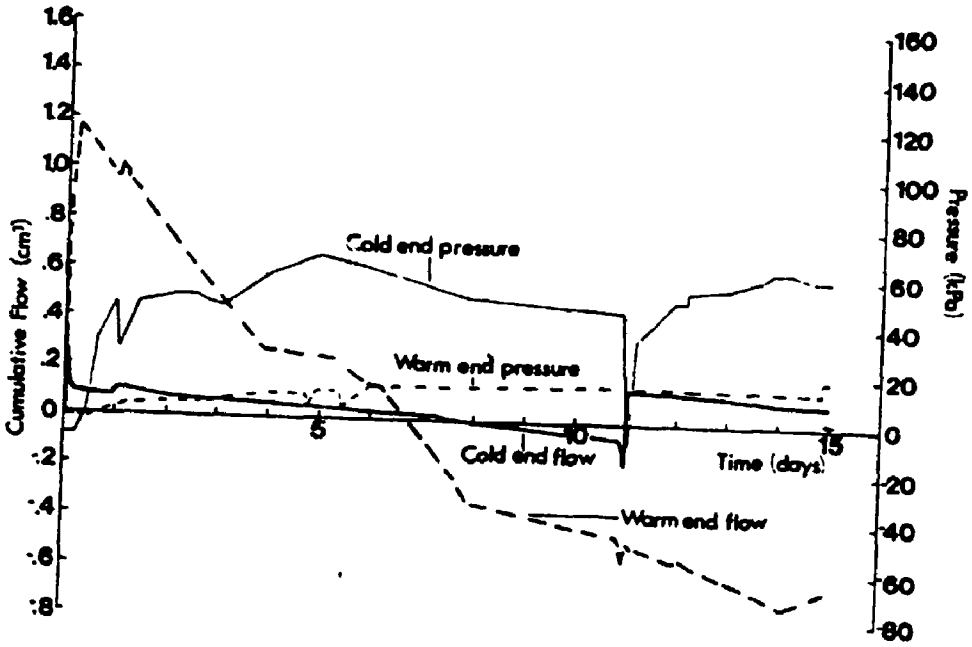

FIGURE 4.3. Cumulative water flow and pressure over time during Caen silt experiment 22. Positive slope for water flow indicates an outflow of water from the sample and a negative slope indicates an inflow of water to the sample. The warm end and cold end temperatures were initially 0.1°C and -0.5°C respectively. A power failure during the tenth day of the experiment resulted in both the warm and cold end temperature increasing. The warm and cold end temperatures were set to the initial values following the power failure. The cold end temperature was increased to 0.03°C on day 21 for a period of 1 hour, the temperature was then lowered to -0.5°C. On day 28 the cold end temperature was increased to 0.06°C for 110 minutes, the temperature was then lowered to -0.5°C.

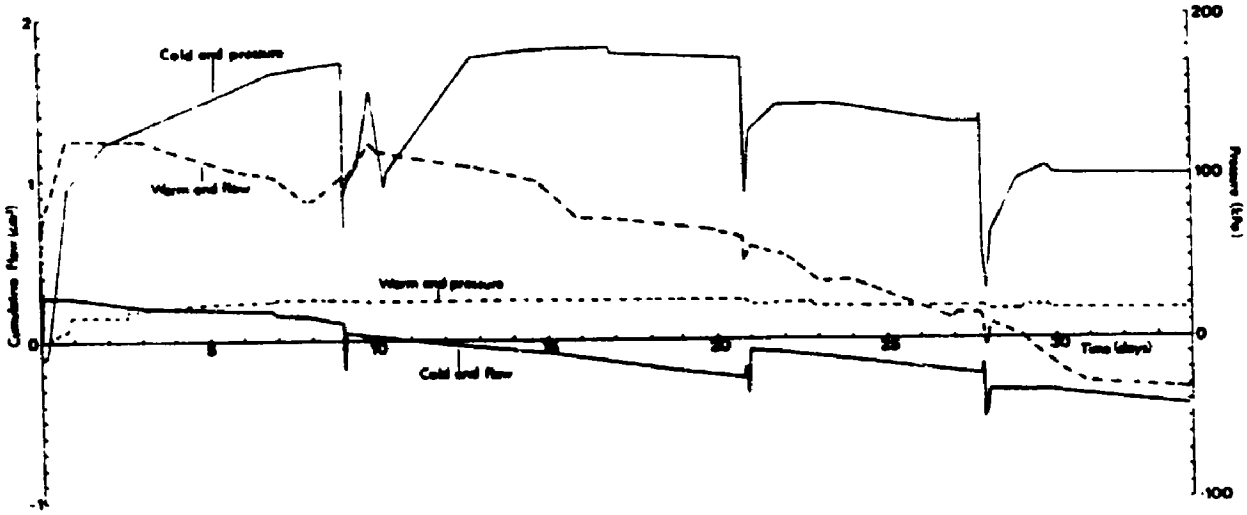

temperature at the cold end was lowered and then increased and reached a maximum approximately 25 to 36 hours later. This peak pressure was generally lower than that reached earlier in the experiment. The pressure at the warm end displayed little change during this time.

b. *water flow*

Water continued to flow into the warm end of the sample when the temperature was raised but at a higher rate. Wood (1985) also observed an increase in the rate of inflow at the warm end in one of his experiments when the temperature at the cold end was raised. The temperature at the cold end in his experiments however, remained below 0°C. Wood (1985) also observed an outflow of water at the warm end in one of his experiments but could offer no explanation for this.

The flow at the cold end followed a similar pattern as that at the warm end in experiments 20 and 22 (figures 4.2 and 4.3). Flow at the cold end followed a different pattern in experiment 21 however. Outflow occurred in experiment 21 after the temperature of the cold end was raised and outflow continued for a short time after the temperature was lowered again (figure 4.1).

c. *observations during abrupt change in temperature (experiment 22)*

A power failure during experiment 22 resulted in an increase in temperature at both ends of the sample for a period of 45 minutes. The maximum temperature reached at

the warm and cold ends could not be determined but the temperatures immediately after power was restored were 0.15°C and -0.15°C respectively. Soil temperatures during the power failure increased by 0.31°C at the cold end of the sample, 0.19°C in the middle and 0.16°C at the warm end. Some melting occurred, especially at the warm end of the sample.

The pressure at the cold end was much lower when power was restored then it had been before the power failure (figure 4.3). The total drop in the pressure at the cold end was approximately 100 kPa. The pressure at the cold end started to increase approximately 15 minutes after the temperature at the cold and warm ends was lowered and continued to rise over the next 17 hours to a maximum of 155 kPa. The temperature at the cold end was adjusted (raised to -0.5°C from -0.53°C) and pressure fell over the next 11 hours to a minimum of 95 kPa and then increased to approximately 180 kPa over the next 10 hours. The peak pressure at the cold end following the power failure was slightly higher (by 8 kPa) than the pressure immediately before the power failure. The pressure at the cold end remained constant over the next 9 hours and then declined slowly to 173 kPa over the next 95 hours. The pressure at the warm end remained almost constant during the power failure.

The water inflow rate at the cold end of the sample

increased as temperature increased at the cold end. Water outflow at the cold end occurred immediately after the temperature at the cold end was lowered and then slowly flowed into the soil again.

Outflow of water from the warm end had been occurring for 24 hours before the temperature increase. Inflow occurred immediately following the temperature change at the warm end. Water was expelled rapidly from the warm end after the temperature of the sample ends was lowered. Outflow continued over the next 15 hours and then inflow commenced.

4.3.3 *Moisture content and observations of ice lenses*

The gravimetric moisture contents at the end of each experiment are tabulated in table 4.1. The moisture content in the warmer unfrozen soil was found to be lower than that of the colder frozen soil.

Visible ice lenses were observed approximately 1.2 cm from the cold end of the sample in a band approximately 0.8 cm thick. Ice lenses were thicker and farther apart at the warmer end where they were 0.075 to 0.09 cm thick and 0.2 cm apart. Ice lenses appeared to be curved and vertical cracks were also observed. The pressure transducer at the cold end was found to be within the zone of visible ice lenses, while the transducer at the warm end was not.

TABLE 4.1. Gravimetric moisture contents at the end of experiments.

Experiment	Moisture Content (% dry wt)	
20	34.3	
21	25.3	warm end
	37.8	cold end
	32.6	average for sample
22	36.8	

4.4 Discussion

4.4.1 *General pressure patterns and water flow*

The general pattern of pressure and water flow is similar to that observed by Wood (1985). The pressure at the cold end increases as water migrates to the colder part of the soil, freezes and accumulates as ice lenses. The maximum pressure reached is less than that predicted by the Clausius-Clapeyron equation and is apparently controlled by the creep properties of the frozen soil. As the ice pressure builds in the frozen soil it will deform and stress relaxation will occur. This prevents pressure from building to higher levels and allows ice lenses to continue to grow in the soil. The pressures observed at the warm end of the sample are lower than those observed by Wood (1985). The pressure transducer at the warm end was found to be located outside the frozen zone in the present experiments while in Wood's experiments the warm transducer was usually at the frost line. The pressure at the warm end does not rise to approximately 100 kPa and decrease to 30 kPa as Wood found but remains almost constant at 20 to 30 kPa. The unfrozen soil surrounding the pressure transducer does not offer much resistance to deformation and stresses transmitted to this zone are dissipated through deformation of the unfrozen soil.

Larger scale laboratory frost heave experiments were carried out with Manchester silt in a column 20 cm in

diameter and 90 cm high by Smith and Onysko (1990). A cooling plate was placed on top of the sample but the sample was able to move upwards. A rapid rise in pressure (figure 4.4) was observed with the passage of the freezing front at each pressure transducer as ice lenses formed in the soil. The pressures which developed are similar to those observed in the present experiments but soil temperatures were lower. Smith and Onysko (1990) explained their results in terms of the creep properties and thermodynamic conditions of the soil. As internal pressure developed, deformation of the soil matrix or creep was induced. As stress relaxation occurs, the ice pressure drops causing a disequilibrium in the thermodynamic conditions. Some water will freeze in order to restore equilibrium and ice pressure will increase inducing more stress in the soil. This process will continue contingent on a supply of water to the growing ice lens and the necessary release of latent heat during freezing to offset the cooling of the soil. As the soil continues to cool, the hydraulic conductivity decreases and the rate of water flow and ice accumulation will drop below that necessary to offset the stress relaxation due to creep. After reaching a peak therefore, pressure was found to gradually decline. The slow decline in ice pressure observed in the frost pressure cell may also be explained in terms of stress relaxation and creep. Even though the soil sample is confined, some deformation of the soil matrix

FIGURE 4.4. Temperature and pressure data for the soil column experiment of Smith and Onysko (1990).

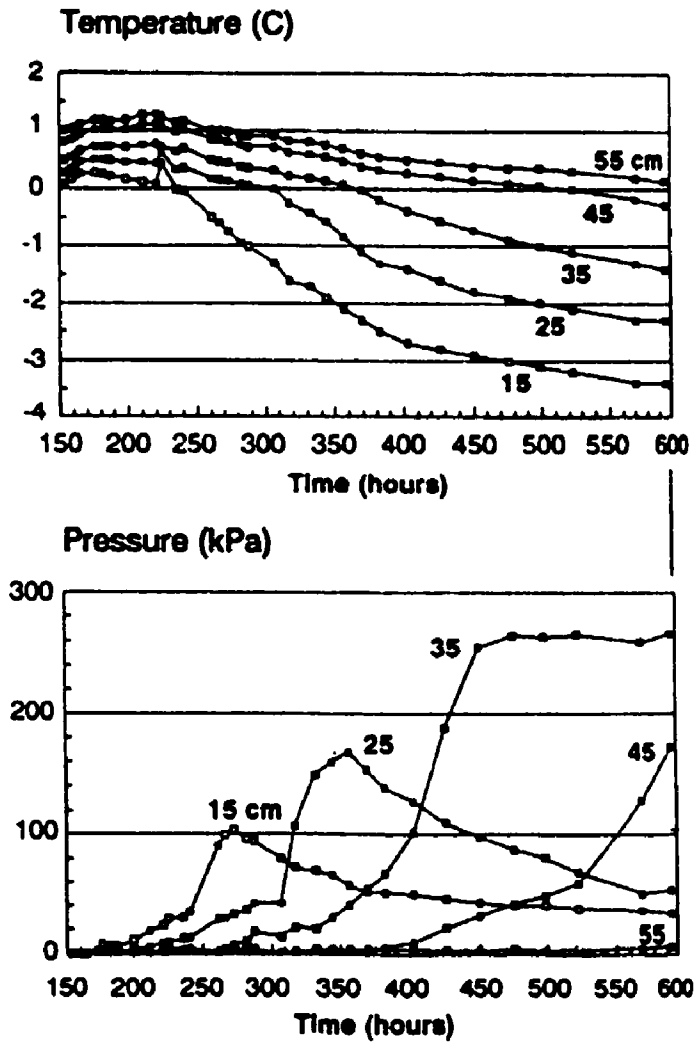

occurs slowly over time in response to stresses which develop within the soil.

Internal soil pressures have also been monitored as part of a field-scale experiment carried out at a controlled environment facility in Caen, France (Geotechnical Science Laboratories 1989). Caen silt was also used in these experiments. Pressures rise as the freezing front passes but they are not observed to relax after the peak pressure is reached (figure 4.5), but level off instead. The pressures are lower overall than those measured in the frost pressure cell and in the experiment of Smith and Onysko (1990), probably due to the fact that the soil is unconfined and is free to expand. Higher pressures were observed at a site adjacent to a sandy soil than at a site located 4 m from the sand-silt boundary. The soil located some distance from the sand would encounter less resistance to heave than the soil near the non frost heaving sand. These observations support the idea that higher pressures develop when the resistance to heave is greater.

Water flow patterns are also similar to those observed by Wood (1985). Water is initially expelled from the sample at the warm end as pore water in the soil freezes and expands and then inflow occurs in response to the suction gradient. Inflow is rapid at first as the soil has a higher hydraulic conductivity earlier in the experiment than it does later when the temperature is lower. Suction gradients

FIGURE 4.5. Temperature and pressure data for the Caen experiment in Caen silt (a) next to the sand-silt boundary and (b) 4 m from the sand-silt boundary (Geotechnical Science Laboratories 1989).

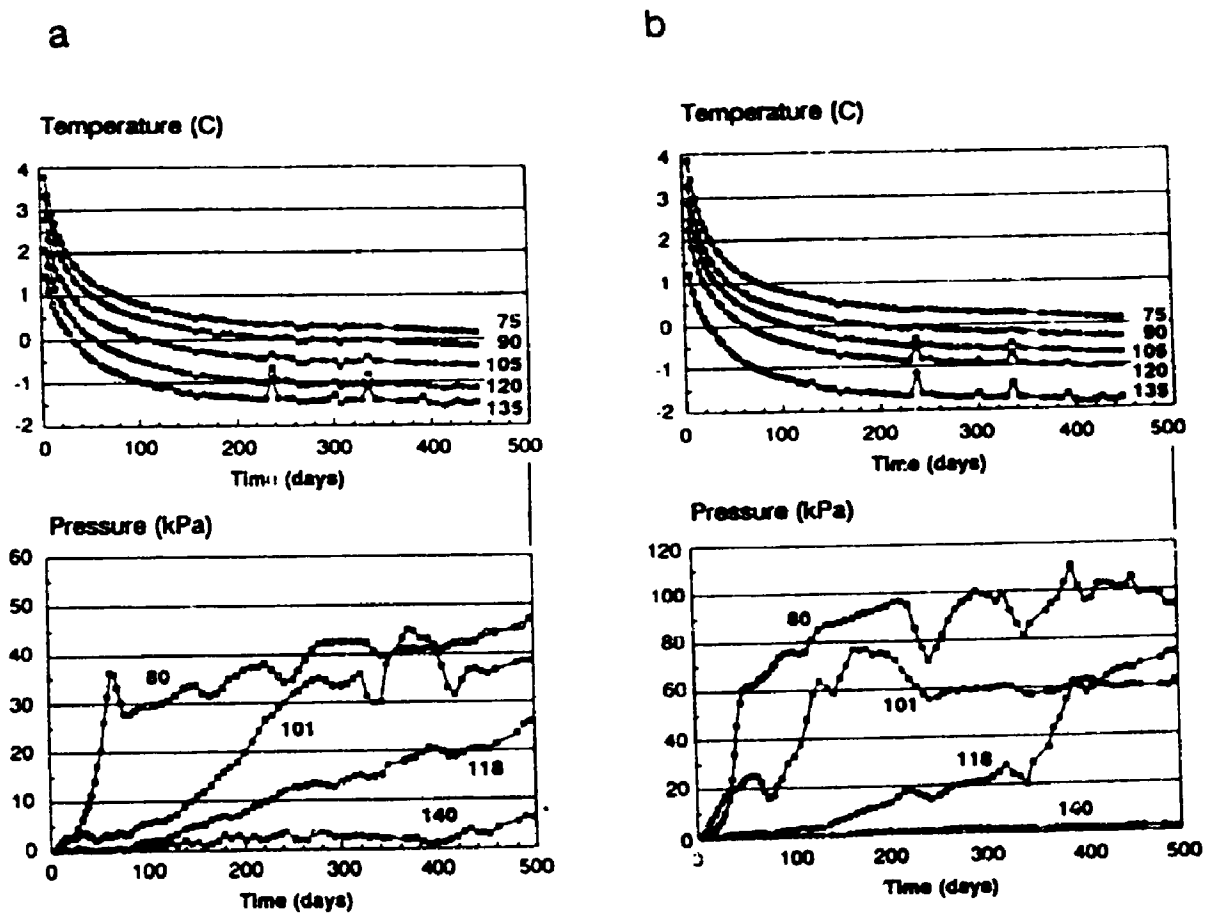

are larger and the resistance to deformation is lower in this part of the experiment than later and a large amount of ice accumulation can take place during this time. As temperature decreases the hydraulic conductivity of the soil decreases, the rate of water migration declines, the soil becomes more resistant to deformation and ice accumulates at a lower rate.

4.4.2 *Pressure and water flow during temperature change*

a. *water flow*

As temperature was increased at the cold end, some melting of ice occurred. Water flows into the soil at the cold end in response to the suction gradient that develops when the temperature gradient reverses and occupies the space previously occupied by ice. Water flows in at both ends of the sample toward the colder central portion of the soil. The flow rates are higher than those occurring before the temperature change because the hydraulic conductivity is greater at higher temperature. Lundin (1989) also observed a rapid inflow of water when temperature at the cold end was raised. As the temperature is lowered again water will freeze and expand, resulting in an expulsion of water from both ends of the sample. A greater amount of water is expelled from the cold end because there is a greater change in temperature at this end of the sample (eg. figure 4.2) and therefore more water freezing. Water inflow occurs at the warm end as the temperature and suction gradients are

established again.

There was an outflow of water at the cold end during experiment 22 following the temperature increase at the cold end. This may be the result of an osmotic gradient that develops between the soil and the reservoir when the temperature changes but this does not appear to occur in the other experiments. It is also possible that as ice melts at the cold end of the sample, some consolidation of the soil takes place as ice lenses continue to grow in the middle of the sample. This would result in some water being forced out of the soil. A sudden drop in ice pressure at the cold end may occur similar to that observed in the ice sandwich experiments as the temperature increases. Ice would flow or creep in the direction of lower ice pressure and melt and flow into the reservoir.

In the experiments done by Wood (1985) where the end temperatures remained constant there were inconsistencies in the direction of flow at the cold end. Wood (1985) suggests there should be no flow at all because the pressure of the unfrozen water is atmospheric. Small volume changes due to thawing at the cold end as minute quantities of lactose diffuse through the membrane would result in the inflow of water. The inflow of water observed was usually small (average inflow approximately 0.6 mm^3h^{-1} over the duration of the experiment) and it may be largely due to evaporation loss from the capillary tubes. Lundin (1989) found that

evaporation was generally in the range of 0.5 to 1.0 mm^3h^{-1} and evaporation rates during the present experiments were found to range between 0.2 and 0.3 mm^3h^{-1}. At low flow rates the error may be up to 100%. Wood (1985) also suggests that flows at the cold end may be the result of freezing or thawing of segregation ice near the cold end in response to minute deformations within the soil. In an experiment where Wood (1985) raised the temperature at the cold end, outflow was observed at the cold end before the temperature change and outflow continued after the temperature change. No explanation however, is offered for this.

b. *pressure*

As the temperature increases at the cold end, thermodynamic equilibrium is disturbed and pressure rapidly decreases at the cold end as soil temperature changes. The pressure decrease is more abrupt than the pressure increase during freezing. Wood (1985) suggests that this is the result of the irreversible nature of consolidation. Pressure builds up slowly during freezing because of gradual deformation (creep) and consolidation of the soil between ice lenses. When the temperature increases, the soil thaws but the pores in the soil between ice lenses do not expand to their original size and pressure falls rapidly. The resistance of the frozen soil to deformation also decreases as soil temperature increases. Water flows toward the central part of the sample in response to the suction

gradient and ice forms in this part of the soil. Growing ice lenses will meet less resistance and ice pressures will not build up. Thermodynamic disequilibrium occurs again when the temperature at the cold end is lowered and the pressure at the cold end increases. The resistance of the frozen soil to deformation also increases and ice pressure increases as the creep rate decreases. The maximum pressure reached after the temperature change is generally less than the peak pressure reached before the temperature change. Wood (1985) observed a decrease in the peak pressure at the cold end when the temperature gradient across the sample was reversed. Wood (1985) suggested that ice lenses did not form at the "new" cold end of the sample because significant quantities of water could not migrate from the "new" warm end of the sample through the central portion of the soil which remained frozen during the temperature change. In the present experiment, ice lenses may form slowly at the cold end of the sample when it refreezes as water migrates slowly through the central portion of the soil.

An increase in creep of the frozen soil would also explain a decrease in ice pressure (Lundin 1989). Over time the frozen soil will deform and this will result in stress relaxation. Ice pressures decrease gradually over time as the frozen soil deforms. The resistance of the frozen soil is less when the soil refreezes after the temperature change than it was before because deformation of the soil has

already taken place. As the soil froze initially, there was a rearrangement of the particles and consolidation of the soil. When the soil refreezes, this deformation does not have to occur for ice to accumulate again. Ice lenses would tend to grow where they had grown previously. Heave was found to be greater with each successive freeze cycle at the Caen experimental pipeline site (Geotechnical Science Laboratories 1989). The Caen results and the ones of the present experiment would suggest that the resistance of the frozen soil decreases with each freeze cycle and deformation that occurs during each freeze cycle is not reversible.

4.5 Links Between Ice Sandwich Experiments and Caen Silt Experiments

The layer of ice in the ice sandwich is analogous to an ice lens in frozen soil and the process occurring at the ice-water interfaces represent the processes occurring in the soil pores. Frozen soil therefore, can be thought of as consisting of many small ice sandwiches. The processes occurring in the ice sandwich experiments should also occur within a frozen soil.

Ice and frozen soil deform slowly or exhibit creep (see figures 2.4 and 2.5) when an external load is applied. The ice sandwich experiments show that creep may occur in response to a thermodynamically generated stress.

Stresses develop in a frozen soil at the ice-water interfaces as they do in the ice sandwich. Pore ice in the

soil should respond in a similar manner to an applied stress as the ice sandwich does. Pore ice would deform slowly and this would result in a deformation of the frozen soil matrix.

An ice lens will continue to grow if the release of latent heat during freezing is sufficient to offset the cooling of the soil. While this is dependent on the hydrologic conditions, creep of the frozen soil must occur if ice is to continue to accumulate and if latent heat is to be released at a sufficient rate. The rate of ice accumulation and the heave rate therefore depends on the creep rate of the frozen soil.

The ice pressures which develop in the ice sandwich experiments and the Caen silt experiments will be controlled by the creep properties (the factors influencing this were discussed in chapter 2) of the ice and the frozen soil as well as the thermodynamic conditions. The decrease in ice pressures that occurred over time in both the ice sandwich and the frozen soil illustrate the time-dependence of the rheological behaviour (creep properties) of ice and frozen soil.

The results of these experiments show that the thermodynamic and hydraulic models discussed earlier may not adequately describe the frost heave processes. The rigid ice model of O'Neill and Miller (1985) does consider the movement of ice and thermally induced regelation but they

assume that the ice does not deform and behaves as a rigid body. The rheologic properties of the frozen soil are not considered in their model. The results of the present experiments suggest that the rheologic properties of the frozen soil must also be considered. A model which links the thermodynamic and rheologic equations can be used to describe the pressures which develop within freezing soils. Models of this type could then be used to predict the rate of ice accumulation and the rate of heave.

CHAPTER FIVE

ICE LENS DISTRIBUTION AND ORIENTATION

5.1 Introduction

An important issue in frost heave studies is the distribution and orientation of ice lenses and the associated distribution and direction of stresses and displacements of soil. A study of ice lens distribution and orientation should provide information on the distribution of stress in the soil and the factors which control the frost heave process.

The distribution and orientation of ice lenses depend, quite generally, on the thermal regime of the soil because this determines where freezing will occur and to some extent, the rate of water migration within the freezing zone. The thickness and spacing of ice lenses are influenced by the cooling rate. It has also been suggested (Carlson and Nixon 1988, National Research Council 1984, Shumskii 1964 and Taber 1930) that the orientation of the ice lenses depends on the heat flow direction and that the ice lenses form perpendicular to the thermal gradient. Observations of ice lens distribution and orientation and of the thermal regime should provide information on the importance of the thermal conditions in the frost heave process.

The strength characteristics of the frozen material and

the pattern of stress in the ground, will also influence the location of ice lenses and their size. The nature of the deformation of freezing soil and the resulting displacements depend on shear stresses in a complex manner. The shear stresses are related in a complex manner to the forces generated by growing ice lenses. The orientation of ice lenses therefore may reflect the mechanical properties of the frozen material.

To obtain information on the factors which influence ice lens orientation and distribution, examinations were made of the ice in soil around a chilled buried pipe at a field scale at an experimental facility. This was achieved through a comparison of the ice lens patterns with the thermal regime and with the heave characteristics of the soil. Another goal of this work was to use the ice lens pattern to determine the direction of stress which develops during freezing of the soil.

5.2 Description of Experimental Facility

The study was part of a major experiment carried out at the Station de Gel at Caen, France. The Station consists of a refrigerated hall 18 m long, 8 m wide and 5 m high with a trough below of 1.7 m depth (figure 5.1). The base of the trough is defined by the bedrock and has been covered with sand to provide a level surface. An impermeable plastic membrane has been used to seal the base and boundary of the

FIGURE 5.1. Longitudinal section of trough (Geotechnical Science Laboratories 1988).

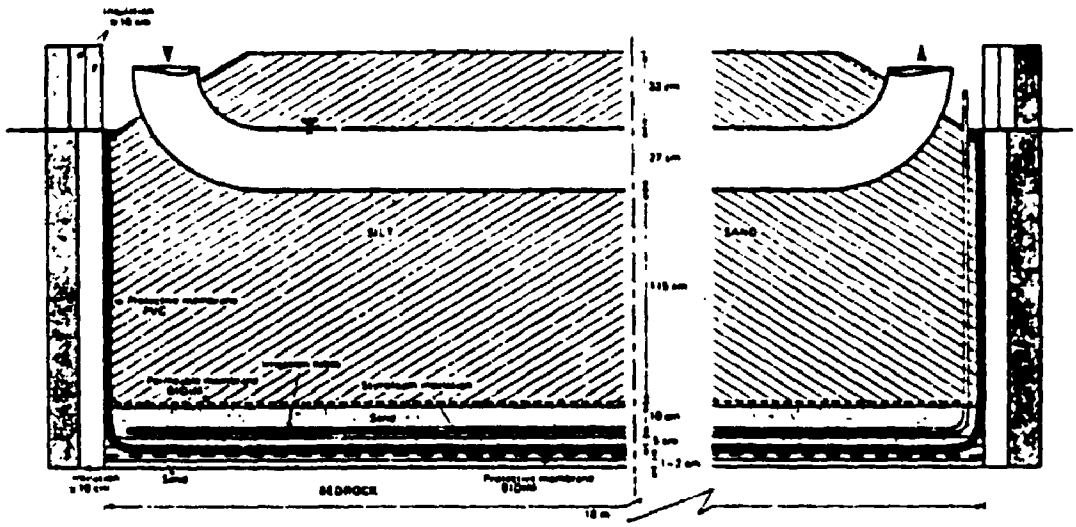

trough. Irrigation tubes placed on the base of the trough provide a supply of water. Non-frost susceptible Snec sand and frost susceptible Caen silt have been placed in each half of the trough. Table 5.1 summarizes the characteristics of the two soils. An 18 m long steel pipe, 273 mm in diameter was buried at a depth of 30 cm. The pipe is connected to a refrigeration system which circulates air of the desired temperature.

The thermal, hydrologic and heave characteristics are measured regularly. Soil and pipe temperatures are monitored with thermistors and thermocouples (figure 5.2). Heave of the soil was determined with magnetic heave devices (Mackay and Leslie 1987 and Smith and Patterson 1989) which allowed the measurement of differential heave in 10 cm layers of soil. Surface heave and pipe heave were determined by optical levelling. Time domain reflectometry probes were used to determine the distribution of water during freezing of the soil. Piezometers and boreholes allowed verification of the water table level during the course of the experiment. For a full description of the layout and all experiments being carried out, see Geotechnical Science Laboratories (1982, 1988 and 1989).

The water table was maintained at a depth of 90 cm below the ground surface, during the freezing of the ice lenses to be described. The freezing period lasted 468 days during which the air temperature was maintained at a nominal

TABLE 5.1. Characteristics of soils used in experiment (from Wood 1985).

	Caen Silt	Snec Sand
%Sand	4	94
%Silt	74	6
%Clay	22	0
Liquid limit (% dry wt)	28.5	--
Plastic limit (% dry wt)	21.0	--
Plasticity (% dry wt)	7.5	--
Mineralogy	Quartz with calcite and chlorite	Quartz with some calcite

2

FIGURE 5.2. Location of instrumentation and sampling sites.

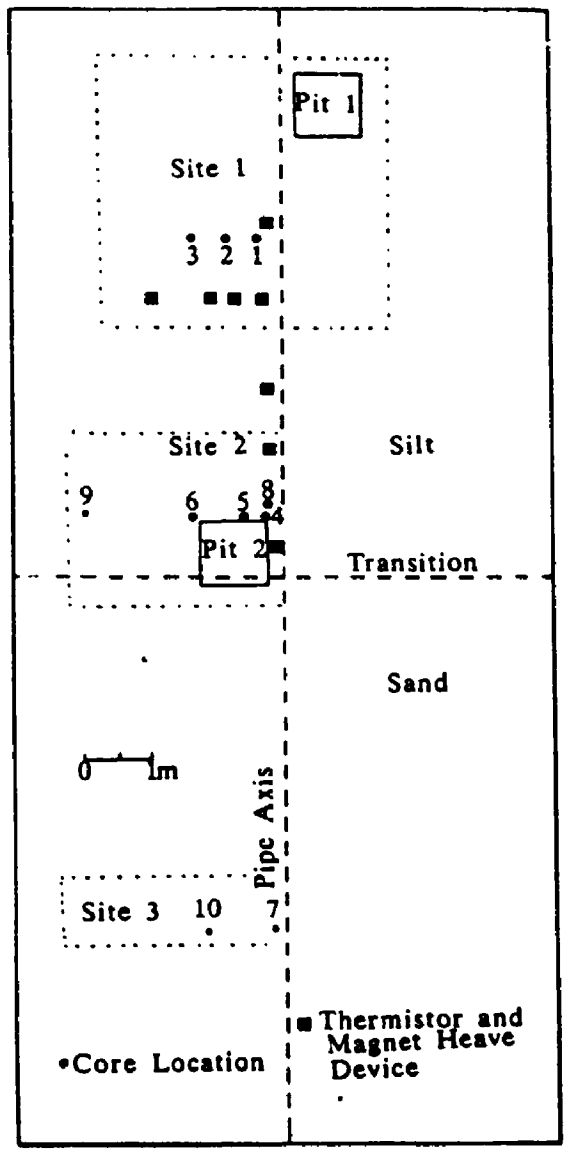

-0.75°C and the pipe temperature at -5.25°C. There were short-term fluctuations around these values.

5.3 Removal of Soil Cores and Pit Excavation

Cores of frozen soil, 10 cm in diameter were obtained to examine the distribution and orientation of ice lenses and to determine moisture content and bulk density. The silt was cored at three points (numbered 1, 2 and 3) at site 1 (figure 5.2) and at five points (numbered 4, 5, 6, 8 and 9) along a transect adjacent to the sand-silt transition (site 2). Two cores (numbered 7 and 10) were also removed from the sand at site 3 (figure 5.2).

Coring was performed with a Sedidrill 100 (Seditech S.A.) with a nitrogen cooled auger, developed by the Centre d'Experimentation Routiere from that described in Van Vliet-Lanoe et al. (1987). The nitrogen cooling system ensured that no melting of the soil occurred during drilling. Before coring, a small hole was drilled through the depth of the soil and a piece of dowelling inserted to act as a marker so that the orientation of the core in situ is subsequently known.

The cores were kept in a frozen state and cut in half lengthwise with a diamond saw along a surface perpendicular to the pipe. One half was used for ice lens observations and preservation and the other was used for moisture content determinations.

In addition to coring, two pits approximately 1 m^2 in

plan and 60 cm deep were excavated next to the pipe. Pit 1 was located in the silt at site 1 (figure 5.2) and pit 2 was at the sand-silt transition (site 2).

5.4 Procedure for Observing Ice Lenses

Frozen cores were cut in half to get a flat surface which was representative of a surface perpendicular to the pipe. The surface was then scraped with a knife to get a smooth surface and to make ice lenses visible. A similar procedure was also used to make ice lenses visible on the walls of the pit. Ice lenses were observed on the wall perpendicular to the pipe and on the wall parallel to the pipe approximately 1 m from the pipe.

The position and orientation of ice lenses in the cores and pits were mapped. The preferred orientation of lenses was determined by measuring the angle (to the nearest degree) that ice lenses dipped from the horizontal and the direction of dip. Ice lens thickness and the distance between lenses were measured and recorded. The number of lenses within a soil layer were counted when lenses were large. Other characteristic of ice lenses were also noted such as any curvature, their length and continuity. Maps showing the distribution and orientation of ice lenses were produced and all cores and pits were photographed.

5.5 Density and Moisture Content Measurement

Half of each frozen soil core was used to determine gravimetric and volumetric moisture content and dry bulk

density throughout the frozen soil profile. The frozen cores were cut into sections approximately 10 cm long where possible. The height and diameter of each half cylinder was measured to the nearest millimetre and the sample volume was calculated. The weight of the frozen sample was determined to the nearest 0.1 g. After placing the sample in a drying room for 48 hours, the dry weight of the sample was measured. The weight of water was calculated as the difference between the frozen and dry weights. Moisture content and density were computed as follows:

Gravimetric moisture content = (Water wt /dry wt)x100 (% dry wt)

Volumetric moisture content = (Vol water/Total vol)x100 (% vol)

Dry density (gcm^{-3}) = Dry wt (g)/Total vol (cm^3)

Note: Volume water = Water wt /Water density

Density of water = 1 gcm^{-3}

It was not possible to determine sample volume (and therefore density and volumetric moisture content) for the entire length of the cores because some sections were broken up. Gravimetric moisture content was however, determined for these samples.

5.6 Orientation of Ice Lenses Perpendicular to Pipe

5.6.1 *Site 1*

a. *cores at site 1*

Figure 5.3 shows the ice lens orientation for each core. The ice lens orientation has been interpolated

FIGURE 5.3. Ice lens pattern in the ground perpendicular to the pipe at site 1. The ice lens orientation has been interpolated between the core sites.

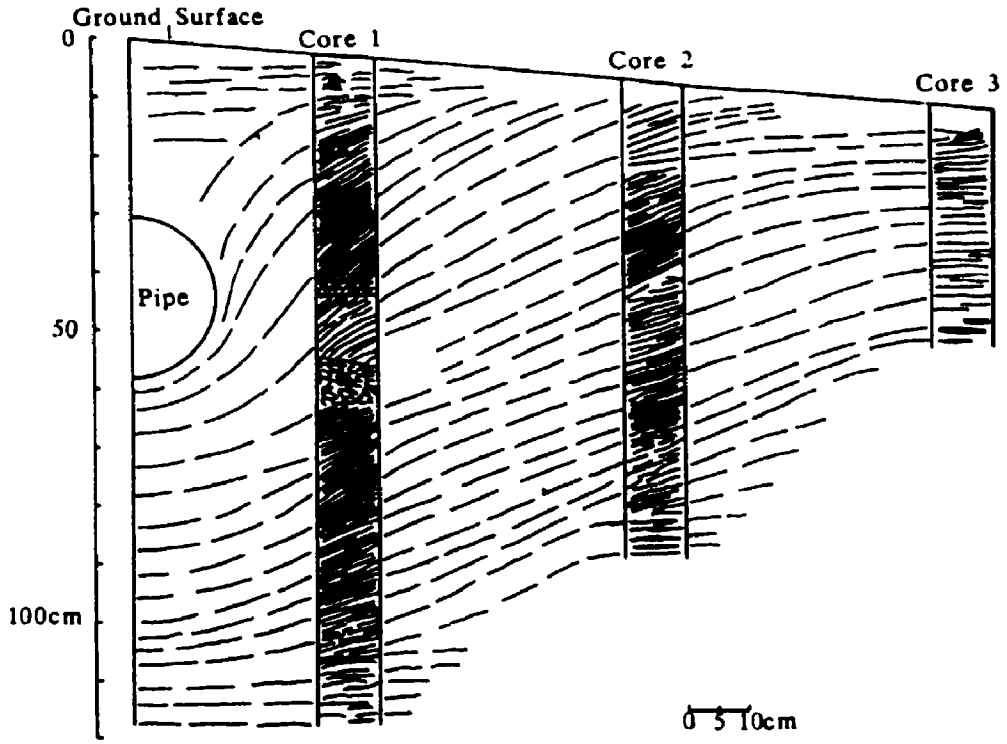

between the cores, between the pipe and core 1 and also for missing sections of the cores. Ice lens data from pit 1 was used to aid interpolation and extrapolation. A map showing the ice lens pattern in the ground perpendicular to the pipe was produced (figure 5.3).

Ice lenses are horizontal at distances greater than 1 m (core 3) from the pipe. As distance to the pipe decreases, ice lenses in the upper part of the ground dip in the direction of the pipe at an increasing angle. Ice lenses are horizontal at the bottom of the frozen zone. The depth of the last ice lens decreases with distance from the pipe. This reflects the change in the position of the freezing front with distance from the pipe.

Reticulate ice veins are found close to the pipe (core 1) at a depth of approximately 40 cm and 60 cm below the ground surface. Extrapolation of data next to the pipe suggests that ice lenses would be vertical next to the pipe but it is also possible that ice veins with no preferred orientation similar to those observed in core 1 would be present here also.

It is difficult to determine the orientation of ice lenses in the soil above the pipe. Data from core 1 and pit 1 suggest that ice lenses should be horizontal near the ground surface but it is not clear if the ice lenses remain horizontal or curve around the top of the pipe.

b. *pit 1*

The ice lens pattern for the wall perpendicular to the pipe in the pit at site 1 is shown in figure 5.4. The right side of the pit is approximately 30 cm from the pipe axis.

There are only a few ice lenses in the upper 10 cm of the ground, within 40 to 50 cm of the pipe and most of these are horizontal. Below this there is an abrupt change in ice lens orientation and ice lenses curve and dip toward the pipe. Generally, as distance from the pipe decreases, ice lenses in the upper 30 cm of the ground dip toward the pipe at an increasing angle, becoming almost vertical next to the pipe.

There is a distinct layer approximately 30 cm below the surface and 50 cm from the pipe. The upper boundary of this layer is marked by a horizontal straight lens extending to a distance of 78 cm from the pipe. This lens then gently dips away from the pipe at an angle which increases from 5° to 15°. This lens ends when it intersects another horizontal lens (which marks the bottom of the distinct layer) 106 cm from the pipe. This ice lens is conspicuous because it shows no irregular curvature along its length while those above and below it are curved. Within the distinct layer ice lenses dip toward the pipe at a distance of 86 to 106 cm from the pipe. Horizontal lenses and lenses which dip away from the pipe are also found in the distinct layer.

Ice lenses dip toward the pipe below the distinct

FIGURE 5.4. Ice lens orientation perpendicular to the pipe in pit 1. The pipe axis is approximately 30 cm from the right hand side of the pit.

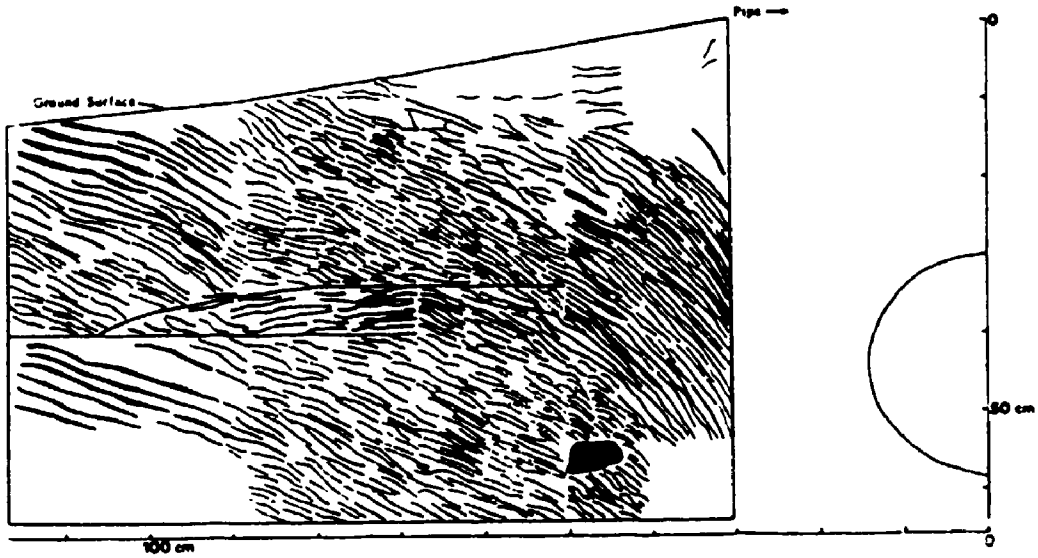

layer. Ice lenses dip gently at an angle of 10° to 20°, 1 m from the pipe. The dip becomes steeper closer to the pipe and was observed to be 50 to 60° at the right side of the pit.

5.6.2 *Site 2*

a. *cores at site 2*

The ice lens orientation at four points at site 2 (which is nearer to the transition) is shown in figure 5.5. The ice lens orientation has been interpolated between cores and for missing sections within cores (figure 5.5) and the ice lens pattern between core 8 and the pipe has been extrapolated. Data from pit 2 (discussed below) were used to aid interpolation and extrapolation. The general pattern of ice lenses is similar to that described for site 1 (figure 5.3).

The upper 30 cm of the ground next to the pipe (cores 4 and 8), contains curving ice lenses which dip toward the pipe at an angle which increases from 23° near the surface to 90° beside the pipe (30 cm below the surface). A large chert particle was found in this part of the ground and ice lenses curve around the top of it while lenses below it are horizontal. Reticulate ice veins are found in the frozen soil next to the pipe 30 to 65 cm below the ground surface. Horizontal ice lenses are found at the bottom of the frozen zone and near the ground surface at distances of greater than 1 m from the pipe (core 6).

FIGURE 5.5. Ice lens pattern in the ground perpendicular to the pipe at site 2. The ice lens orientation has been interpolated between core sites.

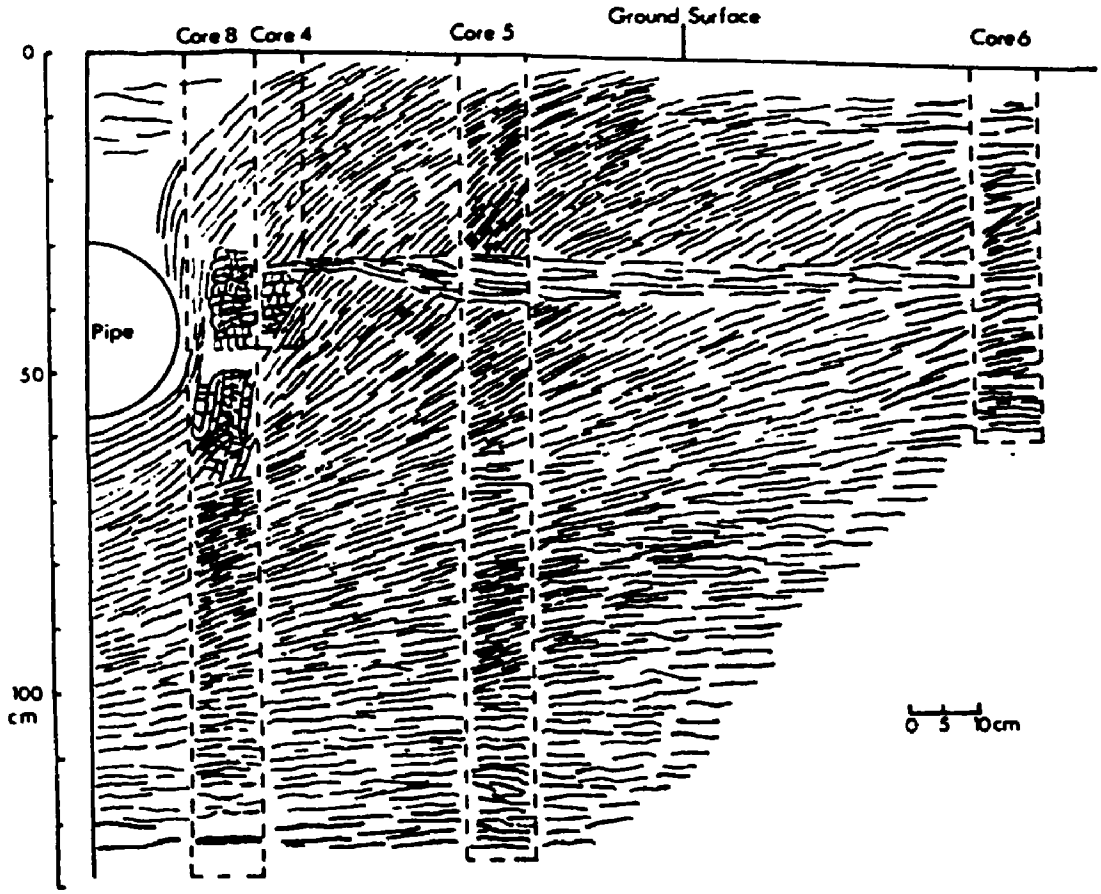

Approximately 35 cm below the surface, 60 cm from the pipe (core 5) ice lenses dip away from the pipe. Data from pit 1 indicate that there is a distinct layer here, in which the ice lenses dip gently away from the pipe (see figure 5.4).

b. *pit 2*

The ice lens pattern perpendicular to the pipe in the pit at site 2 is shown in figure 5.6. The right side of the pit is approximately 25 cm from the pipe axis.

Horizontal lenses are found in the upper 10 cm of the ground next to the pipe. There is an abrupt change in orientation below this as ice lenses dip steeply toward the pipe becoming almost vertical 20 cm below the surface. In the upper 25 cm of the ground, ice lenses are found to dip toward the pipe at an angle that decreases with increasing distance from the pipe. The general pattern in the upper part of the ground indicates that ice lenses generally curve around the pipe.

The ice lens pattern changes abruptly approximately 26 cm below the surface. A distinct layer is found here similar to that in pit 1. Ice lenses dip toward the pipe below the distinct layer at an angle that is less than that in the upper part of the ground.

5.7 Ice Lens Orientation Parallel to the Pipe

The ice lens pattern for the face parallel to the pipe at pit 1 is shown in figure 5.7. This face is approximately

FIGURE 5.6. Ice lens orientation perpendicular to the pipe at pit 2. The pipe axis is approximately 28 cm from the right hand side of the pit.

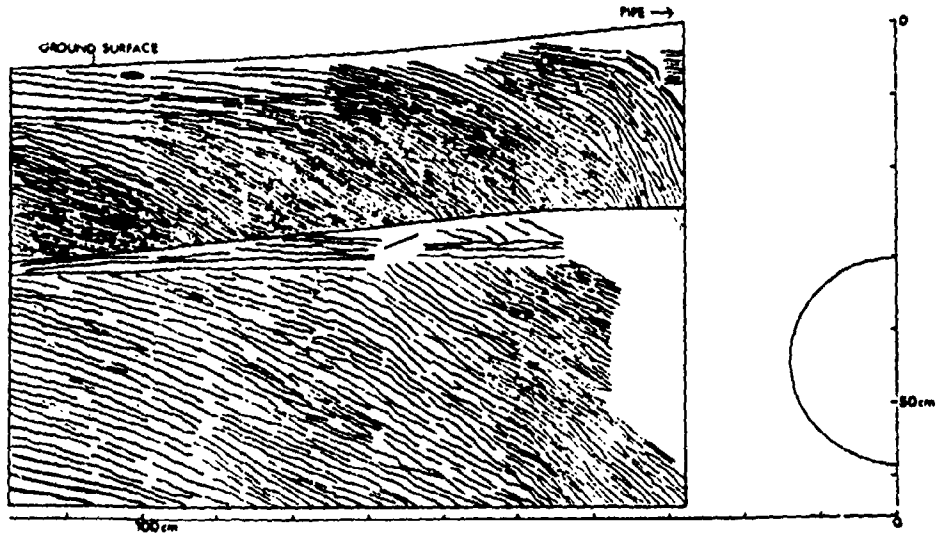

FIGURE 5.7. Ice lens orientation parallel to the pipe in pit 1. The pit wall is approximately 130 cm from the pipe axis. The right side of the pit is closer to the sand.

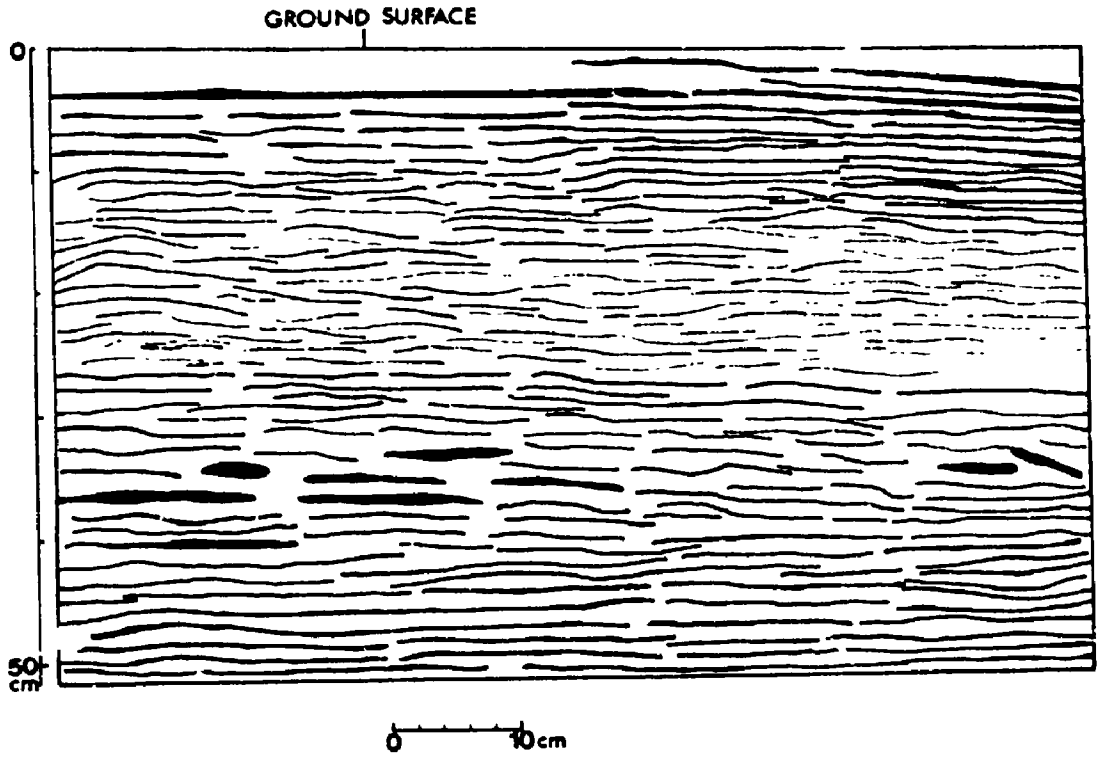

130 cm from the pipe axis. In the upper 35 cm of the ground, ice lenses dip slightly in the direction of the sand (approximately 5°). At greater depth the ice lenses are horizontal.

The ice lens pattern parallel to the pipe near the sand-silt transition (pit 2) is shown in figure 5.8. The pit wall is approximately 115 cm from the pipe axis. Ice lenses generally dip toward the sand at an angle that increases as distance from the sand decreases. The dip angle is less than 5°, 80 cm from the sand and is as high as 20° next to the sand. The ice lenses tend to follow the boundary between the silt and the sand.

A distinct layer was observed approximately 26 cm below the surface in pit 2. The top of this layer is marked by a straight horizontal lens which bends sharply to dip 10° in the direction of the sand, 50 cm from the sand. The lens then dips at an angle which decreases and becomes horizontal next to the sand. A thin layer of coarse material was found below this lens. Four lenses that dip 5° away from the sand and one lens which arches upward were found within the distinct layer. The bottom of this layer is marked by a continuous horizontal lens.

Ice lenses show sharp bending or deformation in a zone 35 to 40 cm from the sand. This bending is obvious below a depth of 30 cm. Ice lenses bend down toward the sand. On either side of this zone the deformation of ice lenses is

FIGURE 5.8. Ice lens orientation parallel to the pipe in pit 2. The pit wall is approximately 115 cm from the pipe axis.

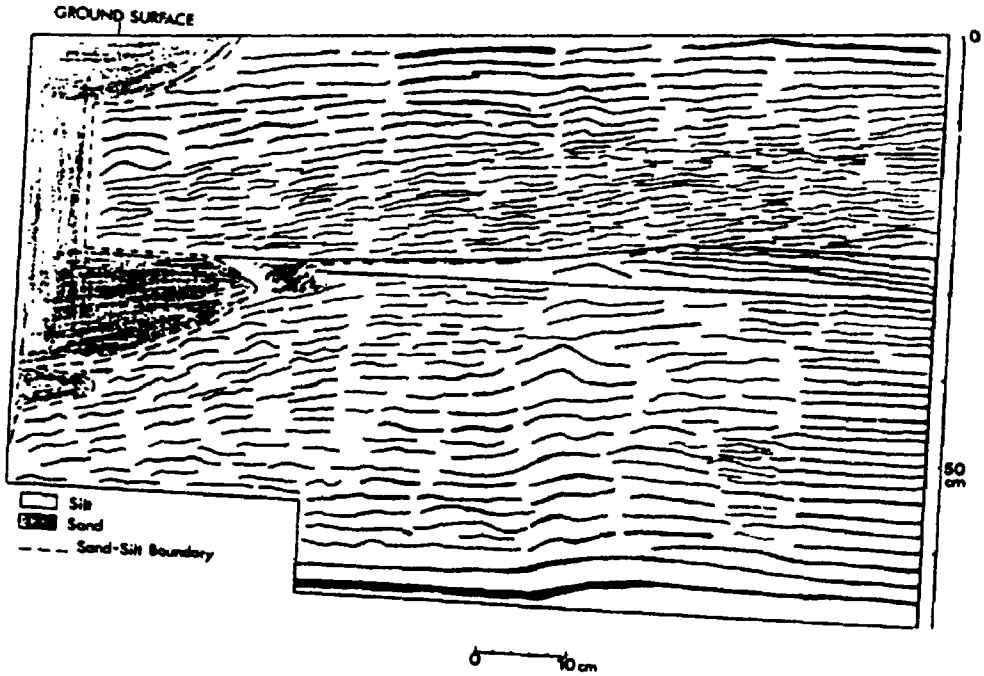

much less.

5.8 Comparison of Orientation of Lenses Sites 1 and 2

The same general pattern of ice lenses was observed perpendicular to the pipe at both sites. Ice lenses at site 2 appear to have a steeper dip in the upper part of the ground than those at site 1. Ice lenses at site 2 are also found at a greater depth than those at site 1.

The distinct layer present in the cores at site 2 and in both pits was not observed in the cores at site 1. The layer may also be present at that location but may have been between core locations or may have been missed due to gaps in the cores.

Ice lenses in pit 1 on the wall parallel to the pipe are almost horizontal or dip slightly toward the sand while in pit 2 the lenses dip at a greater angle especially closer to the sand. The ice lenses in pit 1 exhibit very little curvature or bending. There is sharp bending of ice lenses in pit 2 especially in a zone approximately 40 cm from the sand.

5.9 Ice Lens Thickness and Spacing

5.9.1 *Vertical variation*

a. *site 1*

Ice lenses are small (less than 1 mm thick) and closely spaced in the upper 70 cm of the ground, 35 cm from the pipe (core 1 in figure 5.9) Ice lens spacing and thickness increases with depth near the bottom of the frozen zone.

FIGURE 5.9. Vertical variation in ice lens thickness and spacing at site 1.

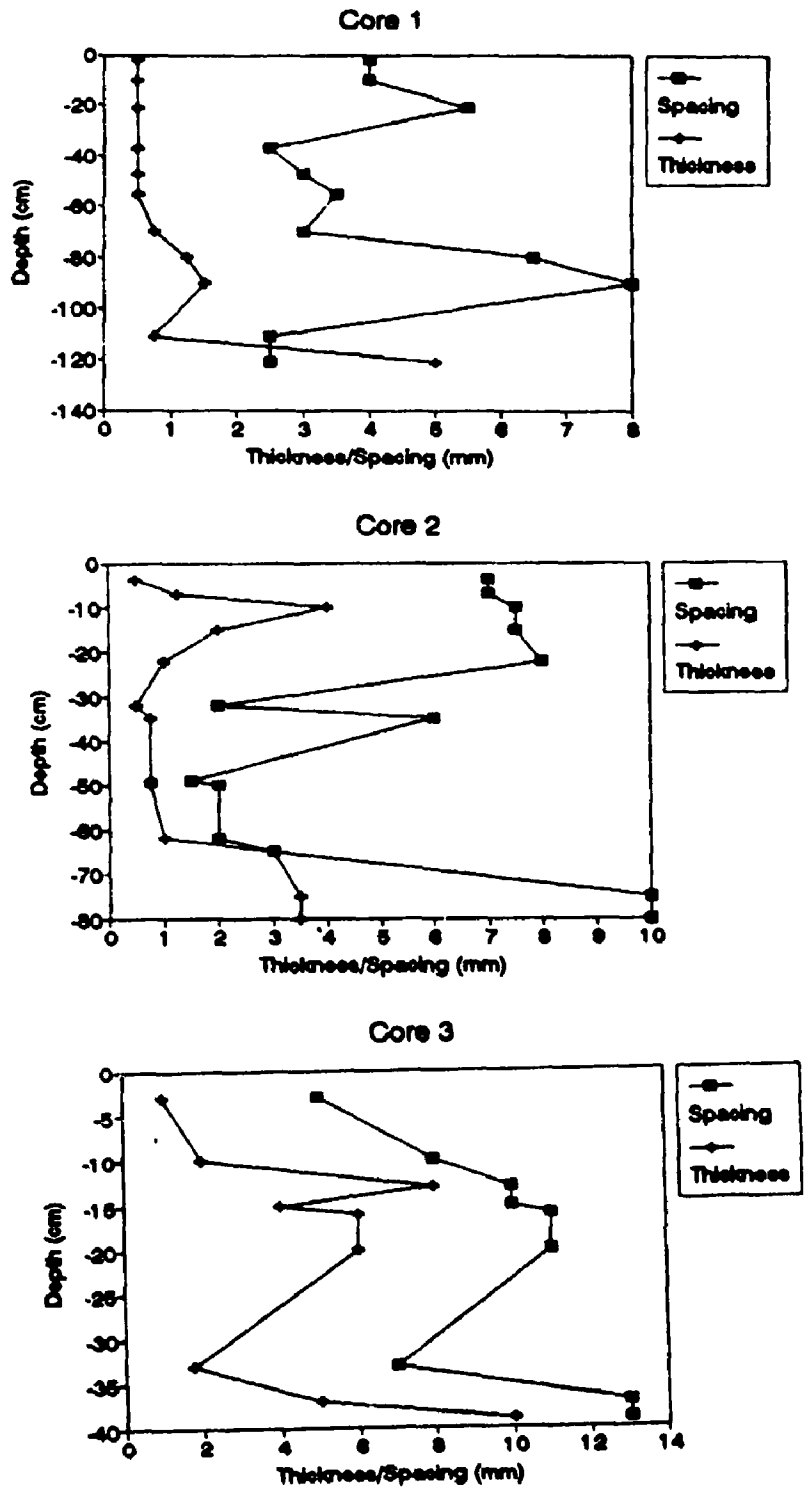

At core 2 (83 cm from the pipe), ice lenses approximately 4 mm thick are found in the upper 15 cm of the ground and at the bottom of the frozen zone (figure 5.9). Small (less than 1 mm thick) closely spaced ice lenses are found at pipe level (30 to 60 cm below the ground surface).

At 135 cm from the pipe (core 3), large ice lenses up to 8 mm thick are present in the upper 21 cm fo the ground (figure 5.9). There is a gap in the core between a depth of 21 and 33 cm and it is possible ice lenses become smaller here because smaller lenses are found at a depth of 35 cm. Ice lenses increase in size with depth in the lower part of the frozen soil where lenses may be up to 10 mm thick and 13 mm apart.

b. *site 2*

Ice lenses are generally small (less than 1 mm thick) and closely spaced next to the pipe (core 4 and 8 in figure 5.10) in the upper metre of frozen soil. A few larger lenses, 1 to 2 mm thick are present 75 to 100 cm below the surface. The soil at the bottom of the frozen zone contains larger lenses. There is a 40 mm section below a depth of 118 cm which contains no ice lenses and the last ice lens is 10 mm thick and is found 123 cm below the surface.

The average thickness of ice lenses at core 5 (58 cm from pipe) is approximately 1 mm (figure 5.10). Lenses 2 to 5 mm in thickness were scattered throughout the frozen soil.

Ice lens spacing and thickness decreases with depth

FIGURE 5.10. Vertical variation in ice lens thickness and spacing at site 2.

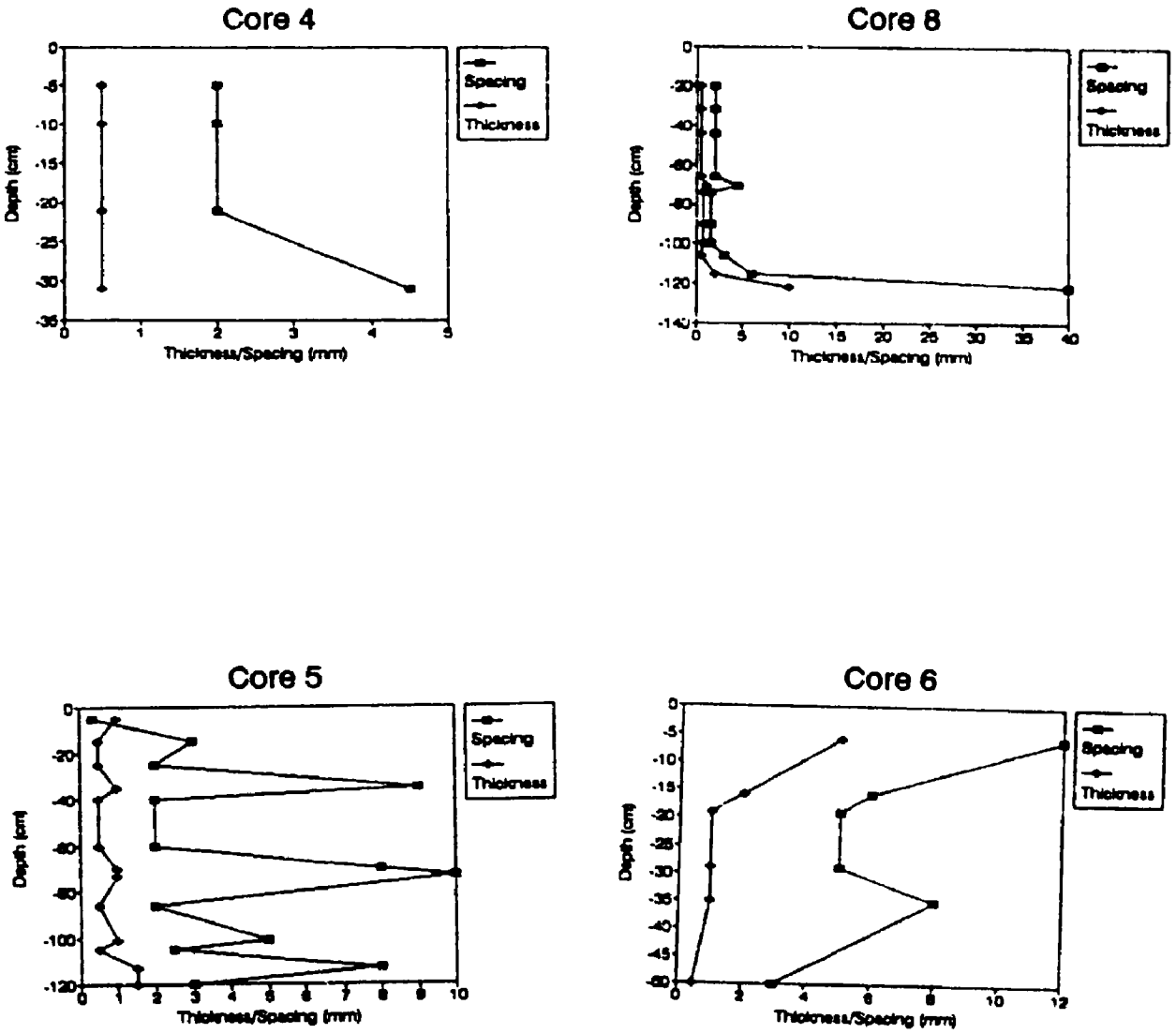

135 cm from the pipe (core 6 in figure 5.10). Most ice lenses in the lower part of the frozen zone are small but a few larger lenses (1 to 3 mm thick) are present.

5.9.2 *Variation in ice lens thickness perpendicular and parallel to the pipe*

The core data (figures 5.9 and 5.10) and the data from the pits (figures 5.4 and 5.6) indicate that for any given depth, ice lenses increase in size with distance from the pipe. Ice lenses appear to be larger at the top and bottom of the frozen zone than they are at a depth which corresponds to the pipe depth.

Ice lenses generally appear to be larger at site 1 than at site 2. This would suggest that ice lens thickness and the distance between them increases with distance from the sand.

5.10 Description of Thermal Regime

Isotherm maps of the ground temperatures (data provided by Geotechnical Science Laboratories 1989) perpendicular to the pipe at site 1 have been constructed for selected days of the freeze cycle (figures 5.11, 5.12 and 5.13). Isotherms were generally horizontal before the cooling cycle started and heat flow was directed upwards.

The 0°C isotherm propagated out from the pipe as the freezing cycle commenced. Further away from the pipe however, vertical heat flow is more important and the 0°C isotherm propagated downward from the surface. Over time, a

FIGURE 5.11. Ground temperature (°C) and soil layers exhibiting heave at site 1 on days 5, 19 and 61. Isotherm interval is .1°C for day 5 and .5°C for days 19 and 61. The dashed isotherm lines have been extrapolated beyond the data range. "New Heave" refers to the most recent layer to exhibit heave for the date shown. The layer exhibiting heave is defined by the magnet location.

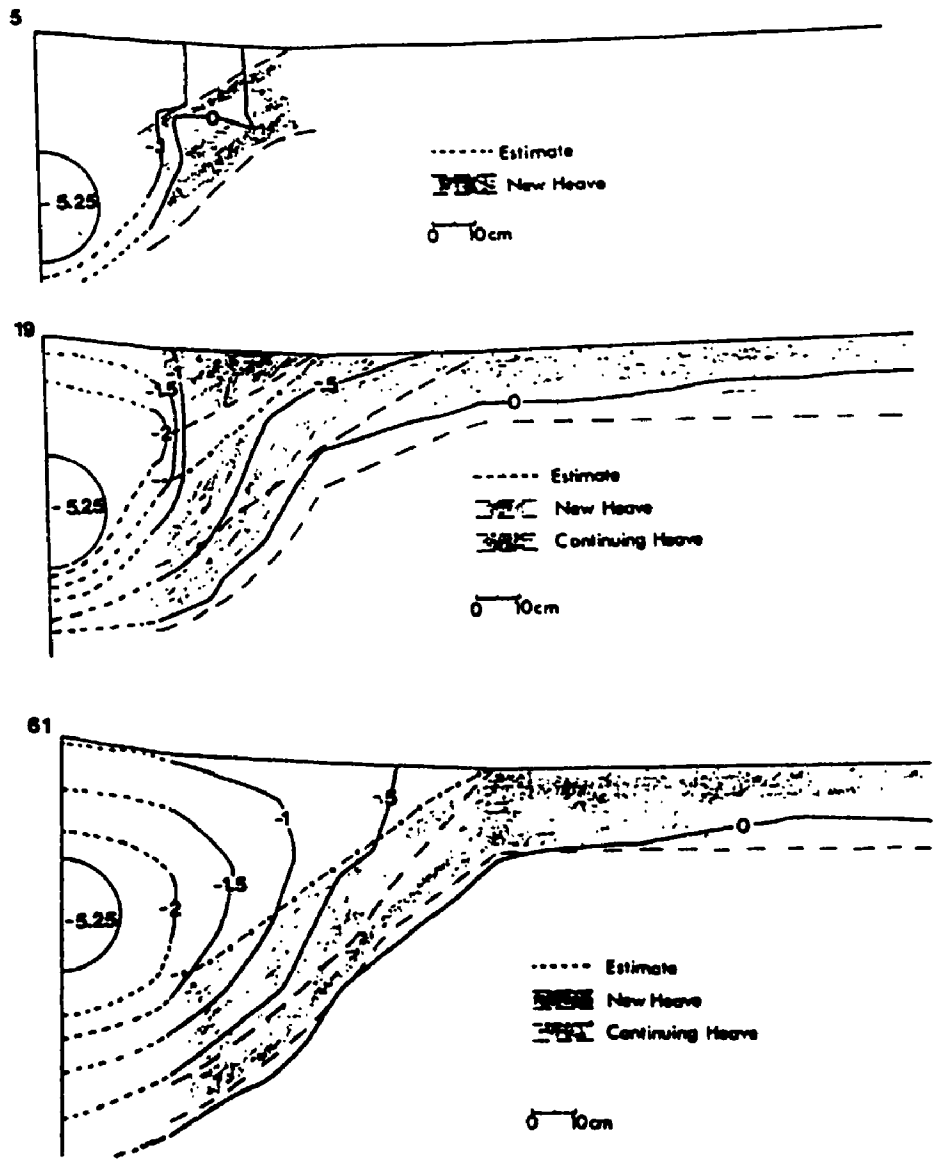

FIGURE 5.12. Ground temperature (°C) and heave zones at site 1 on days 100 and 203. Isotherm interval is .5°C. The dashed isotherm lines have been extrapolated beyond the data range. "New Heave" refers to the most recent layer to exhibit heave for the date shown. The layer exhibiting heave is defined by the magnet location.

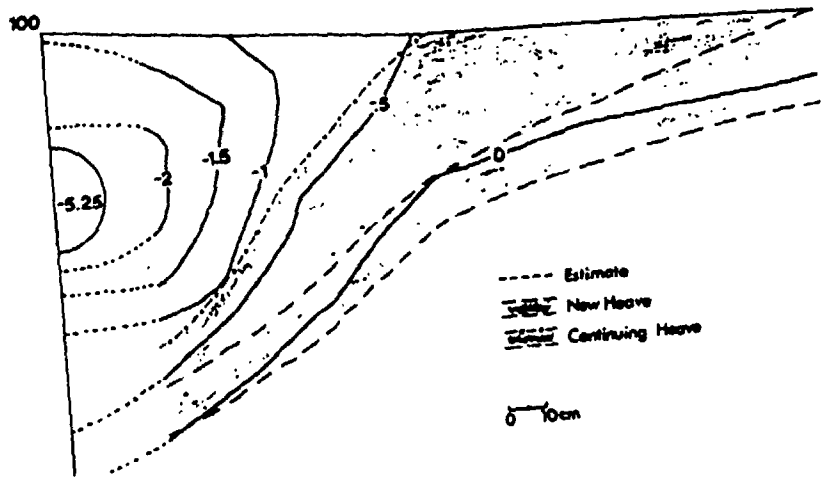

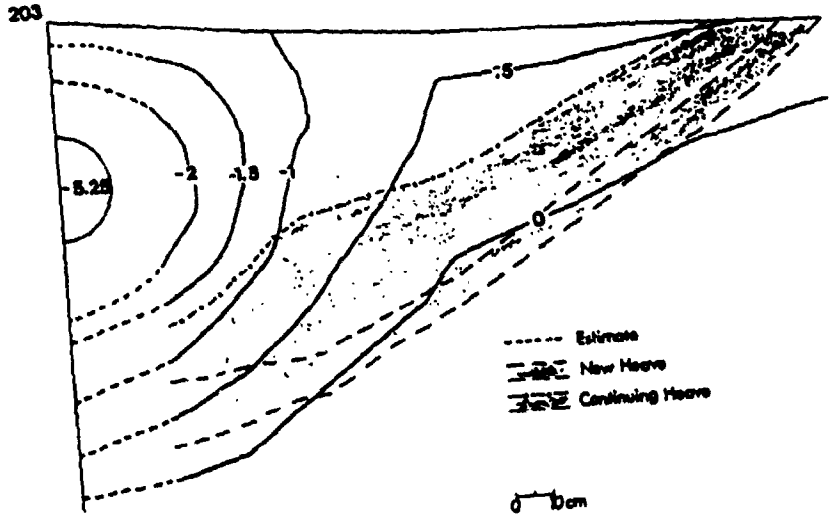

FIGURE 5.13. Ground temperature (°C) and heave zones at site 1 on days 301 and 447. The isotherm interval is .5°C. The dashed isotherm lines have been extrapolated beyond the data range. "New Heave" refers to the most recent layer to exhibit heave for the date shown. The layer exhibiting heave is deflined by the magnet location.

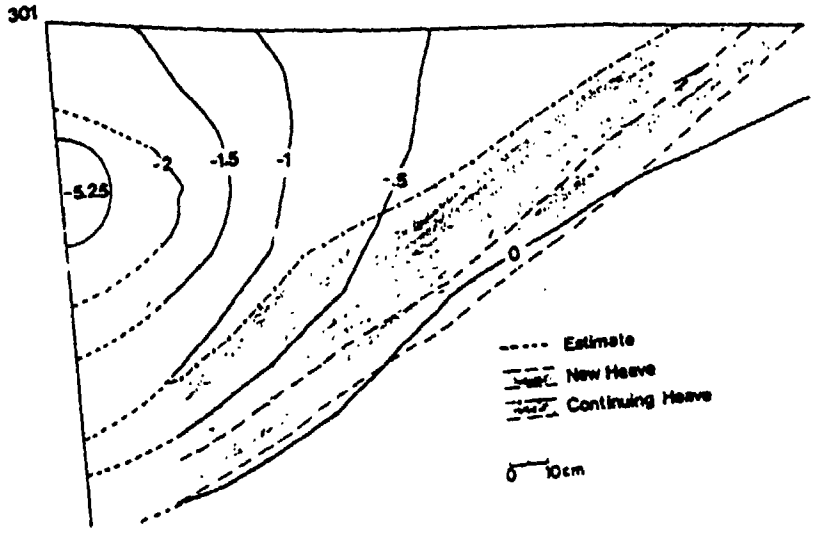

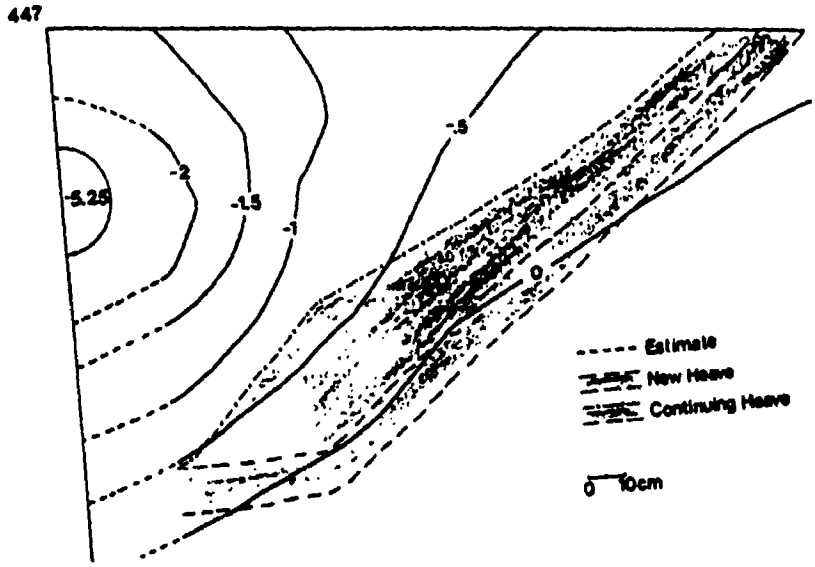

circular pattern of isotherms is found to exist around the pipe. There is a strong lateral heat flow component beside the pipe and as distance from the pipe increases, the vertical component of heat flow is dominant.

Initially the rate of penetration of the 0°C isotherm is high and is approximately 0.15 cmh^{-1} but this decreases to between .001 and .004 cmh^{-1} towards the end of the freeze cycle. Temperature gradients are also large at the start of the freeze cycle, especially near the pipe. Temperature gradients were measured in zones where heave was occurring. The gradient is greater than $6^{o}Cm^{-1}$, 35 cm from the pipe but decreased to $2.8^{o}Cm^{-1}$, 83 cm from the pipe and $1.9^{o}Cm^{-1}$, 135 cm from the pipe. Temperature gradients decreased at the end of the freeze cycle and were $2.8^{o}Cm^{-1}$, $2.2^{o}Cm^{-1}$ and $1.7^{o}Cm^{-1}$, 35, 83 and 135 cm from the pipe, respectively.

The compressor shut down on day 233 of the freeze cycle and some warming of the ground occurred (figure 5.14). Between day 230 and day 237, melting occurred in the upper 5 cm of the ground. Near the pipe, ground temperature increased by more than 0.5°C. Beside the pipe, isotherms were vertical and the lateral component of heat flow is important. The ground started to cool again by day 243 and ground temperature returned to that which existed before the compressor shutdown.

5.11 Heave Pattern

The device used to measure differential heave consists

FIGURE 5.14. Ground temperature (°C) following period of warming which occurred on day 233. Isotherm interval is .5°C. The pipe axis is 25 cm from the left side of the diagram.

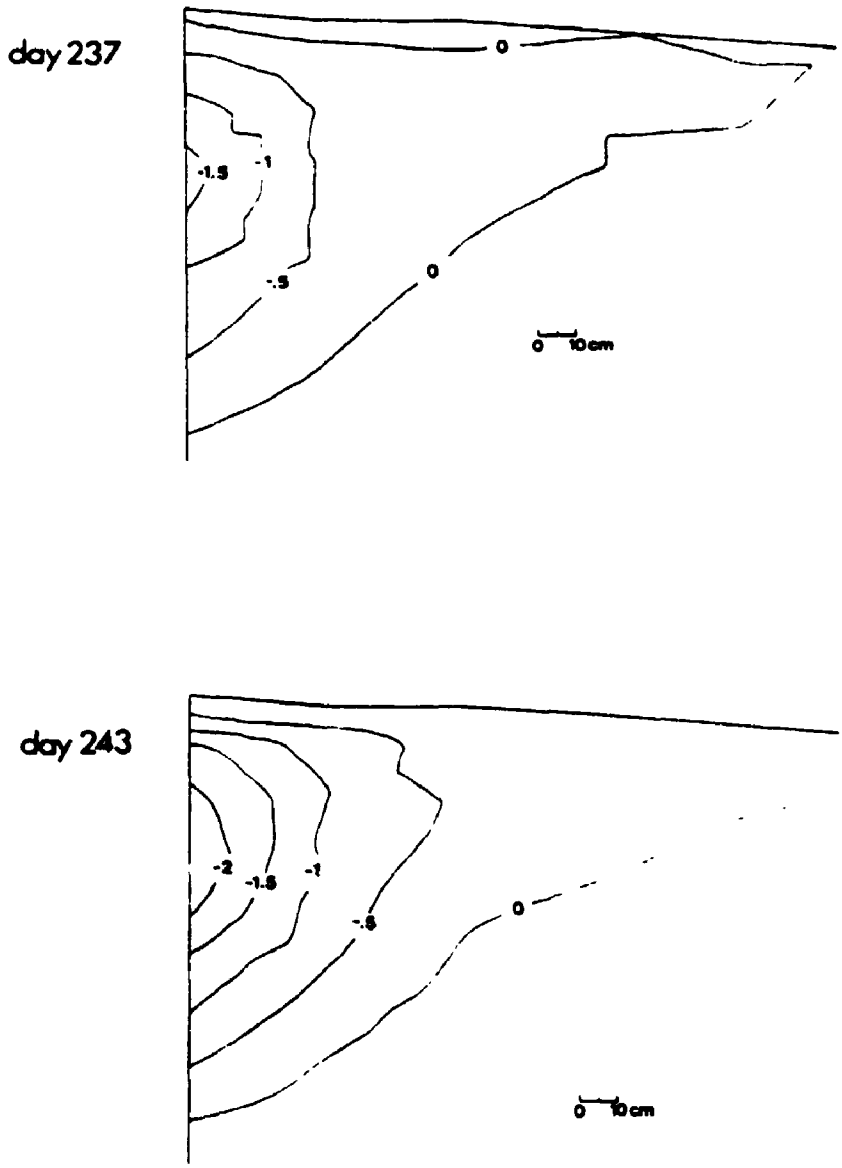

of a series of magnet rings placed approximately 10 cm apart in the soil (MacKay and Leslie 1987 and Smith and Patterson 1989). An access tube passes vertically through the centre of the magnet rings. A magnet sensing device is lowered down the access tube and the position of the magnet rings in the profile is determined with reference to a ring on the surface. The position of the magnet rings can be located to within 0.2 to 0.3 mm. This device allows the monitoring of the expansion (heave) of any soil layer defined by a pair of magnets.

The layer most recently exhibiting heave ("new heave" in figures) on selected dates, site 1, is shown in figures 5.11, 5.12 and 5.13 (data from Geotechnical Science Laboratories 1989). This layer is defined by the magnet location and heave is not occurring throughout the entire layer. Heave begins next to the pipe at a depth of approximately 20 cm during the first five days of the experiment while the surface layer does not start heaving until after day 5. Heave begins at farther from the pipe during the first 20 days of the experiment with the surface layer expanding first. A curved zone of heave similar to the isotherm pattern develops over time. The zone of heave progresses more rapidly through the soil and to a greater depth, next to the pipe. By day 100, heave had stopped 2 m from the pipe but continued next to the pipe until the end of the experiment.

Heave was observed to occur over a temperature range of -0.5°C to 0°C. Temperature and heave data suggest that heave occurs at a lower temperature next to the pipe than farther away. The temperature at which heave occurs may be the same at all locations and the difference suggested by the maps may be a function of the position of the magnets used for the observations. Reasons for the difference in temperature at which heave occurs will be discussed later.

Strain (percent) for each layer at each measurement site is presented in table 5.2. The amount of strain over time for each layer is shown in figures 5.15, 5.16, 5.17. The highest heave rates (strain rates) occur in the uppermost layers.

During the short period of warming (following the compressor malfunction) which commenced on day 233, the heave rate decreased next to the pipe, 82 cm below the surface (figure 5.15). There was no significant change in heave rate at the other measurement locations.

The total amount of strain occurring in each layer, increases with depth below pipe level. A decrease in heave rate and an increase in total strain with depth also occurs at the other sites (figures 5.16 and 5.17).

The greatest total heave (cm) occurs next to the pipe because the ground freezes to a greater depth and therefore heave occurs over a greater depth. The total strain (percent) for the layer of ground frozen (table 5.2),

TABLE 5.2. Total strain and continuing strain in frozen soil at site 1 (from Geotechnical Science Laboratories 1989).

DEPTH (cm)	TOTAL STRAIN (%)	CONTINUING STRAIN (% of total strain)
Location: 25 cm from pipe		
0-23.20	.8	-
23.2-32.8	4	-
32.8-44.6	2	-
44.6-54.6	11	-
54.6-66.97	27	-
66.97-81.36	29	8.4
81.36-93.11	37	16.2
92.11-111.05	45	15.9
Total strain for frozen material = 19.5%		
Location: 63.5 cm from pipe		
0-23.14	14	7.2
23.14-34.04	16	92.1
34.04-46.81	18	59.5
46.81-58.69	24	83.6
58.69-68.94	33	56.1
68.94-86.38	42	29.3
86.38-99.84	12	18.0
Total strain for frozen material = 19.7%		
Location: 1 m from pipe		
0-27.39	34	19.4
27.39-39.02	25	13.5
39.02-52.84	28	32.7
52.84-66.72	46	64.6
66.72-78.55	29	44.8
Total strain for frozen material = 32.2%		

FIGURE 5.15. Differential strain 25 cm from the pipe axis at site 1 (from Geotechnical Science Laboratories 1989). The observations show strain of layers between depths as indicated (eg. 53-63 cm; 63-74 cm; etc.)

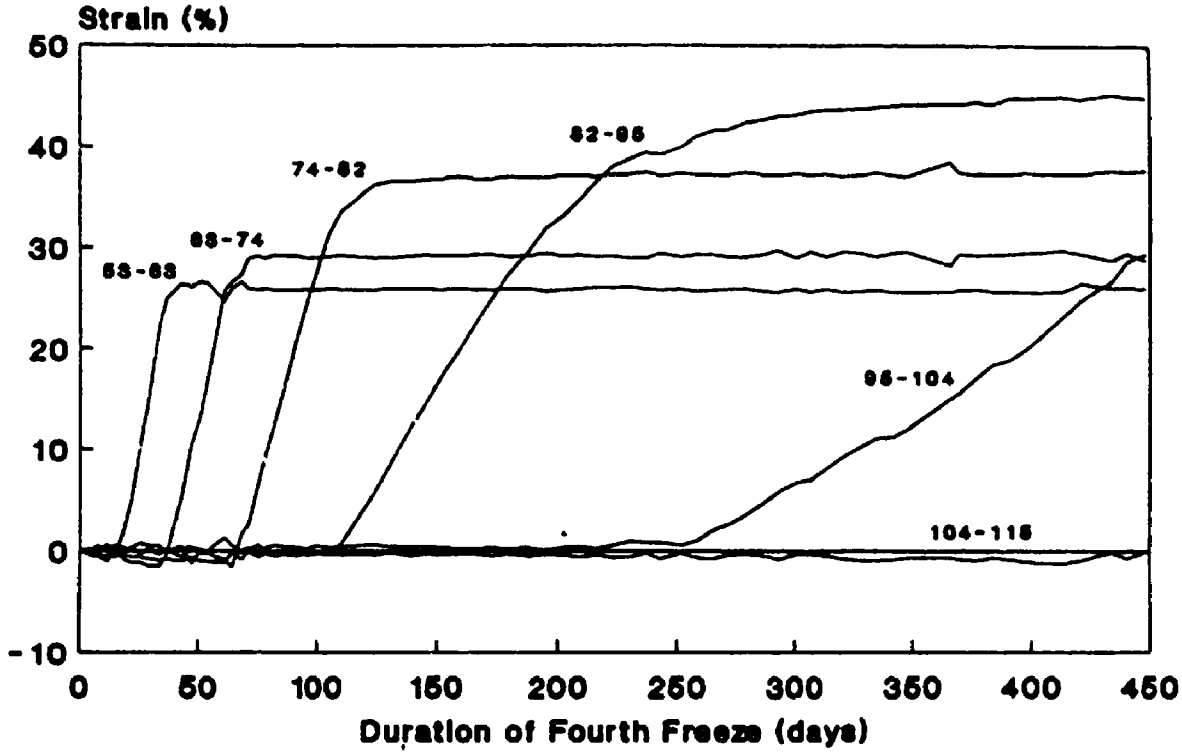

FIGURE 5.16. Differential strain 65 cm from the pipe axis at site 1 (from Geotechnical Science Laboratories 1989).

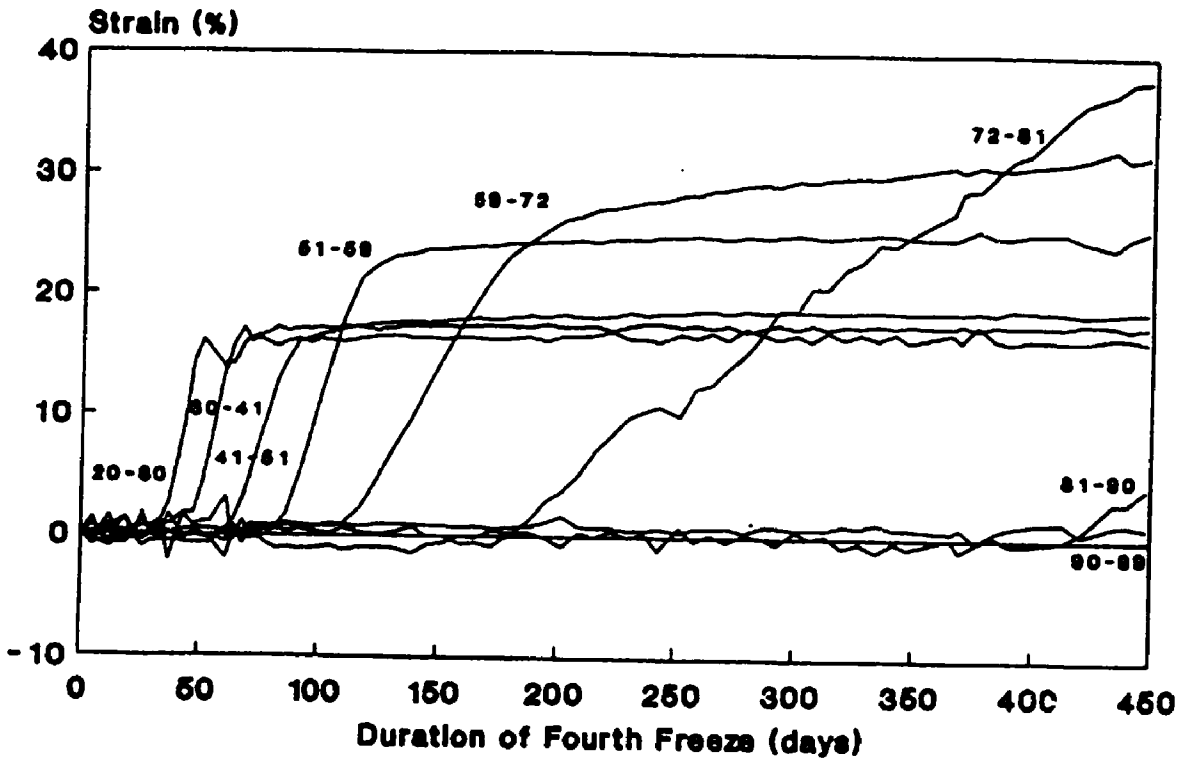

FIGURE 5.17. Differential strain 1 m from the pipe axis at site 1 (from Geotechnical Science Laboratories 1989).

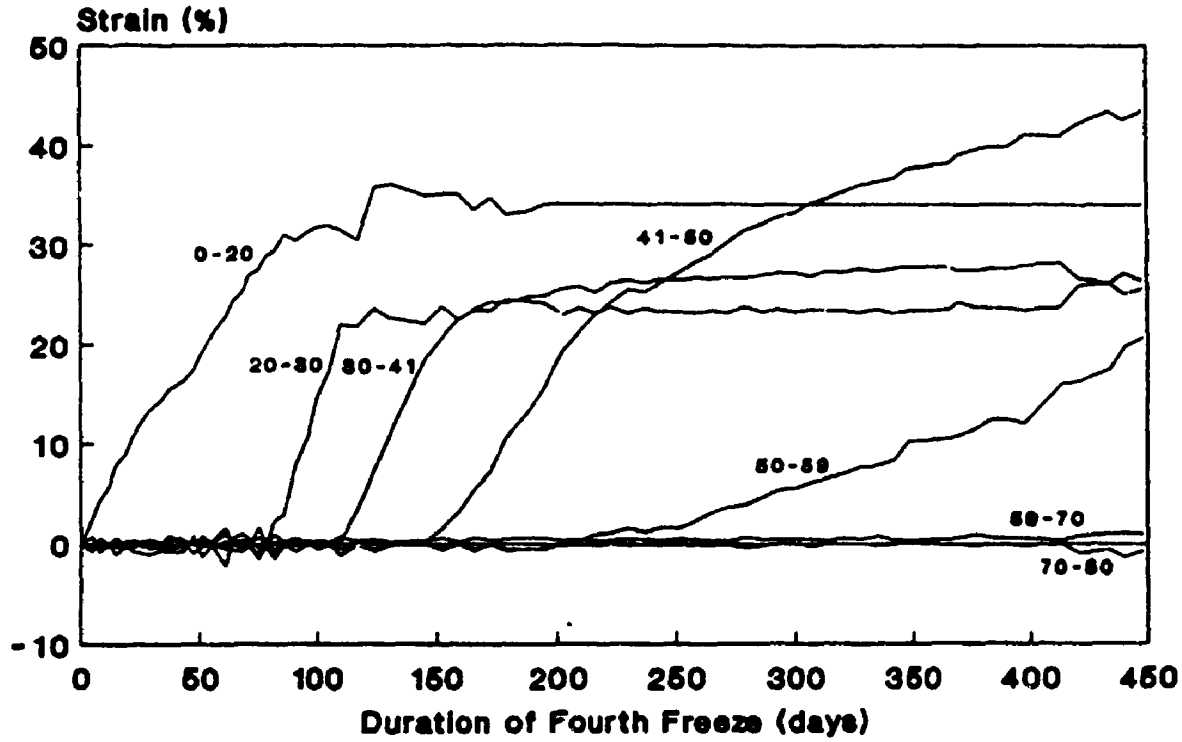

however, is almost two times greater 1 m from the pipe than it is next to the pipe. The total strain 2 m from the pipe is smaller than at the other three measurement locations.

Data from the magnet heave devices (figures 5.15, 5.16 and 5.17) shows that a soil layer may continue to expand as heave commences in the adjacent layer (Smith and Patterson 1989). These data suggest that water migration and ice lens growth continue in the frozen soil behind the warmest ice lens and this is referred to as continuing heave. The soil layer exhibiting continuing heave on selected days is also shown in figures 5.11 to 5.13.

The contribution of continuing heave to the total heave has been determined at three locations at site 1 (table 5.2). These data show that continuing heave can account for a significant portion of the total heave. For example, continuing heave accounts for over 90% of total heave, 20 to 30 cm below the surface, 63.5 cm from the pipe. Continuing heave generally accounts for a greater proportion of total heave at greater distance from the pipe.

The estimates of continuing heave can be used to determine the growth of ice lenses that occurs during continuing heave. It is assumed that the distance between ice lenses remains constant during the time that continuing heave occurs. The average increase in ice lens thickness during continuing heave in soil layers at the core locations at site 1 has been determined by using the average ice lens

thickness in each soil layer (table 5.3).

The increase of thickness of ice lenses during continuing heave increases with distance from the pipe. It is about 0.1 mm at 35 cm, 1 mm at 83 cm and as much as 2.5 mm at 135 cm distance.

Observations of ice lens thickness 135 cm from the pipe at both site 1 and site 2 indicate that ice lenses in the upper part of the soil are larger than those deeper in the soil even though temperature gradients are larger. This is a result of the continuing growth of ice lenses in frozen soil behind the warmest ice lens. Ice lenses near the surface will grow for a longer period of time and will therefore, be larger than those below.

5.12 Moisture Content and Density

5.12.1 *Spatial variation in total moisture content and density*

Gravimetric moisture content (ice and water) and dry bulk density have been mapped for soil perpendicular to the pipe at sites 1 and 2 (figures 5.18 and 5.19). These maps can be compared to those for ice lens pattern and ground temperature. Diagrams showing greater detail of vertical variation in gravimetric moisture content, dry buk density and also volumetric moisture content are presented in Appendix 3.

At site 1 (figure 5.18) there is a general increase in moisture content and a decrease in dry density with depth

TABLE 5.3. Ice lens growth during continuing heave.

DEPTH (cm)	CONTINUING ICE LENS GROWTH (mm)	INITIAL ICE LENS GROWTH (mm)
35 cm from pipe		
66.97-81.36	0.1	0.9
81.36-93.11	0.2	1.3
93.11-111.05	0.1	0.6
83 cm from pipe		
0-11	0.1	0.9
11-23.14	0.1	1.3
23.14-28	0.9	0.1
28-34.04	0.6	0.1
34.04-40	0.4	0.3
40-46.81	0.3	0.4
46.81-58.69	0.4	0.6
58.69-68.94	0.7	0.3
68.94-86.38	1.0	2.5
135 cm from pipe		
0-14	0.3	1.2
14-27.39	1.1	4.9
39.04-45	0.5	1.2
45-52.84	2.4	5.1

FIGURE 5.18. Gravimetric moisture content (a) and dry density (b) in soil perpendicular to the pipe at site 1. The isoline interval for (a) is 10% and for (b) 0.2 gcm^{-3}.

a

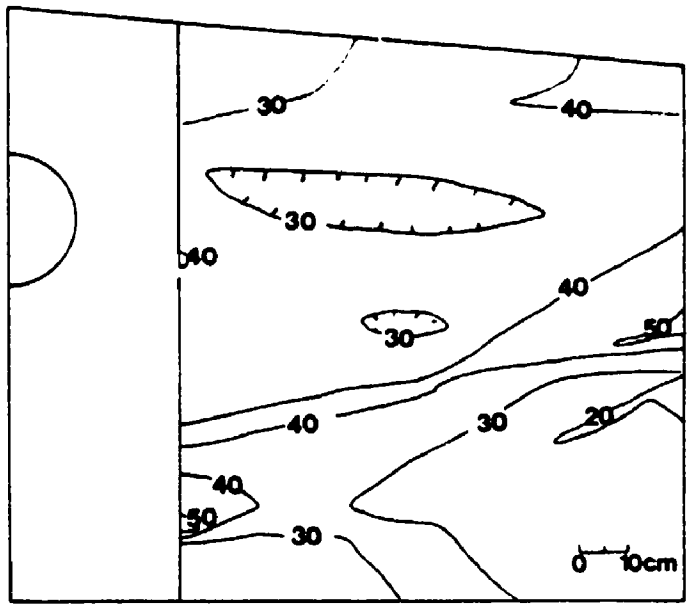

b

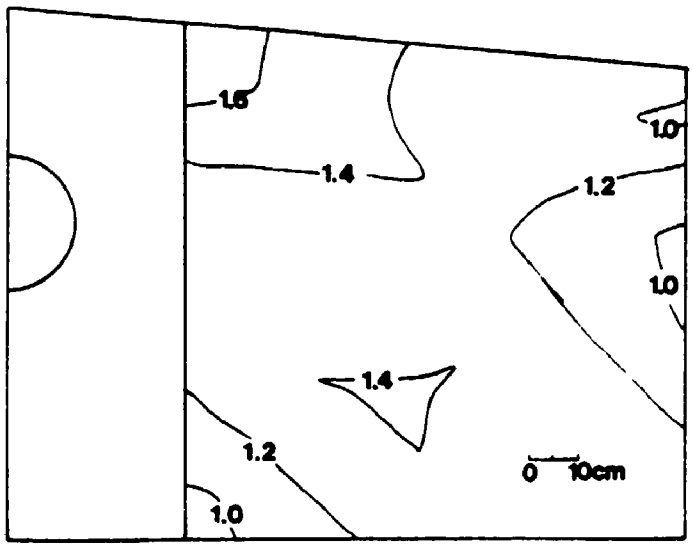

FIGURE 5.19. Gravimetric moisture content (a) and dry density (b) in soil perpendicular to the pipe at site 2. The isoline interval for (a) is 10% and for (b) 0.2 gcm^{-3}.

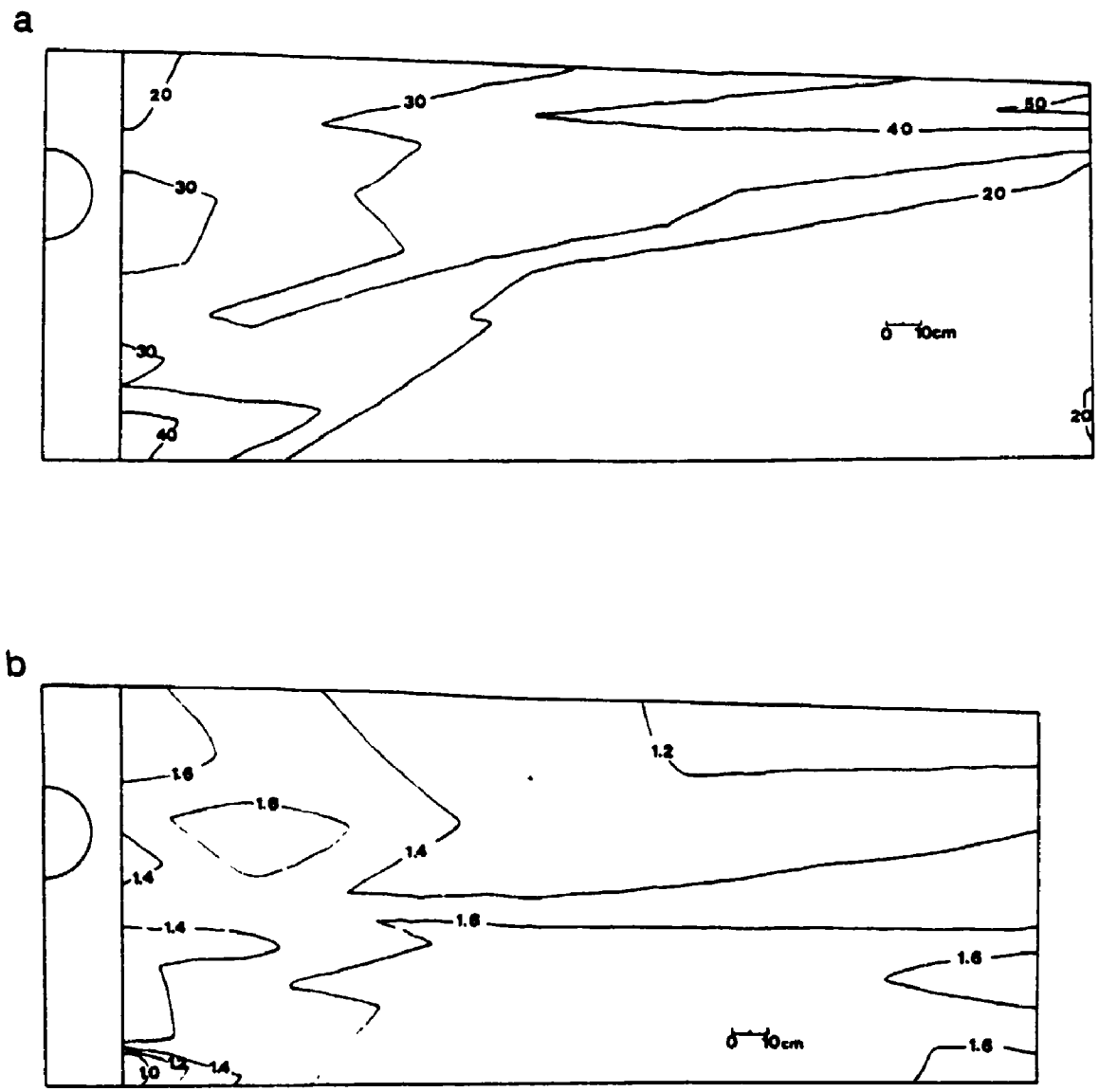

down to the lower limit of the ice lenses. Below the ice lenses, the moisture content drops sharply and density increases. Moisture content in the frozen soil generally increases as distance from the pipe increases and ice lenses become thicker. High moisture contents and low density values are also found near the surface at approximately 1 m from the pipe. This may be the result of continuing heave occurring in the upper layers of the soil and an increase in ice lens thickness over the freezing period. There is also a zone of low moisture content approximately 30 cm below the surface. This coincides with the location of the distinct ice lens pattern which is presumed to result from compaction of the soil.

The increase in moisture content with depth, follows a similar increase in ice lens thickness with depth. Temperature gradients are also smaller at depth, indicating lower freezing rates. These would be conditions suitable for the growth of large ice lenses and therefore a large inflow of water into the freezing zone.

A similar pattern of moisture content and density exists at site 2 (figure 5.19). The highest moisture contents and the lowest density values were found near the surface, 1 to 2 m from the pipe. A high density layer of soil is located at pipe level, approximately 40 to 100 cm from the pipe. The distinct ice lens pattern was found at this location.

Moisture content is generally higher and density is lower at site 1 than site 2. The variation in moisture content along the pipe axis is shown in figure 5.20. The mean gravimetric moisture content at site 1 is 35.4% and the mean at site 2 is 29.7%. A difference of means test was conducted and the mean moisture content at site 1 was found to be significantly greater than that at site 2 at the 0.05 significance level. The mean densities for site 1 and site 2 are 1.27 gcm^{-3} and 1.45 gcm^{-3} respectively and mean dry density at site 2 was found to be greater than that at site 1 at a significance level of 0.05. It may be concluded then, that as distance from the sand-silt boundary increases, the moisture content of the soil also increases and density decreases.

The gravimetric moisture content in the frozen sand was found to be low compared to the silt (figure 5.20). The moisture content of the sand showed little variation with distance from the pipe. Moisture contents were found to be low in the upper part of the frozen sand and increased with depth in the frozen soil.

These observations reflect the difference in the heave characteristics at the three sites. The total heave at site 1 is greater than that at site 2. There is a greater inflow of water into the frozen soil at site 1 which results in greater ice accumulation and higher moisture contents. These results show the influence that the non-heaving sand

FIGURE 5.20. Gravimetric water content in silt at sites 1 and 2 and sand along the pipe axis.

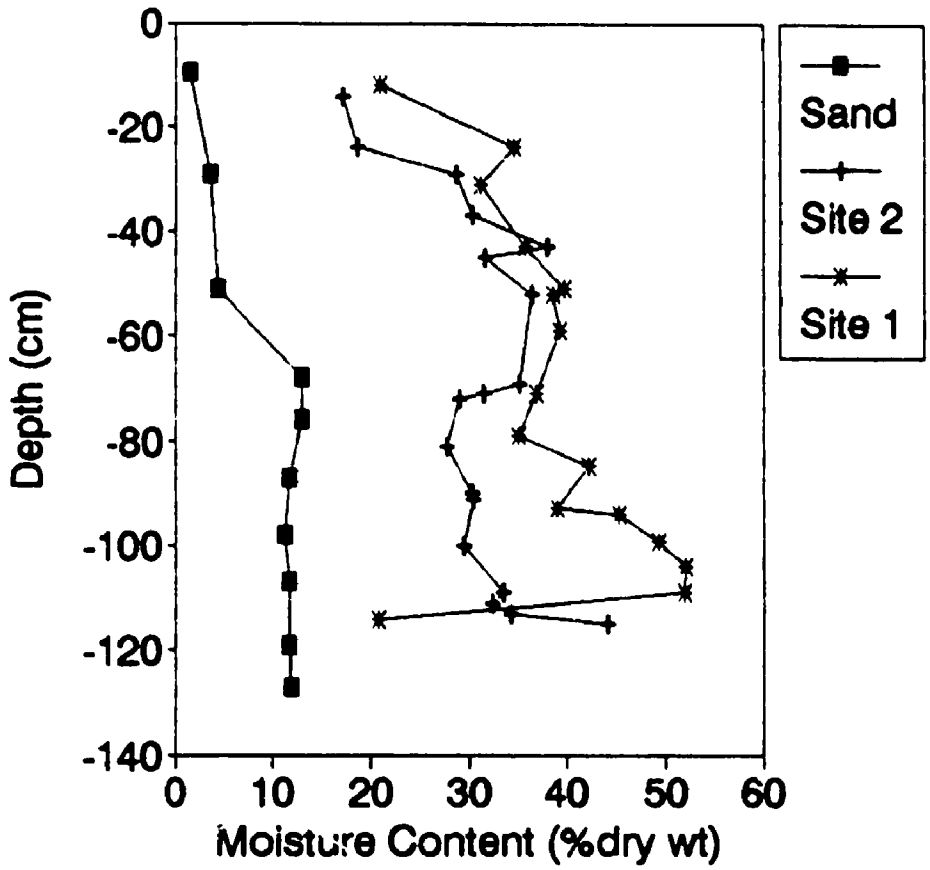

has on the adjacent silt at site 2. Greater resistance to heave and therefore to ice accumulation exists at site 2. This is reflected in the presence of smaller ice lenses and the smaller additions of water to the frozen zone.

5.12.2 *Ice and water contents*

The moisture contents determined for the frozen soil samples can be partitioned between ice and water. The relationship between temperature and unfrozen water content can be used to determine the gravimetric unfrozen water content in a particular soil sample. The difference between this and the total gravimetric moisture content determined for the frozen sample will give the gravimetric ice content.

Unfrozen water content has been determined as a function of temperature using time domain reflectometry (TDR) (Geotechnical Science Laboratories 1988 and Patterson personal communication 1988) for Caen silt samples and an attempt was made to fit an equation to these data. The work of Anderson et. al. (1973) suggests that the relationship between the unfrozen water content and temperature can be represented by a simple power equation:

$$\theta_w = aT^B \qquad (5.1)$$

T = freezing point depression of pure water (°C)

a,B = constants

θ_w = gravimetric unfrozen water content at temperature T (% dry weight)

The coefficients a and B are obtained by a least squares

regression of experimentally measured values of θ_T and T. Values of a and B were found to be related to the specific surface area of the soil (Anderson et. al. 1973 and Anderson and Morgenstern 1973). An equation of the following form was determined for the data obtained by TDR:

$$\theta_w = 15.42T^{-.03} - 6.02 \qquad (5.2)$$

$$r^2 = 0.992 \qquad SEE = 0.679$$

This equation provides a good fit and adequately predicts unfrozen water content for the range of temperatures being considered except for those that are close to 0°C (less than -0.5°C) because data were not available in this temperature range.

Soil temperature during the period of excavation was used to calculate the unfrozen water content for each soil sample. The temperature of the midpoint of each section of core being considered was determined and was used to represent the average temperature of that soil layer. The unfrozen water content at that temperature was then determined and the ice content was then calculated.

Gravimetric unfrozen water and ice contents were determined for the three sampling locations at site 1 and have been plotted as a function of depth in figure 5.21. Volumetric ice and water content were also determined (figure 5.22) but less data were available for these calculations. Unfrozen water content increases with depth because temperature increases with depth. Ice content

FIGURE 5.21. Gravimetric ice and water contents of soil at site 1. The ice lens thickness is also given on each graph.

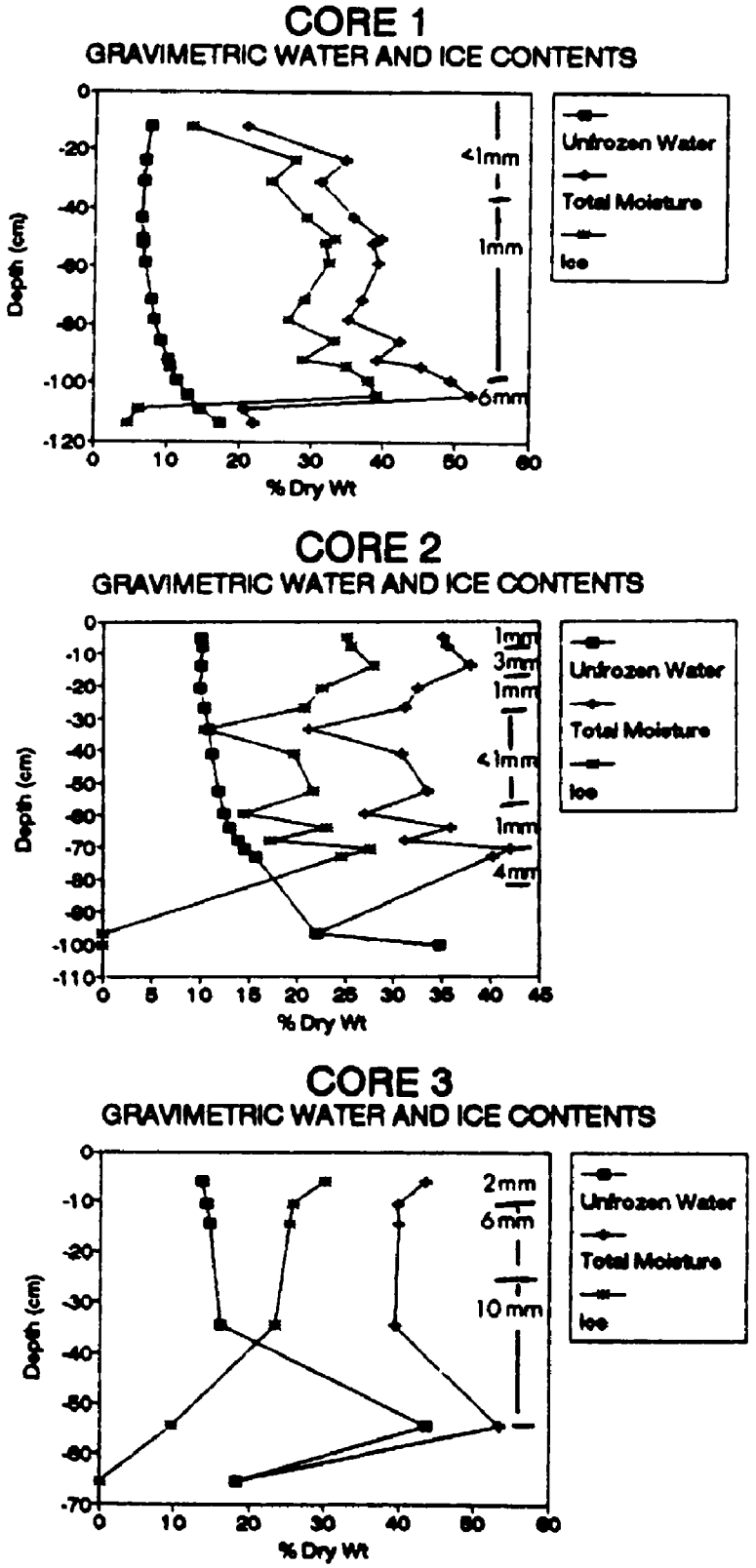

FIGURE 5.22. Volumetric ice and water contents of soil at site 1.

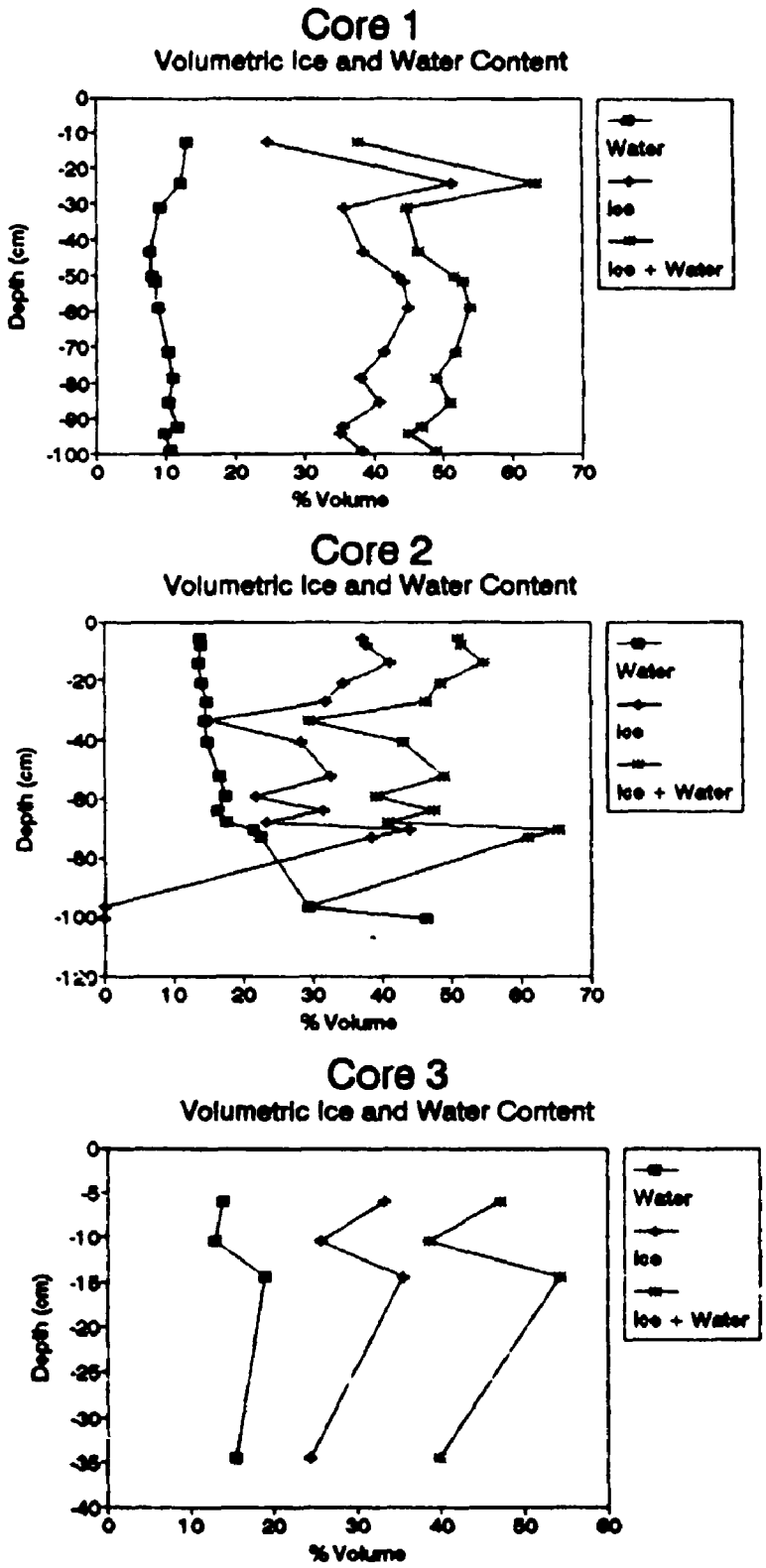

fluctuates with depth but there is a general increase.

Ice lens thickness has been added to figure 5.21 and it is clear that higher total moisture contents and ice contents are associated with larger ice lenses. This indicates the addition of water to the soil and the accumulation of excess ice. The average water content for unfrozen soil is approximately 28% dry weight. It can be seen from figure 5.21 that a large part of the ice content (up to about 56%) is excess ice.

Strain (determined from the magnet heave data) has been plotted against gravimetric ice content in figure 5.23. An attempt was made to fit a linear regression line to the core 1 data. The standard error and r^2 values (13.44 and 0.44) indicate that there is a large amount of scatter about the regression line. The results do suggest however, that a positive correlation exists. Obviously the amount of heave measured by the magnet heave devices should increase as the ice content increases. Expansion of the soil occurs as ice accumulates in the frozen soil. One would expect therefore, that there would be a stronger correlation between these two variables.

To understand the large amount of scatter that exists, an assumption made in the calculation of unfrozen water content must be considered. It was assumed that soil density remained constant during freezing and that the relationship between unfrozen water content and temperature

FIGURE 5.23. Relationship between strain and gravimetric ice content. The regression line has been fitted to the core 1 data (the two outliers were excluded). The equation for the line is:

$$\%strain = 1.79(ice\ content) - 29.33$$
$$r^2 = 0.44 \qquad SEE = 13.44$$

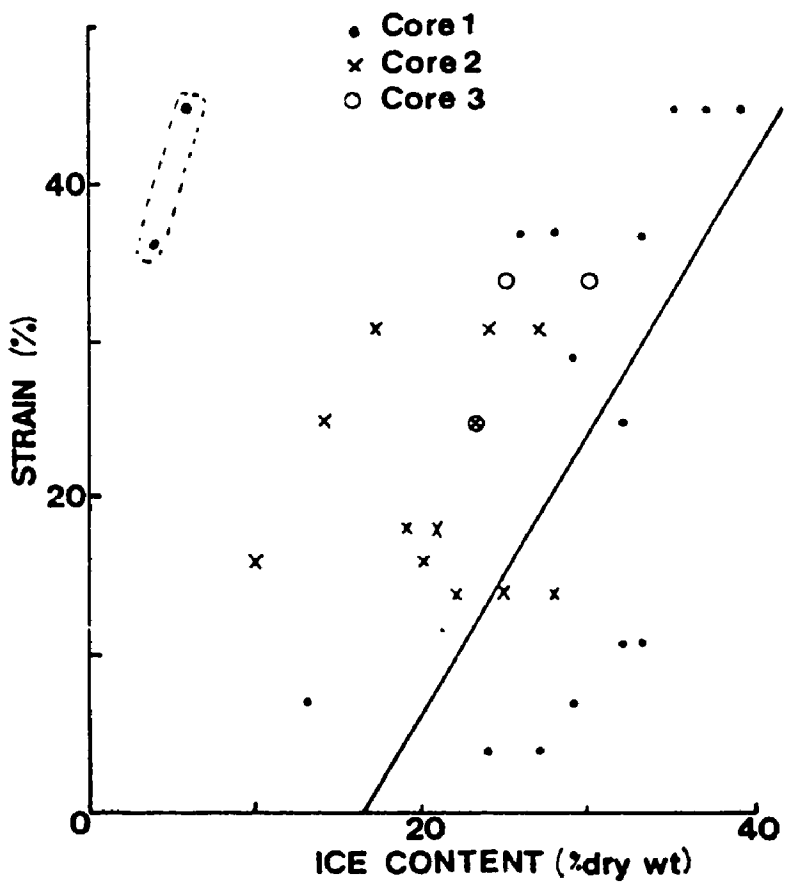

remained constant. Any decrease in density due to freezing and expansion of pore water was considered to be negligible. This appeared to be a reasonable assumption since the unfrozen water is only found in the pore spaces. Any significant changes in density that occur would be due to the accumulation of bulk ice in the form of ice lenses. The gravimetric unfrozen water content would still remain the same because it is expressed as a proportion of the dry soil weight.

As the freezing front progresses, large suctions are created as water is drawn from the unfrozen soil below the growing ice lens. Effective stress will be created in the soil below the ice lens and some consolidation will occur. This results in a decrease in the porosity of the soil and an increase in the dry bulk density. The soil below an ice lens may become desiccated and contain a very small amount of water. The relationship used to determine unfrozen water content therefore, may over-predict the water content of the soil and under-estimate the ice content. This could account for some of the scatter in the relationship between strain and ice content.

Another important point is that expansion of an ice lens may not always be accompanied by an increase in the thickness of the layer of frozen soil. Ice may accumulate as the soil below the ice lens consolidates i.e. the ice layer becomes thicker as the soil layer below becomes

thinner. This could also account for some of the scatter observed in figure 5.23.

CHAPTER SIX

OBSERVATIONS OF ICE LENS ORIENTATION AND DISTRIBUTION IN RELATION TO THE THERMAL REGIME AND OTHER FACTORS

6.1 Relationship Between Freezing Rate and Ice Lens Distribution

Figure 6.1 shows the relationship between the penetration rate of the 0°C isotherm (freezing front) and thickness and spacing of ice lenses at site 1. The relationship appears to be nonlinear with thickness decreasing rapidly with increased cooling rates and then decreasing at a slower rate as the cooling rate becomes higher. The relationship between ice lens thickness and cooling rate was discussed in Chapter 2 and these results suggest a similar relationship. Larger ice lenses will be able to grow where the cooling rate is slower because there will be sufficient time for water to migrate to the freezing front. There is however, considerable scatter and the relationship appears to depend on location which indicates that the thermal regime is not the only factor influencing ice lens thickness and location.

One reason for the scatter in figure 6.1 may be continuing heave. A significant portion of ice lens growth may occur during a period of lower heat flow than when the ice lenses initially formed.

Continuing heave and the accompanying ice lens growth

FIGURE 6.1. Relationship between cooling rate and ice lens thickness and spacing.

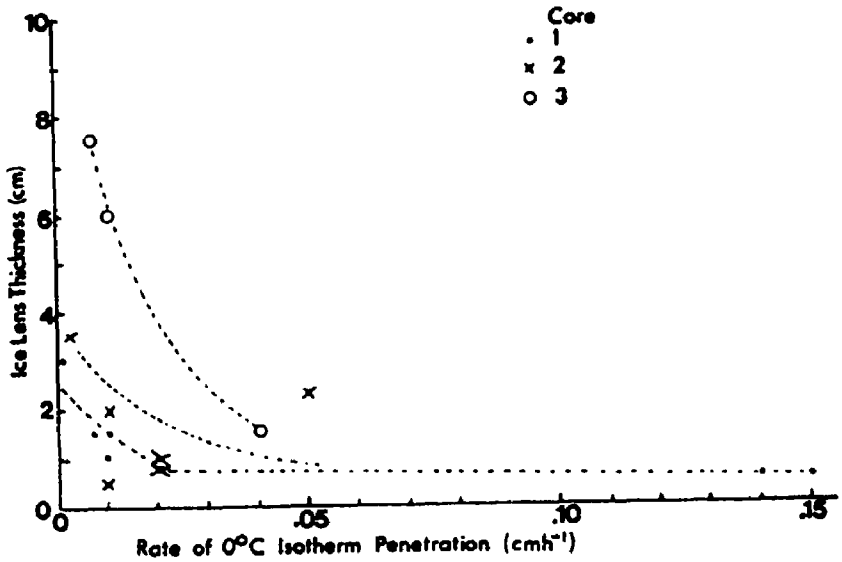

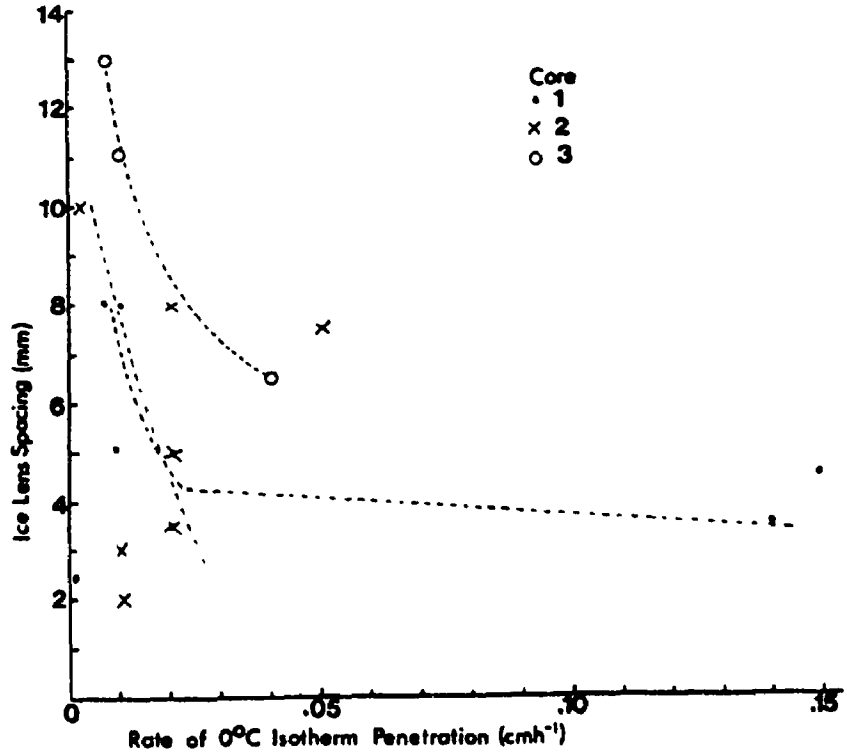

occurs at a slow rate and for this to occur the soil must deform over time. The amount of ice accumulation that will occur during continuing heave will depend on the resistance of the frozen soil. The results from the ice sandwich experiments indicate that pore ice may exhibit creep over time. Redistribution of ice and water through regelation may also occur and this may account for the increase in ice lens thickness which takes place in the frozen soil.

Ice lenses are generally smaller and moisture content is lower near the transition (site 2) than at site 1. The reason for this may be partly due to the higher cooling rate at that site and partly due to the different mechanical conditions. The amount of heave also decreases towards the transition. The non-heaving sand may act as an anchor and offer resistance to heave in the adjacent silt.

6.2 Temperature During Ice Lens Formation

The temperature at which heave and therefore, ice lens formation begins is lower near the pipe (figures 5.11 to 5.13) than it is farther away. The ice pressure (heaving pressure) is related to temperature by the Clausius-Clapeyron equation. Near the pipe it appears that greater ice pressures are necessary to initiate heave. A greater stress must be applied near the pipe to overcome the resistance of the frozen soil.

6.3 Relationship Between Ice Lens Orientation and Isotherm Pattern at Site 1

6.3.1 *Comparison of patterns*

It is generally assumed that ice lenses form perpendicular to the direction of heat flow (Carlson and Nixon 1988, National Research Council 1984, Shumskii 1964 and Taber 1930). The ice lenses therefore, should be parallel to the isotherms since heat flow occurs perpendicular to the isotherms.

The ice lens pattern (figure 5.3) was compared to the isotherm pattern (figure 5.13) that existed just before coring was done (day 447). There is some similarity between the two patterns and it is clear that the chilled pipe acts as a heat sink and influences the ice lens pattern. Both ice lenses and isotherms dip toward the pipe and form a circular pattern but the ice lenses and isotherms are not parallel.

It should be remembered that the isotherm pattern changes through time (see figures 5.11 to 5.13) as the freezing front progresses through the soil. The ice lenses in the upper part of the ground near the pipe for example, formed early in the freeze cycle and the isotherm pattern at that time was different from that at the end of the freeze cycle. This would explain the difference in the two patterns and also explains why there is closer correspondence between the two patterns at the bottom of the

frozen zone.

To properly examine the relationship between the ice lens and isotherm patterns, the isotherm pattern at the time a particular ice lens formed should be considered. Data from the magnet heave devices can be used to determine when a particular soil layer is expanding (heaving) or in other words when ice lenses are forming within the layer. The isotherm pattern in this soil layer during the period of heave can then be compared to the ice lens pattern.

The layer most recently exhibiting heave at site 1 was determined for the following days: 5, 19, 43, 61, 82, 100, 203, 301, 398 and 447. The isotherm pattern in the heaving layer was then determined. A map of the isotherm pattern during heave throughout the freeze cycle was constructed and compared to the ice lens pattern (figure 6.2).

The two patterns are similar and there is better agreement than when the isotherm pattern at the end of the freeze cycle was compared to the ice lens pattern. The two patterns are not parallel over the whole section however. Next to the pipe, (core 1) in the upper part of the ground, the isotherms are almost vertical whereas the ice lenses are not. In one section the isotherms are almost horizontal but the ice lenses still dip toward the pipe. In the lower part of the frozen section there is less difference between the dip of the isotherms and ice lenses but the isotherms are still inclined at a steeper angle than the ice lenses.

FIGURE 6.2. Comparison of isotherm pattern and ice lens patterns at site 1. Isotherm pattern is based on the isotherm pattern in the most recent layer to exhibit heave on a given day.

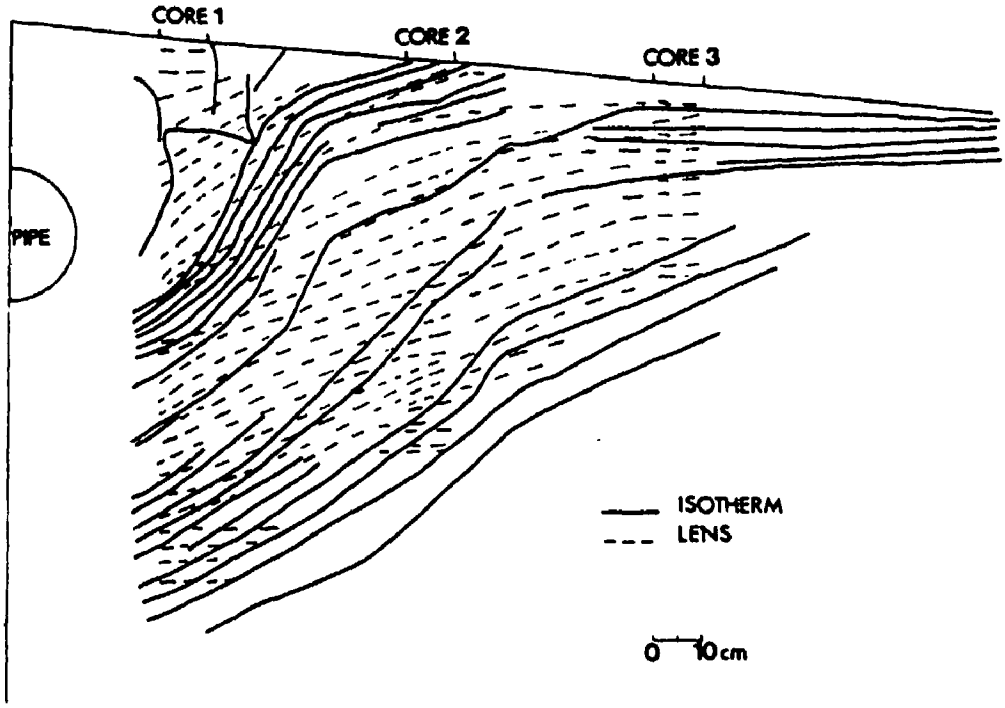

At core 2, the ice lenses and isotherms are parallel in the upper 35 cm of the ground. In the lower part of the frozen section there is a large difference between the two patterns with the isotherms dipping toward the pipe at a greater angle than the ice lenses. At a distance of 135 cm from the pipe, (core 3) both the ice lenses and isotherms are almost horizontal. It appears that at distances greater than 1 m from the pipe, the ice lenses follow the isotherm pattern while closer to the pipe the isotherms dip at a steeper angle than the ice lenses.

The ice lens dip is plotted against the isotherm dip in figure 6.3. There is a large amount of scatter, but it can be seen from the graph that the isotherm dip is generally greater than the ice lens dip. Generally the difference between the isotherm and ice lens dip becomes greater as the isotherm dip becomes steeper (figure 6.3). The isotherm pattern resembles the ice lens pattern when the isotherms are inclined a small amount from the horizontal.

The isotherm pattern during heave throughout the freezing cycle has also been compared to the ice lens pattern in pit 1 (figure 6.4) which is on the opposite side of the pipe from where temperature measurements were made. The assumption is made that the isotherm pattern is the same on both sides of the pipe.

The results are similar to those for the cores (figure 6.2). As distance from the pipe increases, the two patterns

FIGURE 6.3. Relationship between isotherm dip and ice lens dip at site 1. "Difference" refers to the difference between isotherm and ice lens dip angles (isotherm-ice lens).

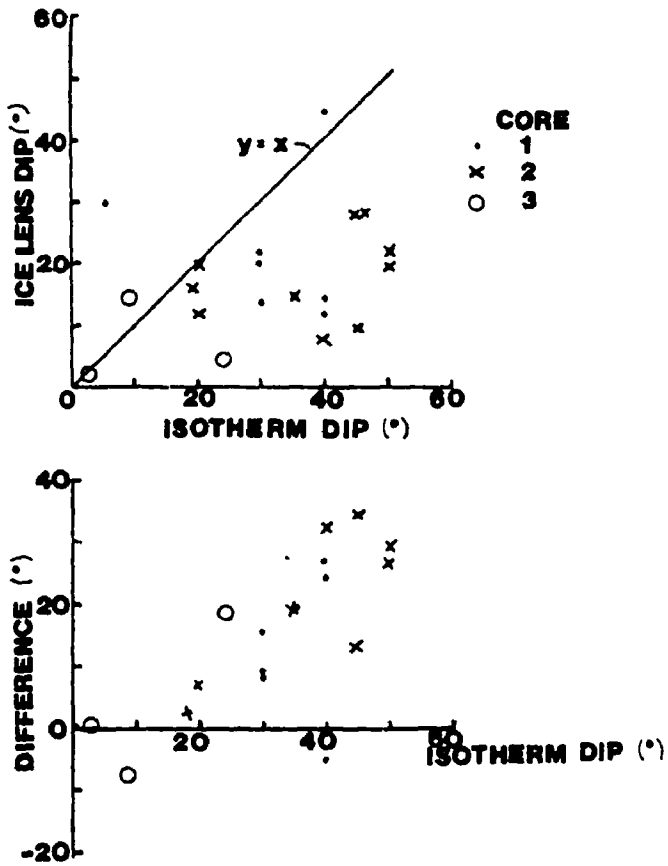

FIGURE 6.4. Comparison of isotherm and ice lens patterns in pit 1. Isotherm pattern is based on the isotherm pattern in the most recent layer to exhibit heave on a given day.

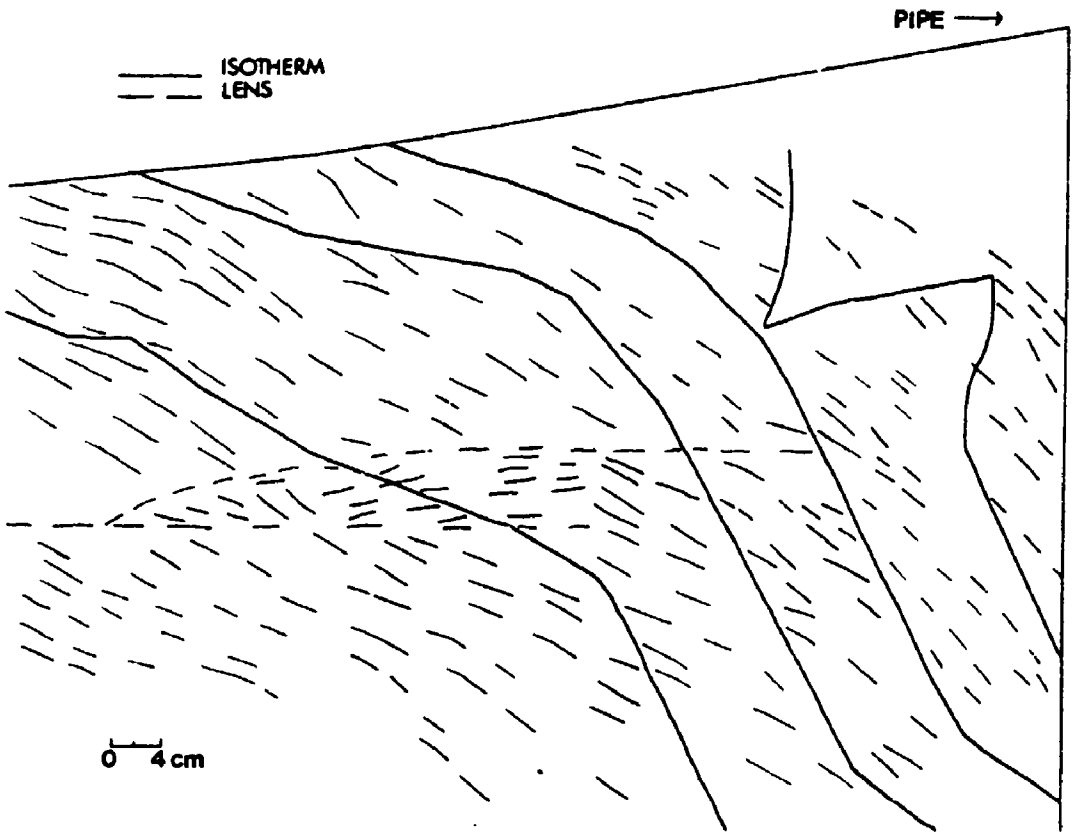

become similar. The isotherm dip is generally larger than that of the ice lenses (figure 6.5). The difference between the angles of inclination of isotherms and ice lenses becomes larger as the isotherm dip increases (figure 6.5). The ice lens pattern in the distinct layer in the middle of figure 6.4 does not match the isotherm pattern.

6.3.2 *Discussion*

The ice lenses and isotherms both show a curved pattern which clearly illustrates that the pipe acts as a heat sink and influences the ice lens orientation. The similarities between the ice lens and isotherm patterns indicate that there is a tendency for ice lenses to form perpendicular to the direction of heat flow. The two patterns are not exactly the same which suggests that other factors influence the ice lens orientation.

Ice can only continue to accumulate if the resistance of the surrounding frozen soil can be overcome. Accordingly there is a tendency for ice lenses to expand in the direction of least resistance which would be upwards. There is a tendency therefore, for ice lenses to be horizontal or parallel to the ground surface. Maximum resistance would be encountered by ice lenses oriented vertically.

It can be seen from figure 6.2 that the two patterns are similar at distances greater than 1 m from the pipe and where the isotherms are close to being horizontal. In this case the direction of heat flow and least resistance are

FIGURE 6.5. Relationship between isotherm dip and ice lens dip in pit 1. "Difference" refers to the difference between isotherm and ice lens dip angles (isotherm-ice lens).

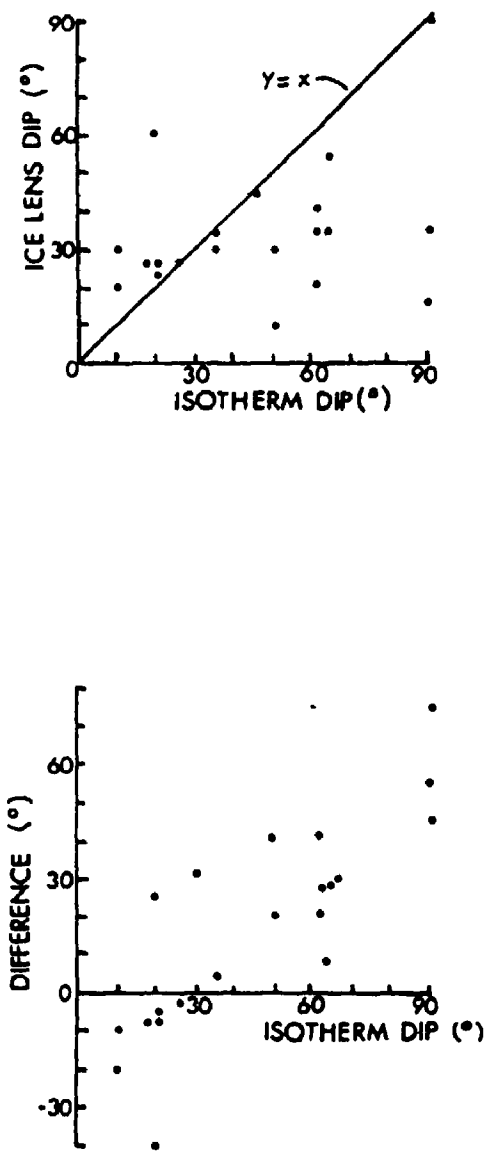

similar and ice lenses will have an orientation that resembles that of the isotherms.

Closer to the pipe, where isotherms are inclined at a steeper angle the two patterns become dissimilar (figure 6.2). The difference between the two patterns becomes greater as the dip angle of the isotherms increases (figure 6.3). If ice lenses were to grow in the direction of heat flow where isotherms are dipping steeply, there would be a large amount of resistance provided by the frozen ground and the pipe. This would not be a preferred orientation for ice lenses There would be a tendency for the ice lenses to expand in a direction that has a larger vertical component rather than a horizontal one. The result would be ice lenses that are inclined at a smaller angle than the isotherms. The resistance of the frozen soil therefore is a factor controlling the orientation of the ice lenses but the fact that the ice lenses are oriented around the pipe indicates that it is not the sole factor.

Other observations also suggest that the mechanical conditions are important in influencing ice lens orientation and distribution. Ice lens thickness also increases with distance from the pipe (figure 6.6). While this increase in thickness is likely due to a smaller temperature gradient there is considerable scatter which suggests other factors may be important. Near the pipe, growing ice lenses dip steeply toward the pipe and probably meet with more

FIGURE 6.6. Relationship between ice lens thickness and distance from the pipe.

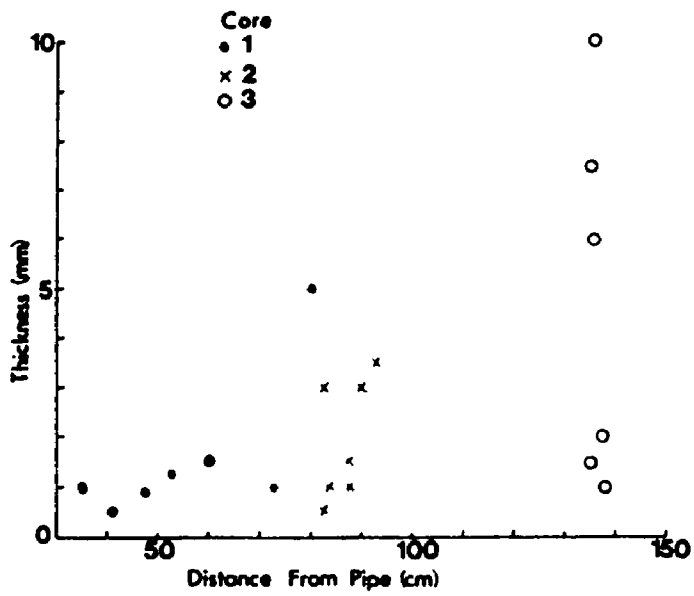

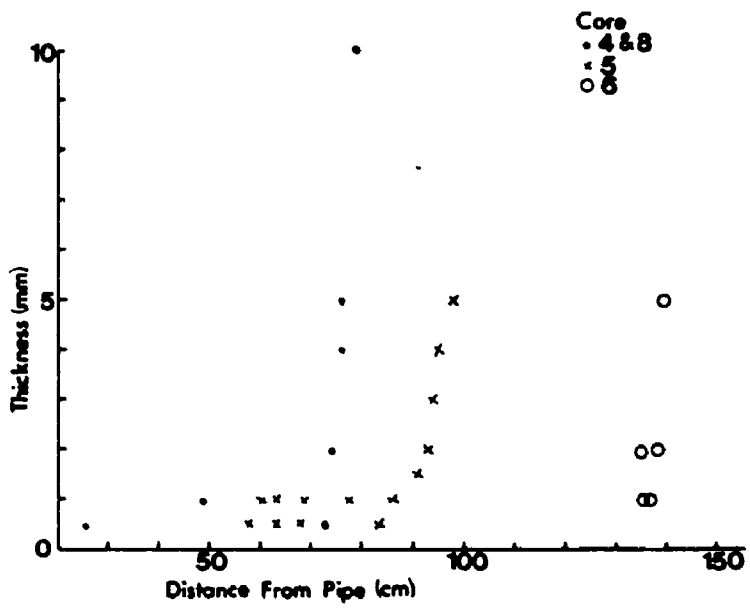

resistance here than at some distance from the pipe. Figure 6.7 shows that ice lenses that dip at a steep angle toward the pipe tend to be smaller and closer together than those that dip at a smaller angle or are horizontal.

The orientation of ice lenses is controlled by at least two factors, the direction of heat flow and the resistance of the frozen soil. Ice lenses will form such that their orientation is somewhere between that of the direction of heat flow and the direction of least resistance.

6.4 Continuing Heave and Ice Lens Orientation

In the above analysis of the relationship between the isotherm and ice lens pattern, only the isotherm pattern in the most recent layer to heave (primary heave - referred to as "new heave" in figures 5.11 to 5.13) was considered when constructing figure 6.2. Heave and growth of ice lenses in the already frozen soil (continuing heave) above this layer was not considered. The possibility exists that ice lenses that still continue to grow while the next layer starts to heave may have an orientation that is different from the orientation they had when they initially formed. This may account for some of the difference between the ice lens and isotherm patterns. To investigate this possibility, the isotherm pattern in the soil layer that continues to heave was determined and compared to the pattern of ice lenses at site 1 (figure 6.8).

Next to the pipe (core 1) the isotherm pattern during

FIGURE 6.7 Relationship between ice lens thickness and ice lens dip.

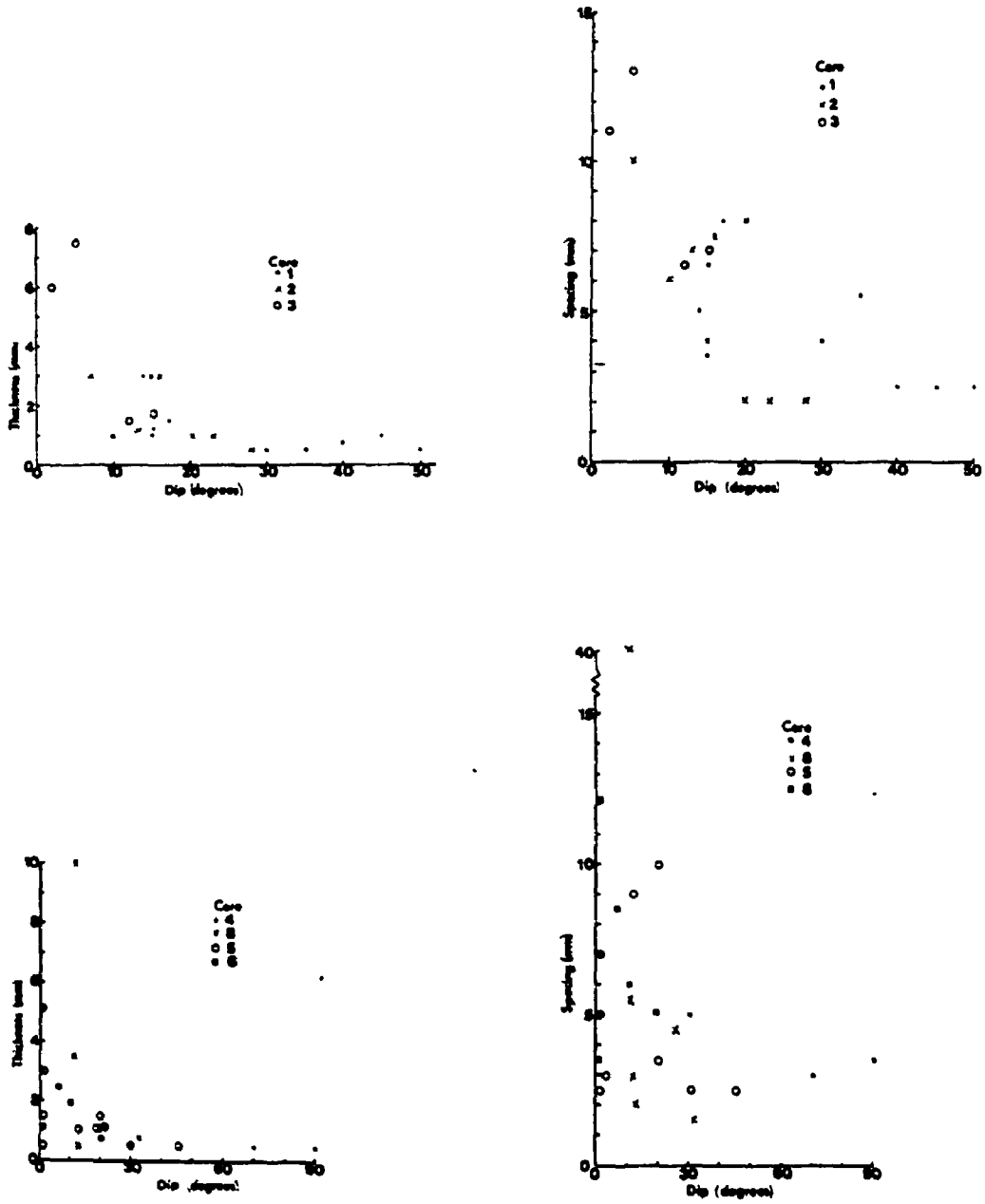

FIGURE 6.8. Comparison ice lens and isotherm patterns during continuing heave at site 1. Isotherm pattern is based cn the isotherm pattern in the layer exhibiting continuing heave on a given dav.

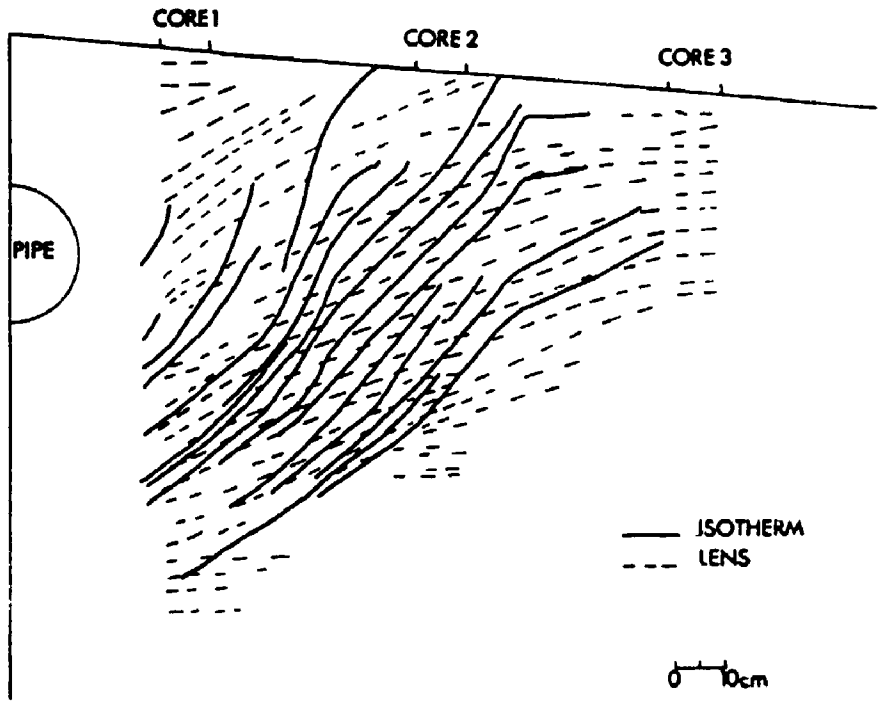

continuing heave is similar to that during primary heave and therefore has the same relationship with the ice lens pattern. At core 2, the isotherms during continuing heave are inclined at a steeper angle than those during primary heave in the upper part of the ground. The difference between the isotherm pattern during continuing heave and the ice lens pattern is greater than the difference between the isotherm pattern during primary heave and the ice lens pattern. In fact, the isotherms during primary heave are almost parallel to the ice lenses in the upper part of the ground. In the lower part of the frozen zone the isotherm pattern during continuing heave is similar to that during primary heave. At distances greater than 1 m from the pipe the two isotherm patterns are the same.

These results do not prove conclusively that the ice lens orientation does not change as the direction of heat flow changes. They do suggest however, that if the orientation of the ice lenses does change, it likely does not change very much. The orientation certainly does not change enough to account for the discrepancy between ice lens and isotherm patterns.

6.5 Ice Veins and the Thermal Regime

Ice bodies exhibiting no preferred orientation were observed next to the pipe (figure 6.9). The pattern of ice veins shows no similarity to the isotherm pattern. These reticulate ice veins have been described by Van Vliet-Lanoe

FIGURE 6.9. Ice veins in frozen soil next to the pipe at site 2, 47 to 71 cm below the surface. The pipe is on the left side of the photograph.

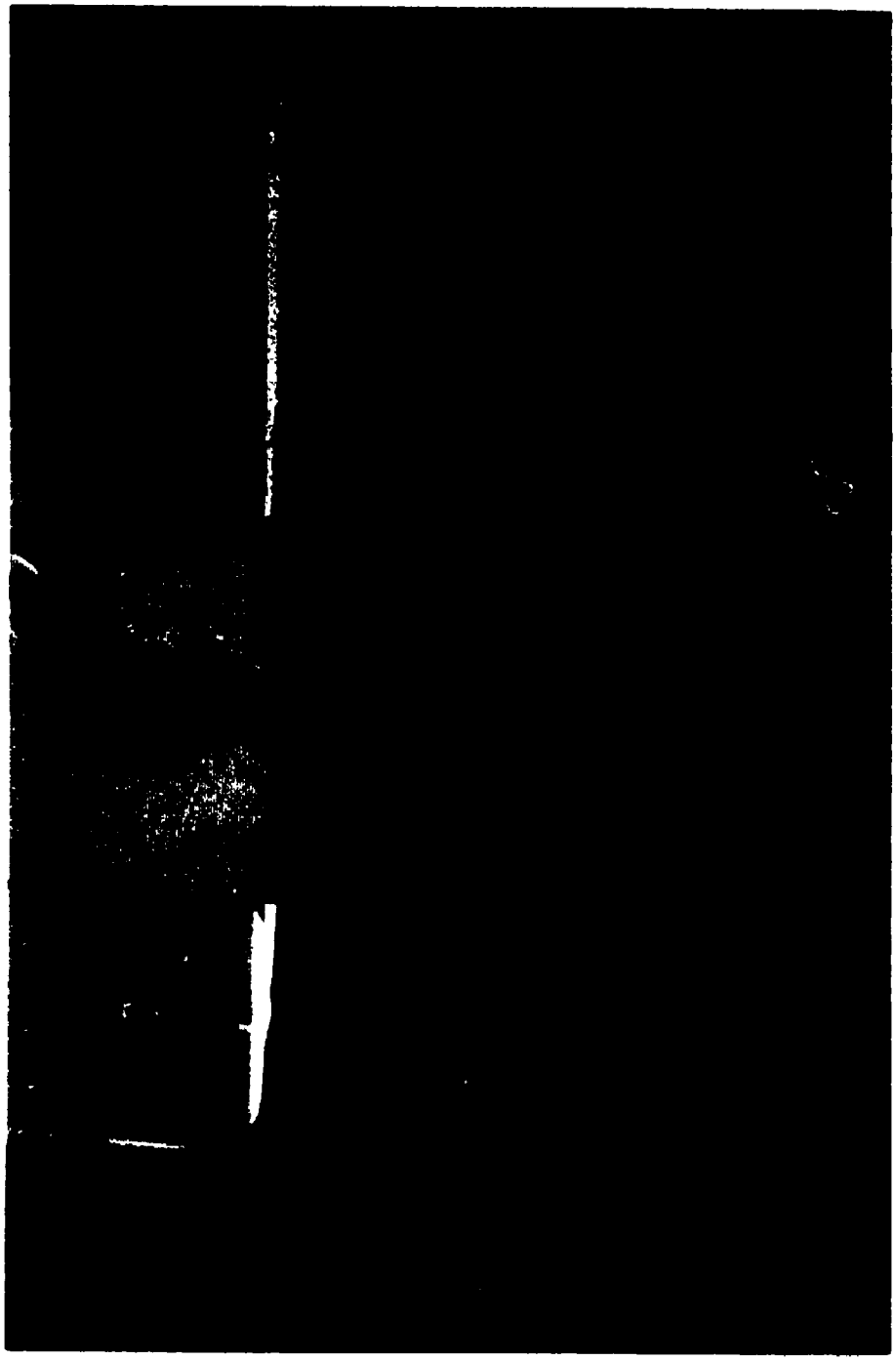

et al. (1985) and have a similar pattern to that described by Mackay (1974). The ice was observed to surround hard compacted aggregates of soil. Mackay found reticulate ice veins in lake and marine clays in northern Canada in which ice surrounded clay blocks free of visible ice lenses. The blocks were overconsolidated and released little water during thawing. Mackay proposed that reticulate ice veins grow in preference to ice lenses because of restrictions on the flow of water which is a requirement of ice lens formation. Water drawn from the frozen and unfrozen soil causes shrinkage of the clay and cracks form. The shrinkage cracks fill with ice as water is drawn from the adjacent soil blocks. McRoberts and Nixon (1975) suggested that large suctions created by an advancing freezing front will create high effective stress in the unfrozen soil below, resulting in consolidation and cracking if there is no access to water. Water which fills the cracks and freezes is obtained from consolidation of the soil.

The growth of ice veins is favoured by a steep temperature gradient and low permeability in structureless soils. These conditions would exist next to the pipe where ground temperature and permeability are low. The veins that were observed at the experimental site were likely formed by cracking associated with consolidation because they are found where the temperature gradients were steep and the soil freezing was rapid (Dupas and Van Vliet-Lanoe 1988 and

Van Vliet-Lanoe et al. 1985). Water flow to this location would therefore, be limited. The existence of the veins indicates that the rate of heat flow as well as the direction of heat flow determines the location and pattern of ice lenses.

It should also be noted that there is no net addition of water to the area of the soil containing the ice veins. The ice veins derive their water from the adjacent soil blocks (Mackay 1974) and there is no formation of excess ice. This is supported by the moisture content observations (figures 5.18 and 5.19). Moisture content of the frozen soil containing the ice veins tends to be low compared to frozen soil containing ice lenses of a preferred orientation.

6.6 Ice Lens Orientation in the Distinct Layer

The ice lens pattern in the distinct layer observed in pits 1 and 2 and in the cores at site 2 (figures 5.4, 5.5 and 5.6) shows no similarity to the isotherm pattern. Clearly factors other than the direction of heat flow are important in determining the ice lens pattern at these locations. The fact that ice lenses are horizontal in the distinct layer would indicate that they are growing in the direction of least resistance and that the mechanical properties of the soil are the major controlling factors on ice lens formation. It is not clear however, why horizontal lenses are found in this particular layer. The distinct

layer is located at the level of the pipe and it is possible that the pipe offers resistance to ice lenses growing towards it. The distinct soil layer may also be explained in terms of the soil properties.

Carlson and Nixon (1988) concluded from observations of horizontal ice lenses around a buried pipe at a Calgary test site that ice lens orientation is controlled by stratigraphic factors rather than heat flow direction. There were textural changes at the Calgary test site of silt to clay which were thought to be responsible for the horizontal orientation of lenses. Lithic discontinuities or stratification of sediment can influence the location of ice lenses (Van Vliet-Lanoe 1985) through local changes in hydraulic conductivity and porosity. Ice lensing will generally follow the bedding in stratified sediment whereas in uncompacted sediments the location of the ice lenses will be influenced by the direction of the thermal gradient. At the Caen site there are no textural changes but there could be variations in soil density which would result in variations in hydraulic conductivity. The existence of the distinct layer is not due to random variations in density since it is found on both sides of the pipe and presumably is found along the length of the pipe in the silt section. This layer is at the level of the pipe and it is possible that while the pipe was being installed, equipment and people on the ground surface along the pipe caused some

additional compaction of the soil (Dumoulin et al. 1987). Dry bulk density data (figure 5.19) indicate that this soil layer may have been compacted.

A dense soil layer may offer more resistance to heave and result in ice lenses orienting themselves horizontally. The particles making up the soil may also become aligned in such a way during compaction which only allows for horizontal orientation of ice lenses (Van Vliet-Lanoe personal communication 1989).

The straight ice lens in pit 1 which is horizontal near the pipe and gently dips away from the pipe with distance from the pipe (figure 5.4) could be following the top of the compacted layer. The horizontal lens 6 cm below this is likely following the bottom of the compacted layer.

Penner (1986) observed the growth of ice lenses in varved clay and silt samples and found that lenses tend to grow at the top of the clay layer. The dense soil layer could be acting like the clay layer and the ice lenses are growing along the top of it.

In summary, the existence of the distinct layer shows that factors other than the thermal regime influence the ice lens pattern. Abrupt changes in soil density appear to cause abrupt changes in the ice lens pattern. The ice lenses will tend to grow along the boundaries separating material of different densities.

6.7 Ice Lens Orientation Parallel to the Pipe

The ice lens pattern parallel to the pipe was compared to the isotherm pattern. Figure 6.10 shows the position of the 0°C isotherm 25 cm from the pipe axis on selected days during the freezing period. The 0°C isotherm generally dips in the direction of the sand with the steepest dip occurring at the transition. At the end of the experiment the 0°C isotherm dips approximately 7° toward the sand in the transition zone. It can also be seen from figure 6.10 that the freezing front penetrates to a greater depth in the sand and in the silt near the transition than it does at site 1.

The freezing front penetrated at a higher rate in the sand because the thermal diffusivity of the sand is greater than that of the silt. The apparent thermal diffusivity of the silt near the sand-silt boundary was probably greater than that at site 1. The moisture content of the silt was generally found to be lower in the transition zone and this indicates that there was less water migration and less ice accumulation at this site. The sand would offer resistance to heave in the adjacent silt so that less ice accumulation occurs at site 2 than at site 1. A smaller amount of latent heat was released during freezing of the silt near the transition and the apparent heat capacity was generally lower than at site 1. The result would be a higher apparent thermal diffusivity and a greater rate of frost penetration near the transition than at site 1. The difference in

FIGURE 6.10. Position of 0°C isotherm along pipe axis, 25 cm from the pipe axis (from Geotechnical Science Laboratories 1989).

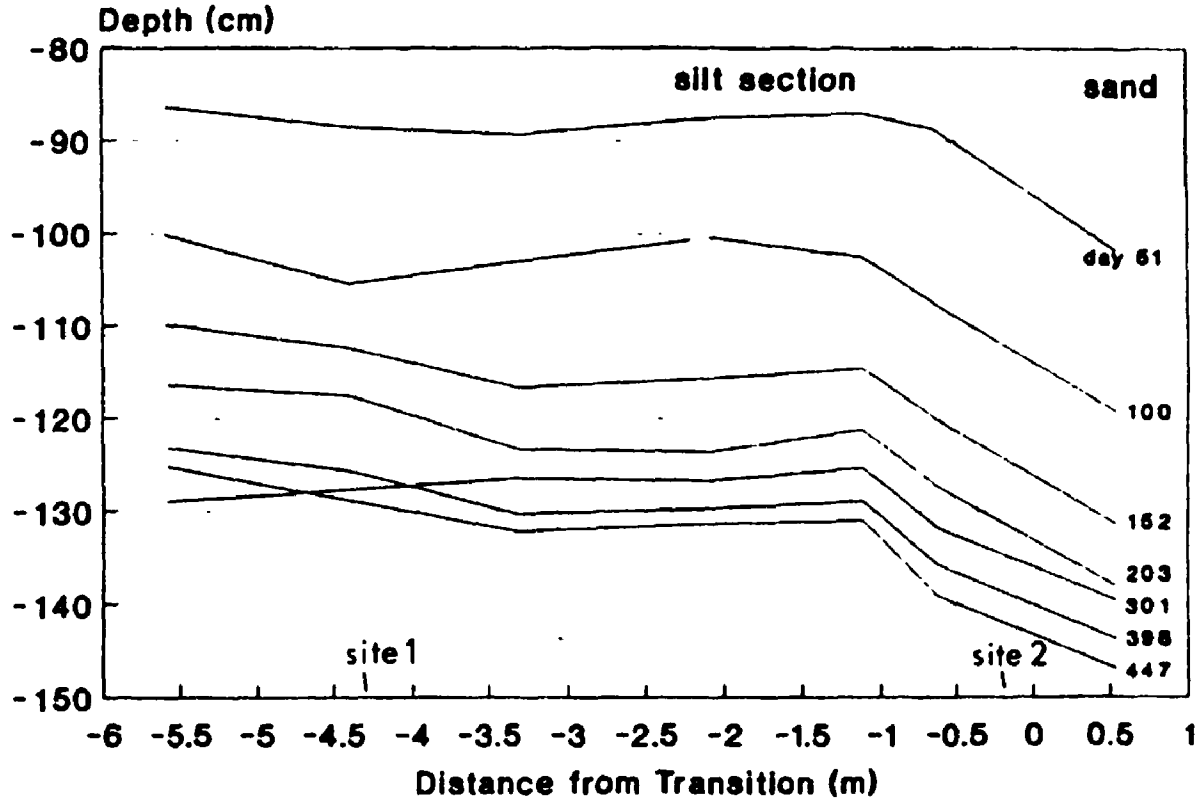

thermal properties was reflected in the difference in the depths of the last ice lenses at the two sites. Ice lenses were found at a greater depth in the silt near the transition than at site 1.

Ice lenses and isotherms were both found to dip toward the sand (figures 5.7, 5.8 and 6.10), indicating that the heat flow direction is of primary importance here in determining the ice lens pattern. Van Vliet-Lanoe (1988) also made similar observations. However, other factors are important in determining the ice lens pattern parallel to the pipe. Ice lenses were found to dip more steeply than the isotherms at the transition and ice lenses appear to follow the boundary between the two soils and were not found in the sand (figure 5.8). Carlson and Nixon (1988) and Van Vliet-Lanoe (1985) found that in stratified materials, ice lenses follow the bedding rather than forming perpendicular to the thermal gradient. The ice lens pattern in the transition zone therefore is influenced by the variation is soil texture.

The sharp bending of the ice lenses 30 to 40 cm from the sand-silt boundary cannot be explained by the heat flow direction but may be explained by the difference in frost susceptibility and heave characteristics of the two soils. The difference in the heave characteristics of the two soils can be seen in figure 6.11. Very little heave occurs in the sand and the amount of heave occurring in the silt decreases

FIGURE 6.11. Surface elevation parallel to the pipe (vertical exaggeration = 40 times).

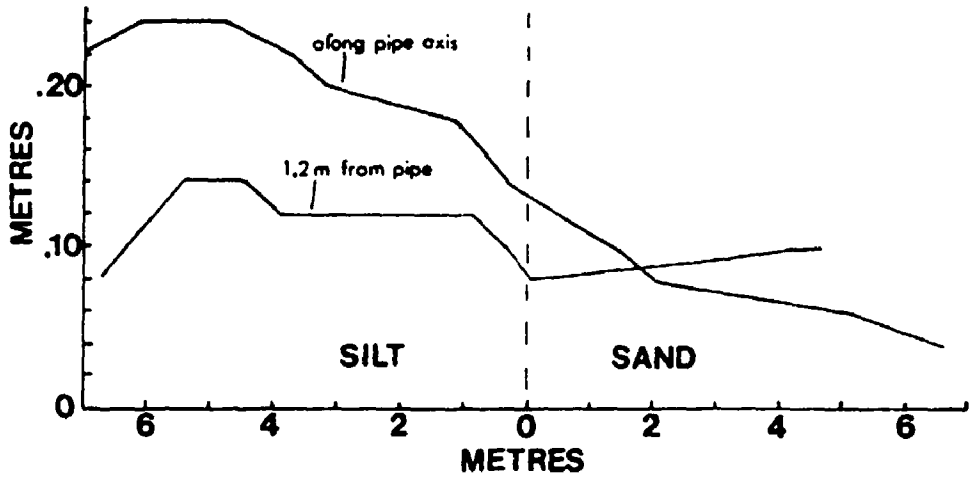

as the sand-silt boundary is approached. As ice lenses grow in the silt, the silt expands and exhibits heave while the sand does not. The frozen sand may act as an anchor and provide resistance to heave in the silt. This is probably responsible for the deformation or sharp bending of the ice lenses that was observed 30 to 40 cm from the sand-silt boundary. Van Vliet-Lanoe also observed that ice lenses bend toward the less frost susceptible material.

The suggestion that the resistance to heave is greater near the transition is supported by soil pressure measurements at the experimental site (Geotechnical Science Laboratories 1989 and Smith and Onysko 1990). Greater pressures were found to develop near the transition than near site 1. Smith and Onysko (1990) suggest that at site 1 the silt is largely unrestrained from heaving while near the transition zone the resistance to heave becomes greater. This would explain the decrease in heave in the silt that occurs towards the transition.

It is clear from these observations, that while the direction of heat flow and the variation in thermal properties influence the ice lens pattern, other factors are also important. The variation in soil texture was observed to influence the orientation of the ice lenses. The differences in the rheologic properties of the two materials also influences the ice lens pattern. The greater resistance to heave offered by the adjacent sand is probably

responsible for the deformation of ice lenses in the silt near the transition.

6.8 Heave Direction and Components

Often, heave is considered to occur in a vertical direction because the ground surface is observed to be displaced upwards and heave measurement instruments (eg. magnet heave devices) measure vertical displacements of soil. Heave occurs perpendicular to the ice lenses because ice lenses expand in that direction. The ice lens patterns observed around the pipe indicate that heave does not always occur in a vertical direction (figure 6.12). Heave is directed toward the pipe near the pipe and at distances of greater than 1 m from the pipe, heave is almost vertical.

Clearly, heave or strain consists of vertical and horizontal components (figure 6.13) and the resultant heave is the sum of these components. The horizontal component and the heave perpendicular to the ice lenses can be resolved using data from the magnet heave devices and the dip angle (α) of the ice lenses (see figure 6.13).

The magnitude of the horizontal component of heave and the magnitude of heave (in cm) occurring perpendicular to the ice lenses at site 1 have been calculated for each soil layer defined by the magnet heave devices (table 6.1). The magnitude of the heave components have also been computed as the percent strain (table 6.1). The ratio between horizontal and vertical components has been calculated and

FIGURE 6.12. Magnitude (given in cm in (a) and as % strain in (b)) and direction of heave components perpendicular to the pipe at site 1.

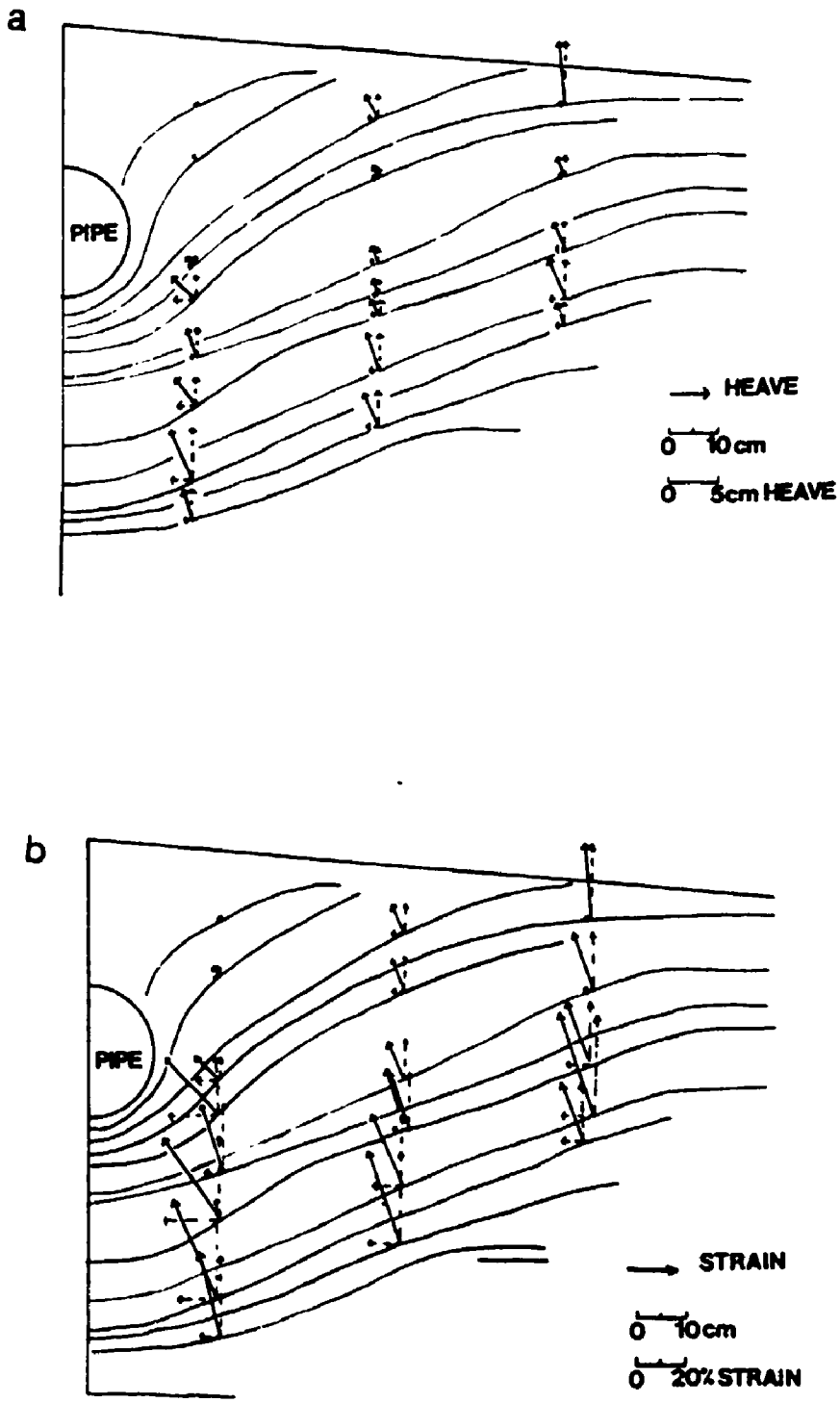

FIGURE 6.13. Resolution of heave components.

Magnitude of horizontal strain = vertical strain x (tan α)

Mag. of strain perpendicular to ice lens = vert. strain/cosα

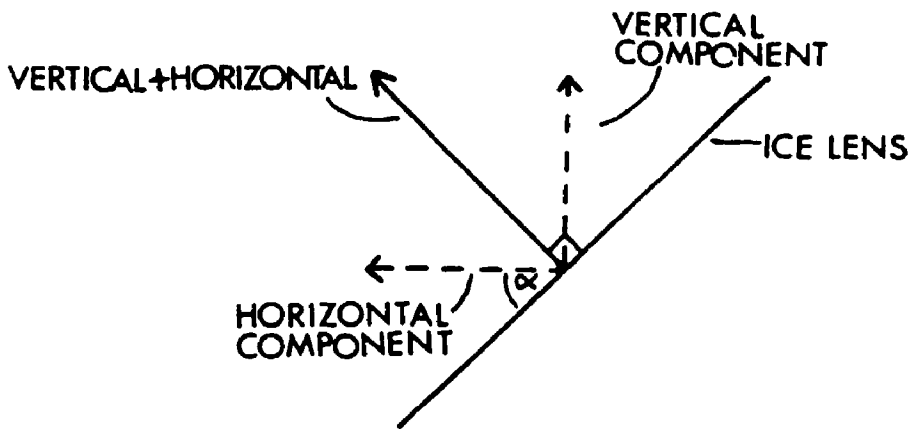

TABLE 6.1. Magnitude of heave components at site 1.

Layer Depth (cm)	Dip of Lens	Heave (cm) V	H	R	%Strain V	H	R	Ratio H/V
25 cm from pipe								
0-23	27°	.17	.09	.19	.7	.35	.8	.53
23-33	32°	.38	.24	.45	4.1	2.6	4.8	.63
44-55	46°	1.02	1.05	1.47	11.3	11.6	16.3	1.03
55-67	42°	2.50	2.24	3.36	25.5	22.8	34.2	.89
67-81	18°	3.30	1.07	3.47	29.7	9.5	31.2	.32
81-93	34°	3.19	2.15	3.85	37.3	25.0	45.1	.67
93-111	23°	5.58	2.37	6.06	45.1	18.9	49.1	.42
111-124	15°	3.63	.97	3.76	36.8	9.9	38.3	.27
63.5 cm from pipe								
0-23	28°	2.83	1.51	3.21	13.9	7.5	15.7	.54
23-34	24°	1.49	.66	1.63	15.8	6.9	17.2	.44
34-47	24°	1.96	.87	2.15	18.1	8.5	19.7	.47
47-59	18°	1.89	.61	1.99	18.9	6.0	19.8	.32
59-69	19°	2.07	.71	2.19	25.3	8.6	26.8	.34
69-86	25°	4.20	1.96	4.63	31.7	14.9	34.9	.47
86-100	21°	3.95	1.51	4.23	41.5	15.8	44.4	.38
1 m from pipe								
0-27	4°	6.96	0.49	6.98	34.1	2.4	34.1	.07
27-39	21°	2.36	.91	2.53	25.4	6.1	27.2	.24
39-53	23°	2.97	1.26	3.23	27.4	11.5	29.9	.42
53-67	23°	4.28	1.82	4.65	44.6	16.9	48.6	.38
67-79	22°	2.54	1.03	2.74	27.3	11.2	29.5	.41
2 m from pipe								
0-27	0°	4.81	0	4.81	22.2	0	22.2	0
27-35	0°	0	0	0	0	0	0	-
35-47	0°	.02	0	.02	.20	0	.20	0

Heave Components
V = Vertical
H = Horizontal
R = Resultant (perpendicular to ice lens)

is presented in table 6.1. Figure 6.12 shows the magnitude of the heave components perpendicular to the pipe at site 1.

The vertical component of heave is generally greater than the horizontal component because ice lenses usually were found to dip at an angle that is less than 45°. At distances greater than 60 cm from the pipe where ice lenses dip at an angle less than 30°, the ratio between horizontal and vertical components is less than 0.5. Near the pipe the horizontal component of heave becomes more important because ice lenses dip at a larger angle. The horizontal and vertical components are almost the same size at pipe level (dip of ice lenses is approximately 45°).

The strain appears to be smaller in layers where the horizontal component is large (where ice lenses dip at a greater angle). Ice lenses expanding in these layers would encounter greater resistance to heave and there would be little accumulation of ice in this area. Ice lens thickness was observed to be smaller here also.

It is also interesting to note that if the ice lens pattern had been the same as the one suggested by the isotherm pattern, the contribution of the horizontal component of heave would have been much larger near the pipe because ice lenses would have dipped toward the pipe at a greater angle. Ice lenses expanding in a horizontal direction would meet more resistance to heave than those expanding in a vertical direction. Ice lenses therefore

would tend to orient themselves such that they thicken in the direction of least resistance and heave will tend to have a greater vertical component.

These results show a complex pattern of heave and suggest that the displacement of the pipe is not simply due to the pipe being lifted up by a force acting in a vertical direction directly below the pipe. Assuming that a similar pattern of heave exists on both sides of the pipe, it appears that the pipe is being squeezed as ice lenses grow around the pipe. Forces directed toward the pipe having a large horizontal component would also cause displacement of the pipe.

Evidence of a horizontal component of heave is also provided by displacement gauges. A series of wooden cylinders approximately 5 mm in diameter and 5 mm in height were placed in a vertical line in the soil before the freeze cycle commenced. At the conclusion of the freeze cycle the soil was excavated and the position of the cylinders was mapped (White personal communication 1989).

Horizontal displacement of the cylinders away from the pipe was found to occur (figure 6.14). The maximum displacement occurred at the level of the pipe where ice lenses have a steeper dip and where the horizontal component of heave is greater.

These results suggest that horizontal stresses develop within the freezing soil and cause displacement of material

FIGURE 6.14. Position of displacement gauges (dots) at the end of the freeze cycle. The vertical lines represent the initial position of the gauges (data collected by T.L. White 1989).

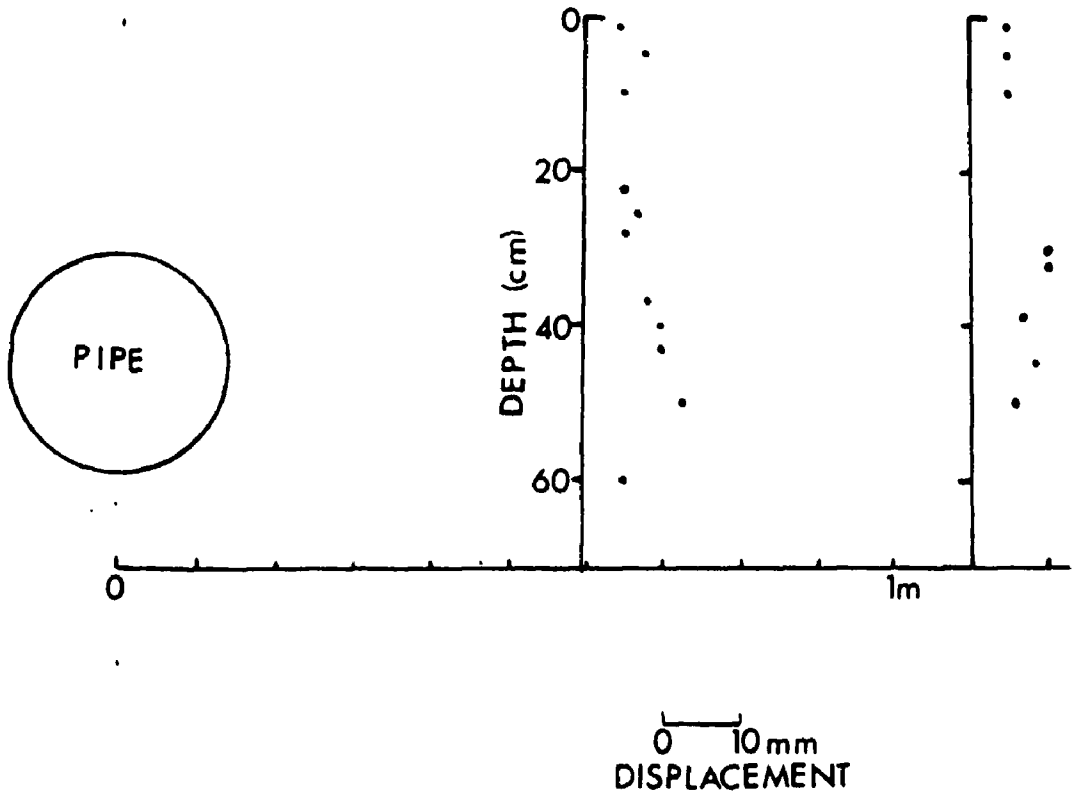

in the direction of least resistance which is toward the unfrozen soil (away from the pipe). This would also suggest that there are two components of heave.

The displacement of the wood cylinders is in the opposite direction to the horizontal heave component that was calculated (figure 6.12 and table 6.1). It is possible that as ice lenses expand, stresses develop in both directions (toward and away from the pipe) with a larger stress being directed away from the pipe in the direction of least resistance.

Observations of ice lens orientation parallel to the pipe suggest that there is a third component of heave that is directed toward the sand. The small amount of heave that is measured in the sand likely originates in the silt at the transition. The observations of the ice lens orientation suggest that the stresses that develop during freezing and the displacements that occur are three dimensional and that a model of frost heave should take this into account.

CHAPTER SEVEN

THERMAL PROPERTIES INTERPRETED FROM A THERMODYNAMIC RHEOLOGICAL PERSPECTIVE

7.1 Introduction

The results of the laboratory experiments (chapters 3 and 4) show that the stresses which develop in a freezing soil depend on the thermodynamic and rheologic conditions of the frozen soil. Observations of ice lens distribution and orientation (chapters 5 and 6) also imply that the resistance of the frozen soil is an important factor controlling ice segregation and heave. Variations in other soil properties such as texture and density also influence ice lens formation.

The experimental results suggest that a frost heave model is required which links together heat and water flow with the rheologic conditions. Shen and Ladanyi (1987) present a theoretical model which couples heat, moisture and stress fields but they do not consider directly, the effect of frost heave on the thermal properties of the soil. The following discussion will consider that not only is the rheologic behaviour important in determining the amount of heave that will occur but also in determining the thermal properties of the frozen material.

7.2 Thermal Properties

7.2.1 *Heat capacity*

The heat capacity for heterogeneous material such as soil is the sum of the heat capacity of the proportional parts (Williams 1982). In the case of soil freezing or thawing, it is convenient to refer to the apparent heat capacity which represents the sum of the true heat capacity and the latent heat associated with the phase change. The apparent volumetric heat capacity may be determined using the following (Smith and Riseborough 1985, Williams 1982 and 1991):

$$C_{vT} = X_s C_s + X_i C_i + X_w C_w + \rho_d L (d\theta_w/dT)_T \qquad (7.1)$$

C_{vT} = Apparent volumetric heat capacity of the soil at temperature T ($Jm^{-3}{}^{o}C^{-1}$)

C_s, C_i, C_w = Volumetric heat capacity of soil mineral component, ice and water

X_s, X_i, X_w = Volume fractions of soil mineral component, ice and water

ρ_d = dry density (kgm^{-3})

θ_w = gravimetric unfrozen water content

$(d\theta_w/dT)_T$ = change in unfrozen water content with temperature at temperature T (slope of unfrozen water content curve)

L = Latent heat of fusion of water

The relationship between unfrozen water content and temperature is required to use equation 7.1 and this relationship was determined for Caen silt as described in chapter five (Equation 5.2). The data were collected by Patterson (personal communication 1988) using TDR (Patterson

and Smith 1981). The slope of the unfrozen water content curve at a given temperature, determined by evaluating the derivative of equation 5.2 is used to determine the apparent heat capacity. The expansion of soil and the accompanying decrease in dry density during freezing must be taken into account in the calculation.

Apparent volumetric heat capacity is plotted as a function of temperature in figure 7.1. The heat capacity (without the latent heat term) has also been plotted for comparison. While the volumetric heat capacity varies with temperature as the relative amounts of water and ice change, this influence is minor compared to that of the latent heat term.

At temperatures close to 0°C the apparent heat capacity decreases rapidly with decreasing temperature (figure 7.1) because the formation of ice decreases rapidly with temperature. Precise determination of unfrozen water content is important at these temperatures because the latent heat term in equation 7.1 may change by orders of magnitude over a very small temperature range.

7.2.2 *Thermal conductivity*

The thermal conductivity of a soil depends in a complex way on the composition of the soil and can be estimated using a geometric mean equation (Johansen 1973):

$$k_T = k_w^{X_w} k_i^{(n-X_w)} k_s^{(1-n)} \qquad (7.2)$$

k_T = thermal conductivity at temperature T ($Wm^{-1}K^{-1}$)

FIGURE 7.1. True and apparent volumetric heat capacity for frozen Caen silt as a function of temperature, calculated for two initial dry densities.

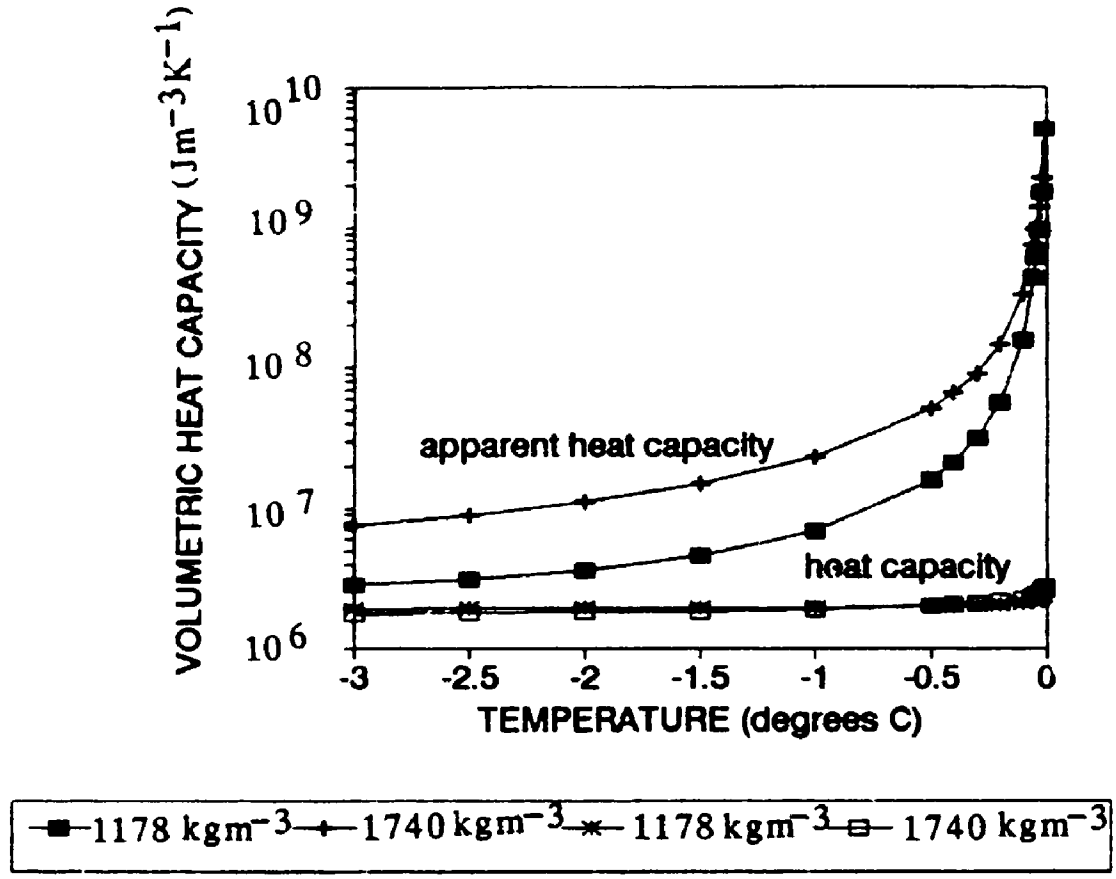

k_w, k_i, k_s = thermal conductivity of water, ice and soil minerals

n = porosity

The thermal conductivity of frozen soil increases with decreasing temperature as the ice content increases (figure 7.2). The increase in thermal conductivity with declining temperature is rapid at temperatures close to 0°C because there is a rapid rise in ice content.

7.2.3 *Thermal diffusivity*

The total thermal response of a soil is represented by the thermal diffusivity (Oke 1978):

$$\alpha = k/C_v \tag{7.3}$$

α = Thermal diffusivity (m^2s^{-1})

Thermal diffusivity may be used to estimate the propagation of a temperature change such as the movement of the freezing front (Lunardini 1981):

$$\frac{\partial T}{\partial t} = \alpha\frac{\partial^2 T}{\partial z^2} \tag{7.4}$$

The apparent thermal diffusivity of Caen silt has been determined using the estimated apparent heat capacity and thermal conductivity (figure 7.3). Thermal diffusivity increases as temperatures fall below 0°C because apparent heat capacity decreases and thermal conductivity increases. The rate of movement of the freezing front will therefore, increase as less soil water changes to ice. Thermal diffusivity will be more sensitive to changes in the

FIGURE 7.2. Thermal conductivity of frozen Caen silt as a function of temperature, calculated for two initial dry densities.

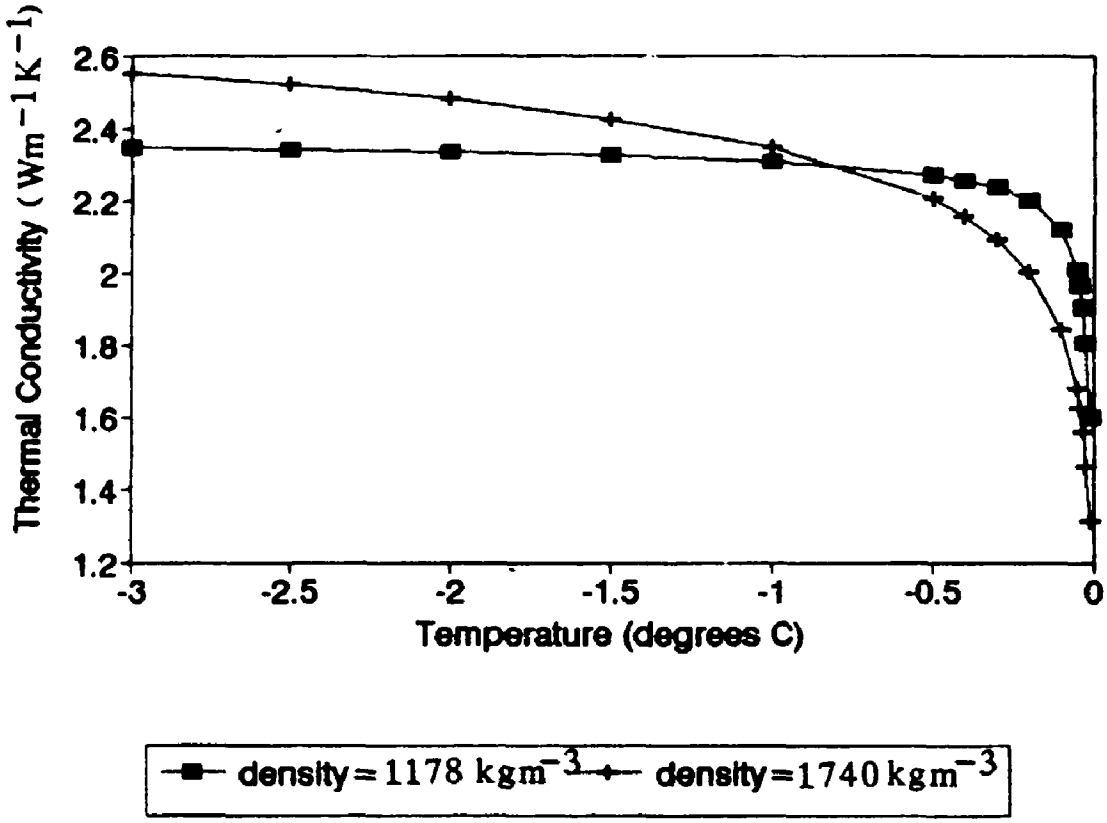

FIGURE 7.3. Apparent thermal diffusivity of frozen Caen silt of two different dry densities.

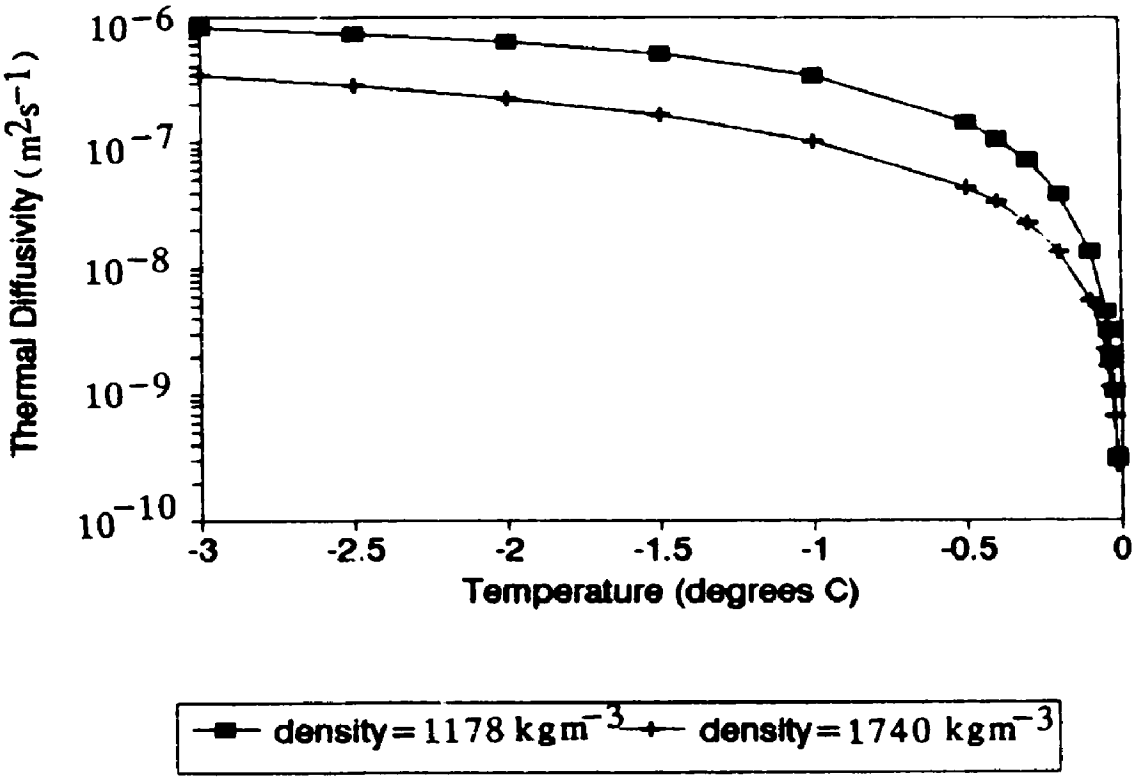

apparent heat capacity which may change through orders of magnitude over a small temperature change especially close to 0°C. It is important then, that the estimation of heat capacity be as accurate as possible. Thermal conductivity does not often vary by more than a factor of two so, small uncertainties in its estimation may be tolerated.

7.3 Water Migration and Ice Accumulation

The ice content of the soil may increase greatly during ice lens formation in response to water migration. Thermal conductivity will initially increase rapidly with ice content (figure 7.4) because ice has a higher thermal conductivity than water. As ice accumulates the thermal conductivity approaches the value for ice as the proportion of mineral soil decreases (dry density decreases).

Ice accumulation has an even more important effect on the apparent heat capacity because a large amount of latent heat is released as migrating water freezes. Lunardini (1981) suggests that the most common way to handle latent heat numerically is as an energy source or sink. The apparent heat capacity is defined to account for the entire enthalpy change including latent heat. It could be argued then, that the latent heat released by the freezing of migrating water should be treated in a manner similar to pore water and therefore, should be included in the apparent heat capacity of the soil.

Kay et al. (1981) incorporate the latent heat released

FIGURE 7.4. Thermal conductivity of frozen Caen silt as a function of volumetric ice content (calculated from equation 7.2).

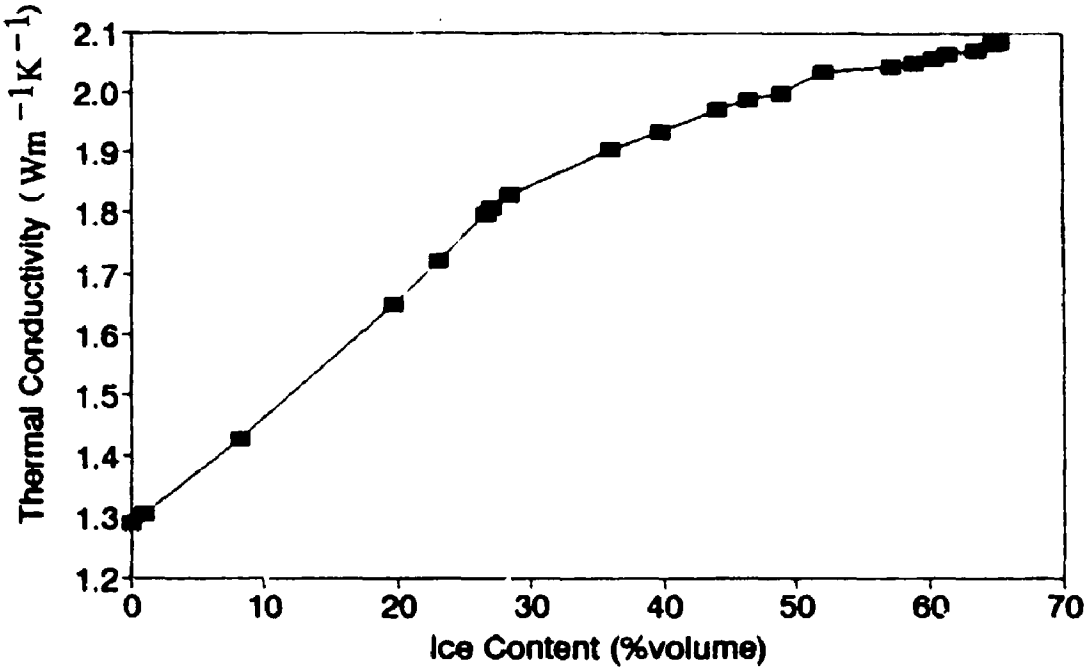

during the freezing of migrating water in the apparent thermal conductivity. Kay et al. (1981) calculated the apparent thermal conductivity for soils of various permeabilities and found that the apparent thermal conductivity could be up to two orders of magnitude greater than the true thermal conductivity. Limited experimental data however, were collected to assess the validity of dealing with the latent heat in this way.

The apparent thermal conductivity considers the amount of heat transported across the frozen fringe to the growing ice lens by conduction and latent heat transfer. The water that enters the frozen fringe is in liquid form and does not release latent heat until the phase change occurs at the ice lens. No heat is transported away from the unfrozen-frozen fringe interface by latent heat transfer since no phase change occurs there. It is argued here then, that there is no latent heat transfer across the frozen fringe because the migrating water does not undergo a phase change until it reaches the ice lens. The latent heat released as migrating water freezes therefore, should not be included in the thermal conductivity.

The thermal diffusivity that is calculated using the apparent thermal conductivity would be larger than that calculated using the true thermal conductivity. The larger thermal diffusivity would appear to suggest that the freezing front would progress at a higher rate through the

soil when water migration and freezing were occurring at a high rate. In reality this would not be the case. The release of large quantities of latent heat would decrease the rate of penetration of the freezing front and therefore result in a smaller thermal diffusivity. Ice lenses continue to grow at a fixed location for an extended period of time if the flow of heat to the ice-water interface occurs at a rate that equals or exceeds the rate of heat removal (conduction away from the ice-water interface) (Lunardini 1981). The latent heat released during ice lens formation will offset the conduction of heat away from the growing ice lens. It makes more sense then, to include the latent heat released by the freezing of migrating water in the apparent heat capacity and use this value in calculating the thermal diffusivity.

The apparent heat capacity was calculated using the heave data collected (see figures 5.15, 5.16 and 5.17) at the Caen pipeline site. The average temperature of a given soil layer marked by the magnet location was determined from the temperature data collected (Geotechnical Science Laboratories 1989) at the site. The apparent heat capacity was determined by first using equation 7.1, and a term was added which considers the latent heat released as migrating water freezes. The amount of ice accumulation over short periods of time was determined from the heave data and the amount of latent heat released per cubic metre of soil was

calculated. The temperature change over this period was also determined and the latent heat released by a unit volume per °C was calculated.

The apparent heat capacity which considers this additional latent heat is plotted through time for a soil layer located approximately 82 cm below the surface, 25 cm from the pipe (crosses in figure 7.5). The apparent heat capacity without the latent heat released during heave has also been plotted for comparison. Freezing in this layer commenced on day 80 and the apparent heat capacity rapidly increases to a maximum as in situ pore water freezes. Once the bulk of the pore water freezes the effect of water migration and ice lens formation becomes noticeable and the apparent heat capacity remains high. There is some scatter due to measurement error but the apparent heat capacity can be up to an order of magnitude greater than it would have been had heave not occurred. The apparent heat capacity is greatest when the heave rate is the largest.

The thermal diffusivity has also been calculated for the same soil layer (figure 7.6). During periods of high heave rates the thermal diffusivity may be an order of magnitude smaller than it would be if heave was not occurring. The release of latent heat during heave can be significant and the result is a retardation of the cooling rate of the soil.

There is another way of dealing with the latent heat

FIGURE 7.5. Apparent volumetric heat capacity for a layer of frozen Caen silt located 25 cm from the pipe, 82 cm below the ground surface. The upper curve ("With heave") includes the component of latent heat released as water migrating to the layer freezes.

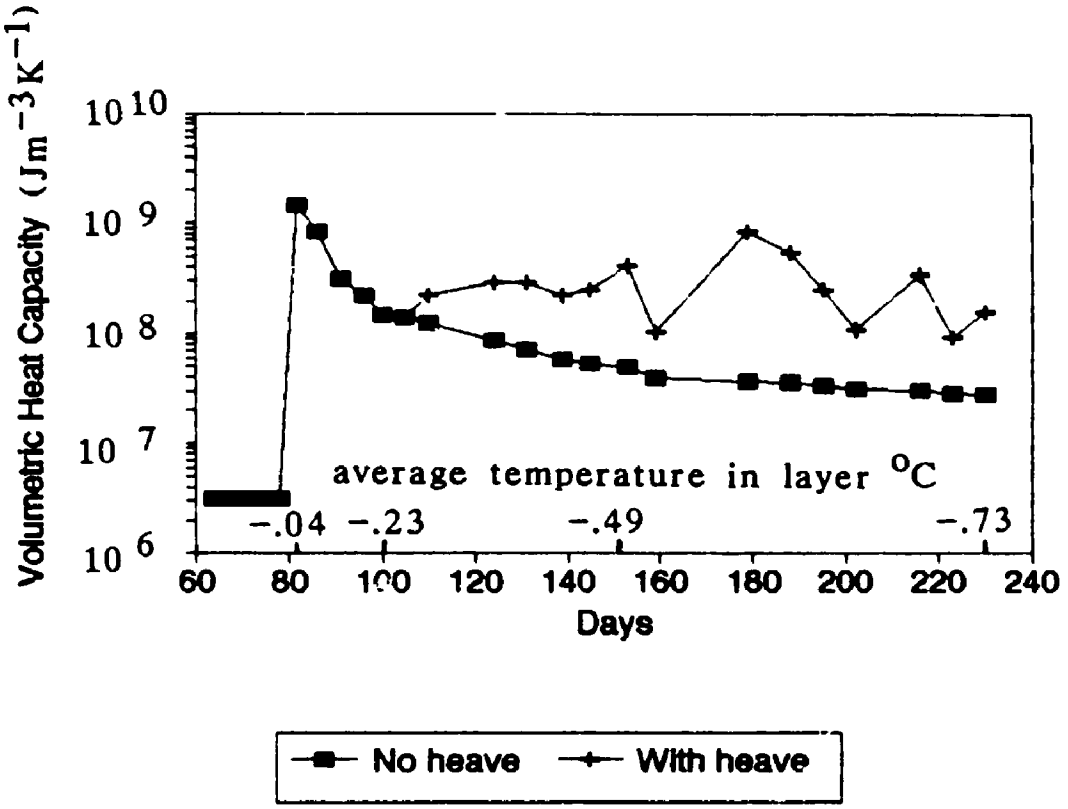

FIGURE 7.6. Apparent thermal diffusivity for a layer of frozen Caen silt located 25 cm from the pipe, 82 cm below the ground surface. "With heave" refers to the thermal diffusivity calculated using the heat capacity which includes the component of latent heat released as migrating water freezes.

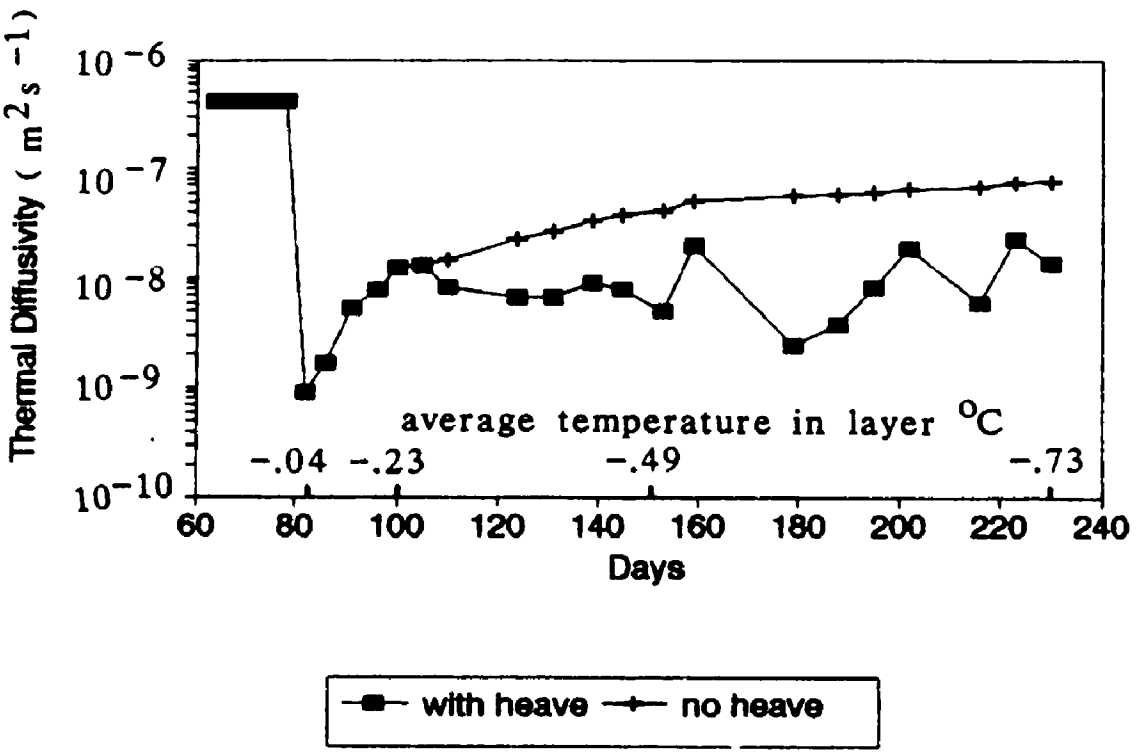

which is liberated during freezing. Konrad and Morgenstern (1980) do not use apparent heat capacity in their heat transfer equations but they do consider the internal heat generation per unit area per unit time:

$$\frac{\partial}{\partial z} k\frac{\partial T}{\partial z} + Q = C\frac{\partial T}{\partial t} \qquad (7.5)$$

This equation is similar to equation 7.4 and the only difference is the addition of the internal heat generation term Q. The internal heat refers to the latent heat liberated as pore water freezes and as freezing occurs at the growing ice lens. It can be seen from equation 7.5 that temperature changes will propagate at a slower rate when there is a large amount of latent heat released within the soil layer. The heat generated as segregation ice forms within the soil layer 82 cm below the surface is shown in table 7.1.

Frost heave models such as the one proposed by Konrad and Morgenstern (1980) consider the zone behind the warmest ice lens to be a passive zone because moisture transfer in this zone is much reduced due to low permeability. The contribution by this zone to total heave therefore, is considered to be negligible. Heat and moisture transfer is only considered in the active zone which consists of the frozen fringe and the unfrozen soil. While most of the segregation heave is associated with the growth of the warmest ice lens (Burn 1990), observations by Smith and

3 of/de 3

PM-1 3½"x4" PHOTOGRAPHIC MICROCOPY TARGET
NBS 1010a ANSI/ISO #2 EQUIVALENT

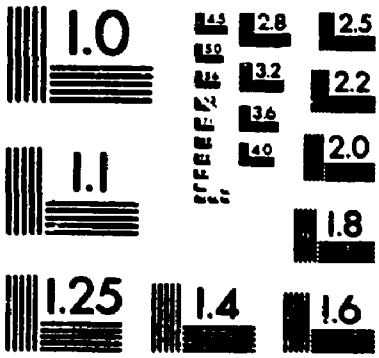

PRECISION℠ RESOLUTION TARGETS

PIONEERS IN METHYLENE BLUE TESTING SINCE 1974

MICRO-D

TABLE 7.1. Heat generated within a soil layer due to latent heat liberation during ice lens formation.

25 cm from pipe, 82 cm below surface

Day	Internal Heat Generation (Wm^{-2})
100	0
105	0
110	4.34
124	13.21
131	14.36
139	14.07
145	11.33
153	10.44
159	11.08
179	9.31
188	6.51
195	7.03
202	3.81
216	5.15
223	4.26
230	2.10

1 m from pipe, 41 cm below surface

Day	Internal Heat Generation (Wm^{-2})	
145	0.29	
152	6.20	
159	8.77	
166	11.61	
173	9.13	
179	18.04	
195	9.79	
202	13.70	Continuing Heave
209	7.54	↓
216	6.54	
258	3.03	
272	3.43	
366	1.80	
370	4.18	
398	1.39	
413	0	
421	2.75	
453	0.62	

Patterson (1989) show that a significant amount of heave is due to accumulation of ice (due to addition of water) in the frozen soil behind the warmest ice lens. Approximately 50% of the strain in the layer 41 cm below the surface, for example, is due to continuing heave (figure 5.17).

The latent heat liberated during continuing heave must also be incorporated into the apparent heat capacity. Figure 7.7 shows that the apparent heat capacity of the soil layer 41 cm below the surface remains high even though the layer is completely frozen and the layer 50 cm below the surface has begun to heave (day 202). The total amount of latent heat released during continuing heave in this layer is $4.73 \times 10^7 Jm^{-3}$ and the temperature decrease during this period is only 0.24°C. Because the temperature change is small, the heat capacity for this period is a meaningless large number. Even though continuing heave requires a temperature gradient, the actual temperatures may not change and a steady state exists with respect to temperature. Latent heat will continue to be liberated and this gives an infinite value for the apparent heat capacity. The internal heat generation may still be calculated for the period of continuing heave and these results are presented in table 7.1. It can be seen that for this particular soil layer, up to 13 W of heat may be generated internally per m^2 during continuing heave.

The thermal conductivity will also vary during

FIGURE 7.7. Apparent volumetric heat capacity for a layer of frozen Caen silt located 1 m from the pipe, 41 cm below the surface. The upper curve ("Heave") includes the component of latent heat relased as water migrating to the layer freezes. Note that the heat capacity remains high during the period of continuing heave.

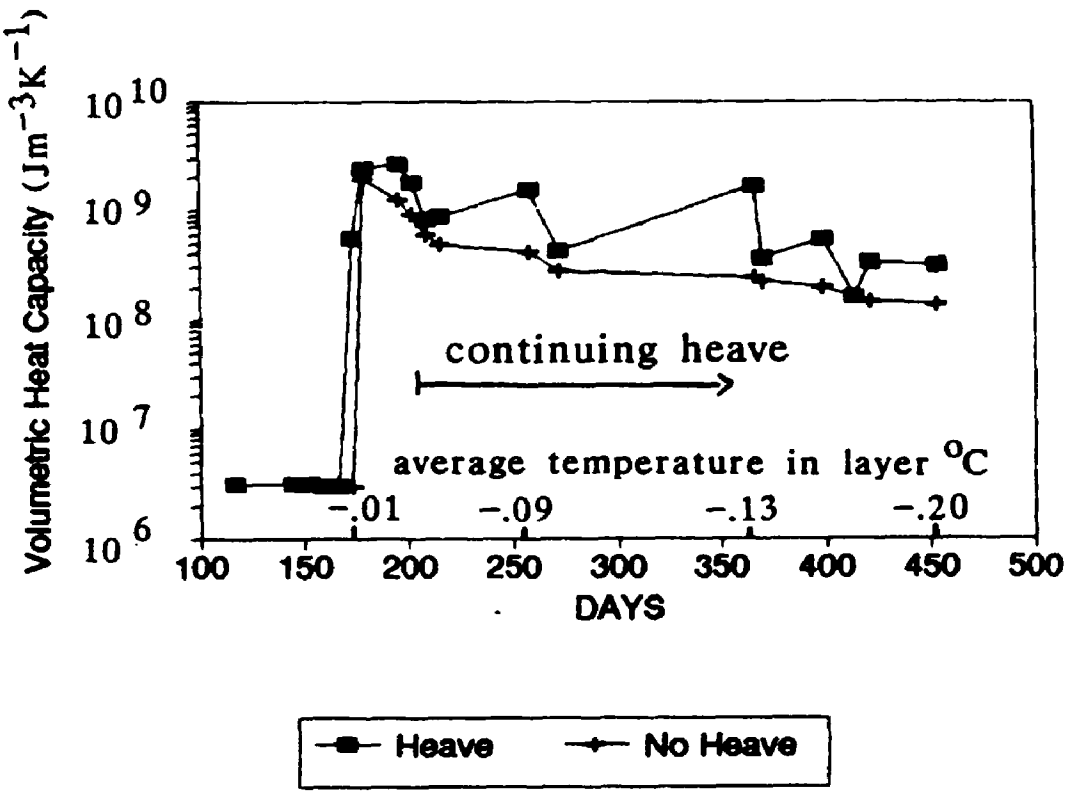

continuing heave as ice continues to accumulate (figure 7.8). It is clear from these results that the thermal properties of the frozen soil constantly change even in the zone that is considered to be passive.

7.4 The Role of Rheologic Conditions

For ice lenses to continue to grow, at a fixed location, the release of latent heat during ice lens formation must be sufficient to offset the cooling due to conduction of heat away from the ice lens. The rate of water migration toward the freezing front therefore, is an important factor in determining the release of latent heat and the apparent heat capacity of the soil. This is dependent on the temperature gradient (which controls the potential gradient) and the hydraulic conductivity (which is temperature dependent). There is clearly a link between the thermal and hydrologic conditions in the frozen soil and models have been developed which couple heat and moisture flow. Equations describing coupled mass and heat transport can be derived using irreversible thermodynamic theory (Prigogine 1967):

$$J_m = -L_m \frac{V_w}{T_2} \frac{\Delta P}{\Delta x} - L_{mq} \frac{\Delta(1/T)}{\Delta x} \qquad (7.6)$$

$$J_q = -L_{qm} \frac{V_w}{T_2} \frac{\Delta P}{\Delta x} - L_q \frac{\Delta(1/T)}{\Delta x} \qquad (7.7)$$

ΔP = Pressure difference $P_2 - P_1$

$\Delta(1/T) = (1/T_1) - (1/T_2) \approx T/T^2$ provided $T = T_1 - T_2$ is relatively small compared to T_1

Δx = distance $x_1 - x_2$

FIGURE 7.8. Thermal conductivity (calculated from equation 7.2) for a layer of frozen Caen silt located 1 m from the pipe, 41 cm below the surface. Note that the thermal conductivity continues to change as continuing heave occurs.

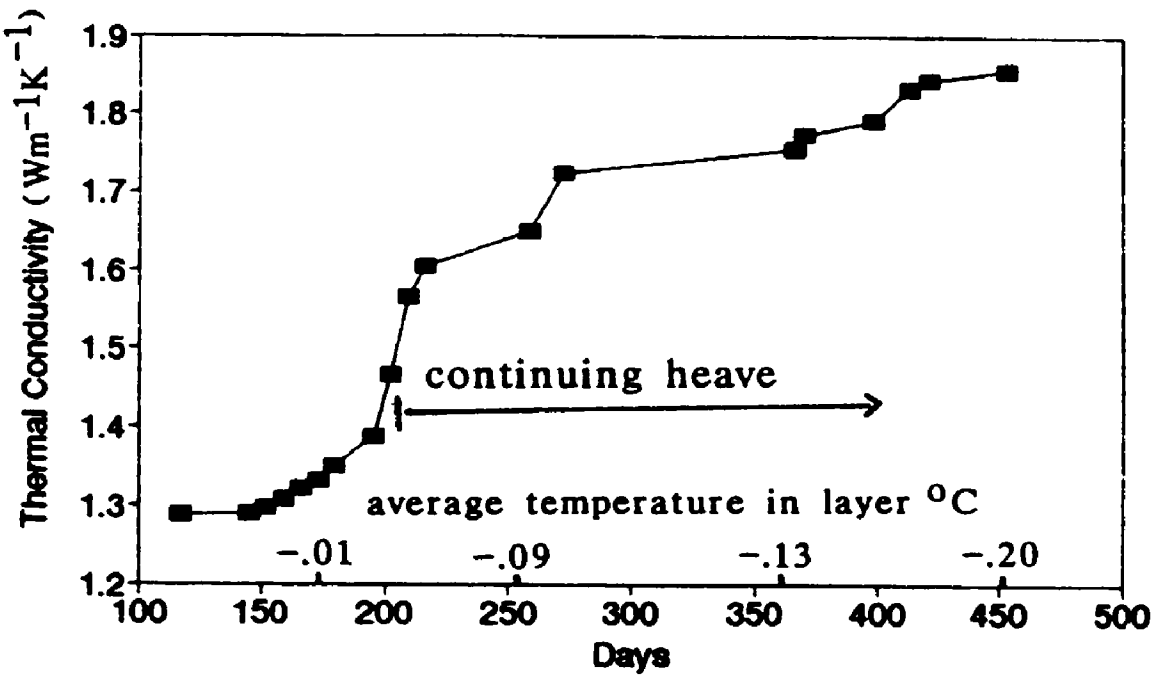

V_w = specific volume of water

J_m and J_q = mass and heat flow rates

T_2 and T_2 = temperature at x_1 and x_2

L_m and L_q = isothermic mass and isobaric heat transfer coefficients

L_{mq} and L_{qm} = cross coefficients for coupled transport

Guymon and Luthin (1974), Harlan (1973) and Kay and Groenvelt (1974) all propose equations for coupled transport of heat and mass in frozen soils. Miller et al. (1975) offers an analysis based on the coupled flow equations which also considers the movement of ice through regelation. The mechanistic theory of ice lens formation presented by Konrad and Morgenstern (1980) also considers the link between heat and mass flow as the internal heat generation term is determined as a function of the velocity of water movement.

None of these models however, include the rheologic properties of the frozen soil which the experimental results presented in this paper suggest are important. Ice will only continue to accumulate if it can overcome the resistance of the surrounding frozen soil. If the resistance offered by the frozen material cannot be overcome, the ice lens will stop growing, latent heat will no longer be liberated at the ice-water interface and the freezing front will progress deeper into the soil. If resistance to deformation is high, the apparent heat capacity of the soil will be low. The thermal diffusivity will be high and the freezing front will progress quickly

through the soil. This link between resistance to heave and the apparent heat capacity is illustrated by the difference in rates of frost penetration between site 1 and site 2 (figure 6.10). The continuing heave observed at the Caen experimental site (Smith and Patterson 1989) illustrates the time dependent behaviour of the frozen soil and ice lenses grow slowly over a period of time as the frozen material deforms under the stress that is continuously applied. The apparent heat capacity therefore, depends on the creep properties of the frozen soil and is also time-dependent.

The thermal conductivity also depends on the rheologic properties of the soil because it depends on the amount of ice accumulation and the location of the ice lenses. Thermal conductivity is also time-dependent as illustrated by its slow change during continuing heave.

It is clear then, that the thermal properties of the frozen soil will be dependent on the rheologic properties of the frozen soil. These interrelationships are summarized in figure 7.9. The rheologic properties therefore, should be incorporated into the mass and heat flow equations described earlier. Even if one is to use the simpler approach of Konrad and Morgenstern (1980), the calculation of the internal heat generation during heave should consider the creep of the frozen soil as well as the velocity of migrating water.

Another aspect that needs to be considered, is that

FIGURE 7.9. Interrelationships between thermal, hydrologic and rheologic conditions of freezing soils.

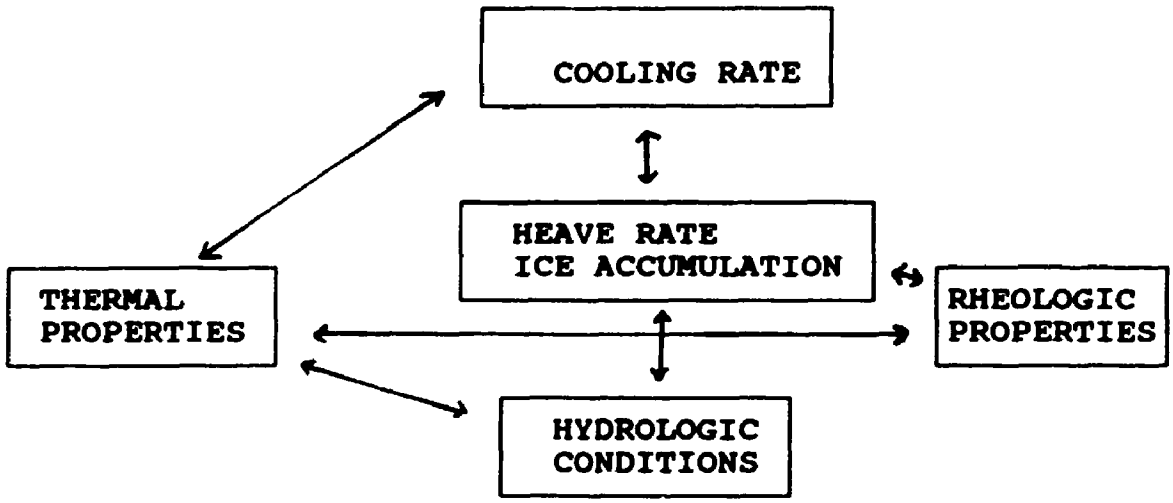

some consolidation of the soil may take place during freezing. The soil below a growing ice lens may become consolidated as water is drawn from it so that the frozen soil between ice lenses may be more compacted than it was before freezing. The soil layers may become consolidated further during continuing heave. This was not considered in the calculation of thermal properties. In fact, only the expansion of the soil due to the freezing of pore water was considered. The unfrozen water content curve varies with soil density as will the thermal properties (eg. figures 7.1 and 7.2). The mechanical properties of the frozen material will also depend on the moisture content and the density of the soil. These factors also need to be considered in a frost heave model.

7.5 Summary

Frost heave is the result of a complex interaction of the thermal, hydrologic and rheologic conditions of the frozen soil. These complex interactions should be incorporated into a frost heave model.

The thermal properties of the soil are time-dependent and therefore difficult to evaluate. It is also necessary to determine how the thermal and mechanical properties of the soil will change during ice formation and with changes in soil density (either increases or decreases).

CHAPTER EIGHT

SUMMARY AND CONCLUSIONS

This thesis has examined the processes of ice lens formation and frost heave. The interaction of the thermodynamic and rheologic conditions in the frost heave process have been analyzed. The studies allow the following conclusions to be drawn.

Ice sandwich experiments showed transport of water substance through an ice layer as a consequence of a temperature gradient (thermally-induced regelation). Creep of the ice occurred in response to a stress which is induced at the cold end when the temperature at the water-ice interface is lowered. Pressures developed in the ice which were dependent on the rheologic properties of the ice. The pressure measurements suggested that ice at temperatures close to 0°C, behaves sometimes as a rigid solid and at other times as a viscous fluid. The magnitude of the ice pressure and the size of the pressure gradient changed over time indicating that the rheologic behaviour of ice changes also. It is proposed that, although the applied conditions in the experiment differed from those likely in nature, the ice in a soil pore will exhibit similar rheologic behaviour and thermally induced regelation will occur.

Observations of the pressure distribution in frozen soil show that the water pressure is a function of the

hydrodynamic and thermodynamic regime and the ice pressure will depend on the creep properties of the frozen material. These two effects will produce a pressure difference (P_i-P_w) that is compatible with the Clausius-Clapeyron equation. Creep and stress relaxation occur over time and this results in a change in the observed ice pressures. Observations made during changes in the cooling plate temperature also show the importance of the rheologic properties and the time-dependence of the frost heave process.

Observations at a field scale facility of ice lens orientation around a buried, cooled pipe showed that ice lenses tend to be orthogonal to the heat flow. The size and spacing of lenses are modulated by the rate of heat flow. The resistance of the frozen soil was also found to be important and the ice lenses also have a tendency to grow with the lenses lying perpendicular to the direction of least resistance. Furthermore, density and texture were found to be important factors influencing ice lens growth and distribution. The location of ice lenses and their orientation therefore, is the result of a complex interaction between the thermal and mechanical conditions.

The orientation of the ice lenses around the pipe suggest that heave and therefore the stress and displacement of soil also have vertical and horizontal components. In the case of the chilled buried pipe, the horizontal component is more important next to the pipe. The results

show a complex pattern of heave and suggest that the displacement of the pipe is not simply due to the pipe being lifted up by a force acting in a vertical direction. The pipe displacement is also a result of the pipe being squeezed from the sides.

Knowledge of the thermal properties of the soil is important in developing a frost heave model. The thermal properties however, are not constant and vary with temperature as the proportions of ice and water change. The determination of the apparent heat capacity is difficult with latent heat being released as water freezes over a range of temperature. Latent heat is also released during ice lens formation and the rate of release of latent heat will depend on the rate of water migration to the growing ice lens. The rate of release of latent heat and therefore, the apparent heat capacity will also depend on the resistance of the frozen material because ice will only continue to accumulate (with release of latent heat) if the resistance of the surrounding frozen soil can be overcome. The rate of ice accumulation and the apparent heat capacity will thus depend on the time-dependent mechanical behaviour of the frozen soil. Latent heat is also released as heave continues behind the warmest ice lens even though temperatures may have reached a steady state. The rate of ice accumulation and the rate of frost penetration depends on a complex interaction between the thermal and rheologic

properties of the freezing soil.

Ice lens formation also depends on the hydraulic conditions and these are related to the thermal conditions. The potential gradients which develop depend on the magnitude of the temperature gradient and the hydraulic conductivity which is controlled by temperature. The rate of water migration and the thermal conditions therefore, are interrelated.

Ice lens formation and frost heave is clearly a function of the hydraulic and thermal conditions (thermodynamic conditions) and a coupled heat and mass flow model is required. Such a model however, must consider the time-dependence of the frost heave process and the significant amount of continuing heave that occurs in the frozen soil behind the warmest ice lens as water migration and creep occur slowly over time. The results of this study have shown that a model is required which considers the thermodynamic, hydraulic and rheologic conditions of the frozen material, their interaction and their dependence on time.

APPENDIX ONE

RESULTS FROM ICE SANDWICH EXPERIMENTS

FIGURE A.1.1. Cumulative water flow and pressure over time during ice sandwich experiment 13. Positive slope for water flow indicates an outflow of water from the sample and a negative slope indicates an inflow of water to the sample.

COOLING PLATE TEMPERATURE (°C)

Days	0-2	2-4	4-7	7-8	8-9	9-10	10-12
Cold End	-.07	-.1	-.11	-.12	-.14	-.06	-.12
Warm End	-.07	-.06	-.06	-.06	-.06	-.06	-.06

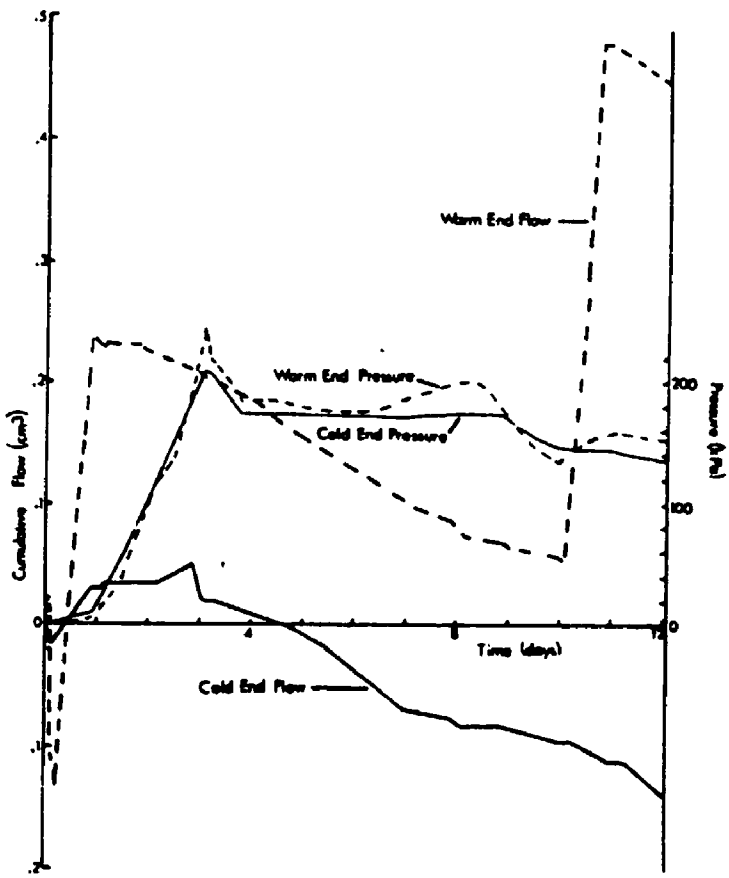

FIGURE A.1.2. Cumulative water flow and pressure over time during ice sandwich experiment 15. Positive slope for water flow indicates an outflow of water from the sample and a negative slope indicates an inflow of water to the sample.

COOLING PLATE TEMPERATURE (°C)

Days	0-1	1-4
Cold End	-.06	-.12
Warm End	-.06	-.06

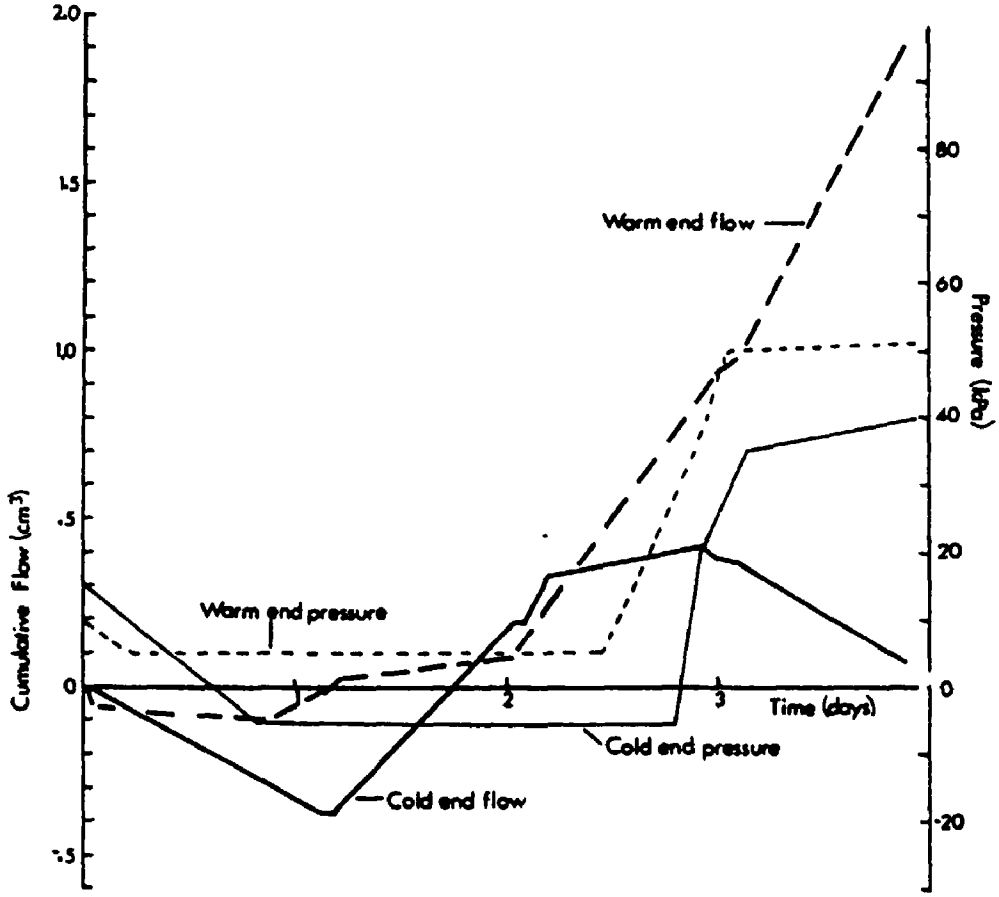

FIGURE A.1.3. Cumulative water flow and pressure over time during ice sandwich experiment 18. Positive slope for water flow indicates an outflow of water from the sample and a negative slope indicates an inflow of water to the sample.

COOLING PLATE TEMPERATURE (°C)

Days	0-1	1-2	2-5	5-14	14-16	16-21	21-26
Cold End	-.08	-.12	-.14	-.14	-.17	-.19	-.20
Warm End	-.08	-.08	-.08	-.08	-.08	-.08	-.08

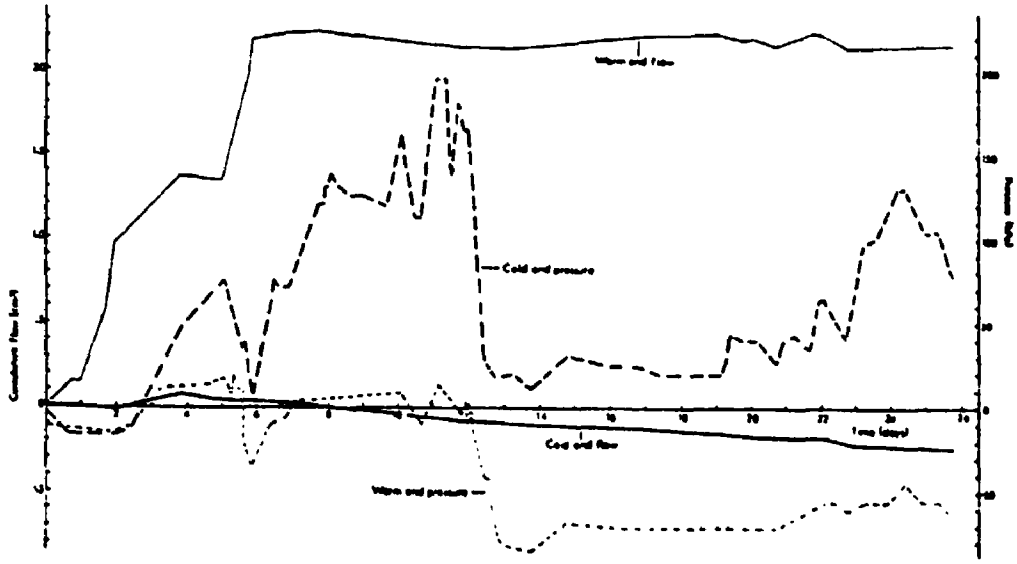

FIGURE A.1.4. Cumulative water flow and pressure over time during ice sandwich experiment 19. Positive slope for water flow indicates an outflow of water from the sample and a negative slope indicates an inflow of water to the sample.

COOLING PLATE TEMPERATURE (°C)

Days	0-1	1-2	2-6	6-8	8-9	9-12	12-13
Cold End	-.08	-.12	-.13	-.14	-.15	-.16	-.17
Warm End	-.08	-.08	-.08	-.08	-.08	-.08	-.08

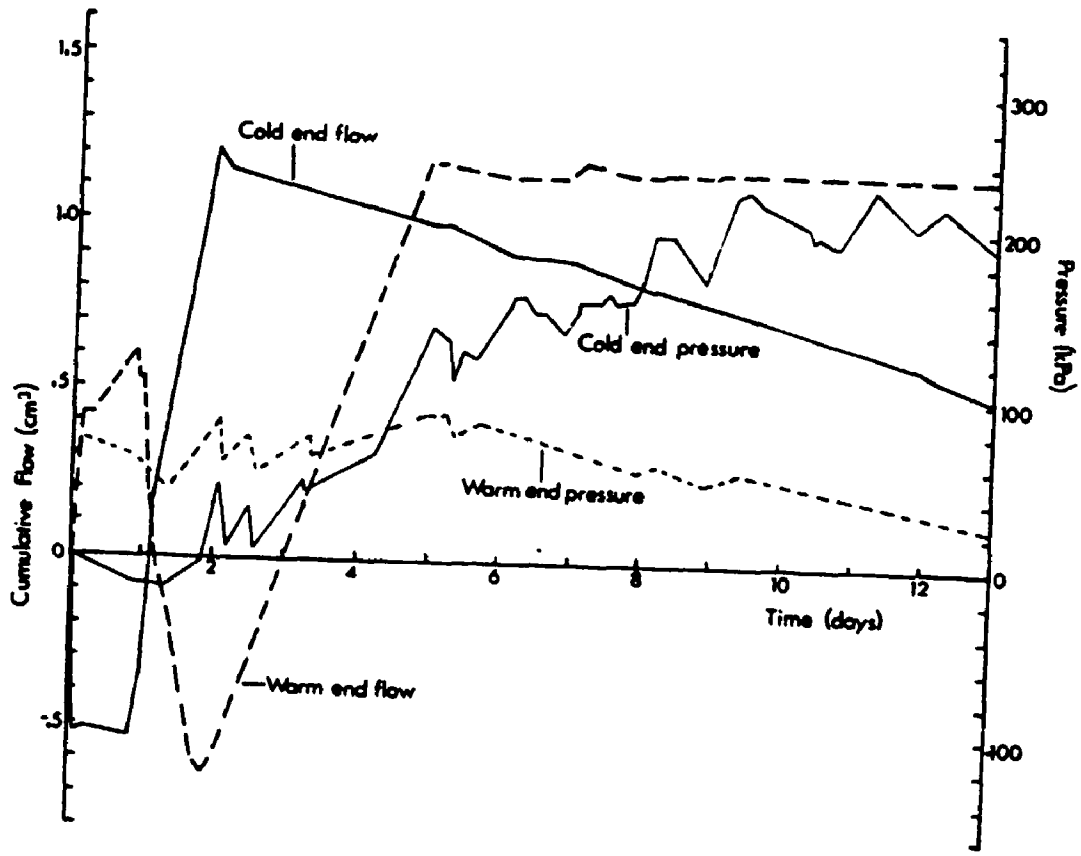

APPENDIX TWO

TEMPERATURE, WATER FLOW AND PRESSURE DATA DURING TEMPERATURE INCREASE IN CAEN SILT FROST HEAVE EXPERIMENTS

FIGURE A.2.1. Sample temperature following temperature increase at the cold end on day 11 of experiment 20.

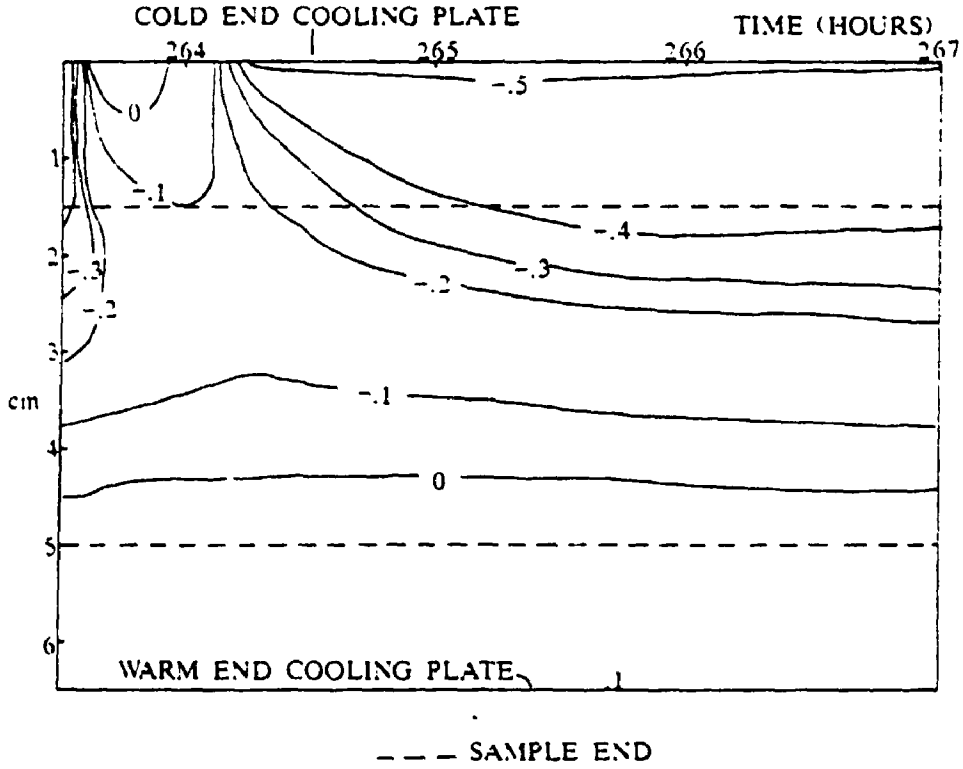

FIGURE A.2.2. Water flow and pressure following temperature increase at the cold end on day 11 of experiment 20.

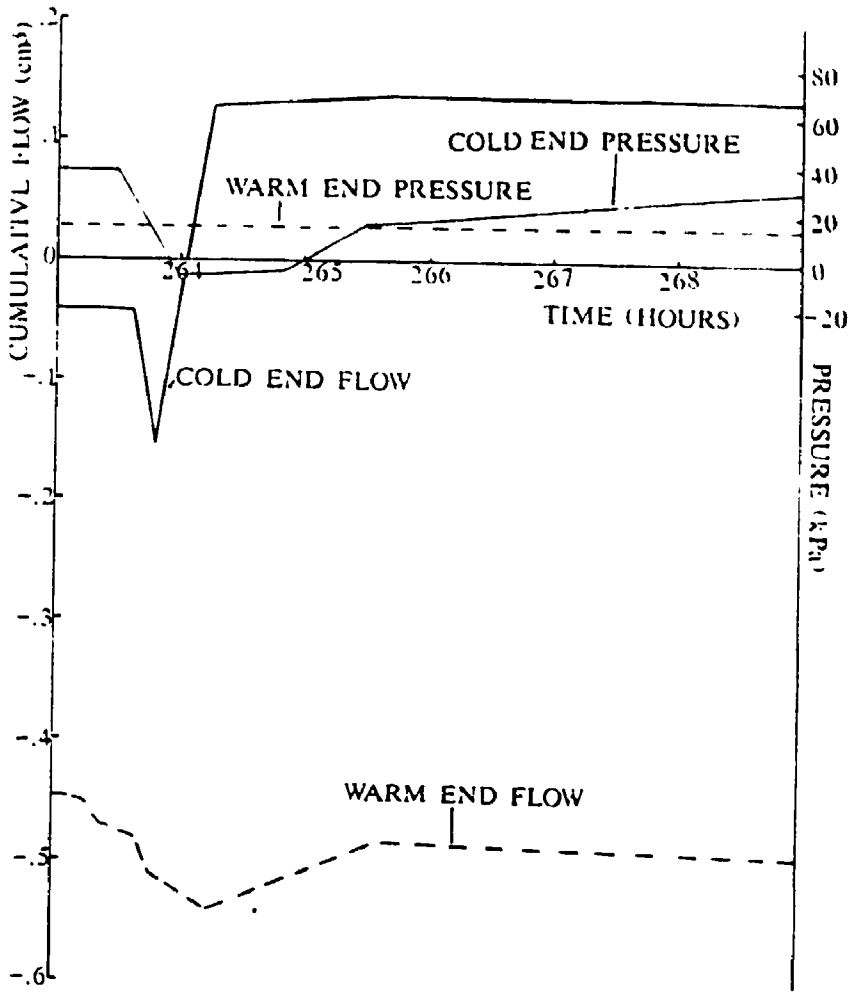

FIGURE A.2.3a. Sample temperature following temperature increase at the cold end on day 17 of experiment 21.

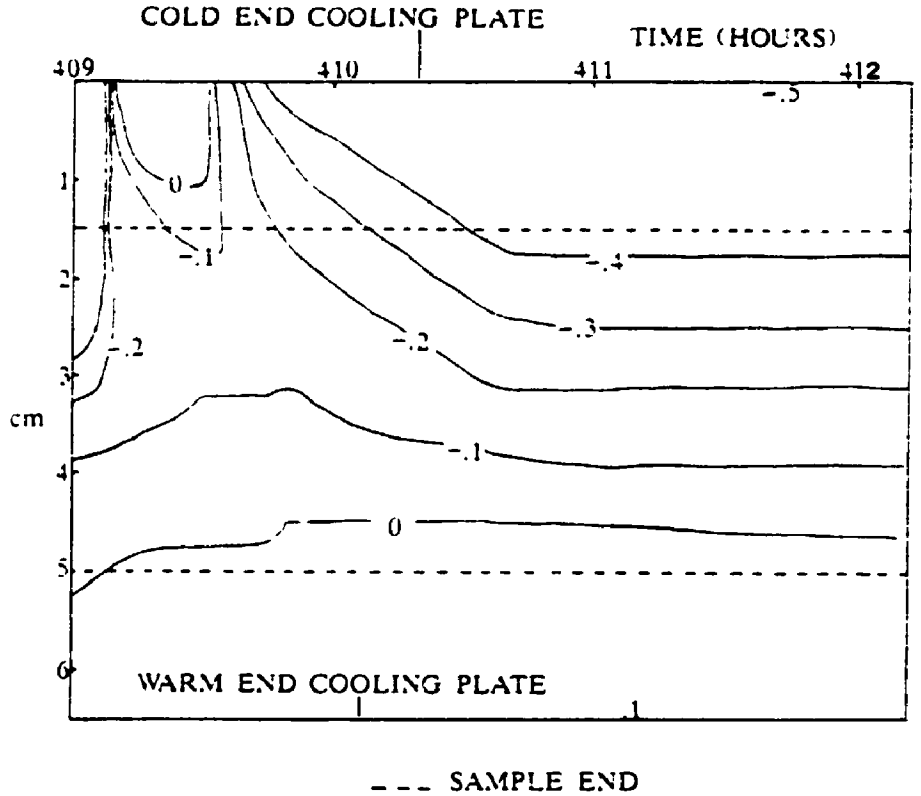

FIGURE A.2.3b. Water flow and pressure following temperature increase on day 17 of experiment 21.

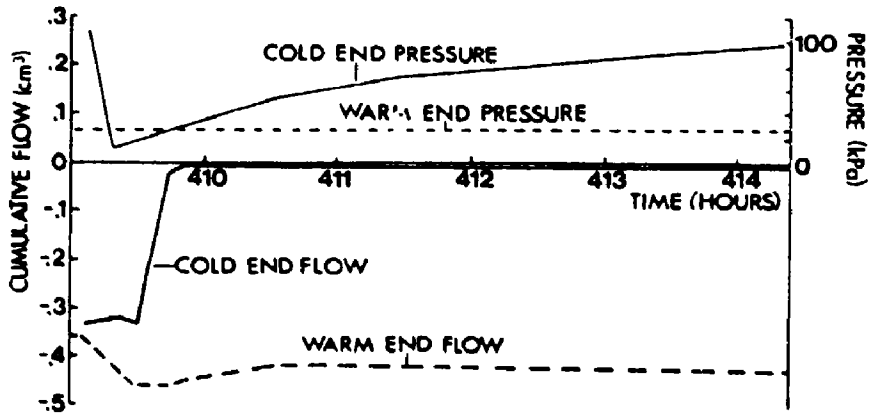

FIGURE A.2.4a. Sample temperature following temperature increase at cold end on day 25 of experiment 21.

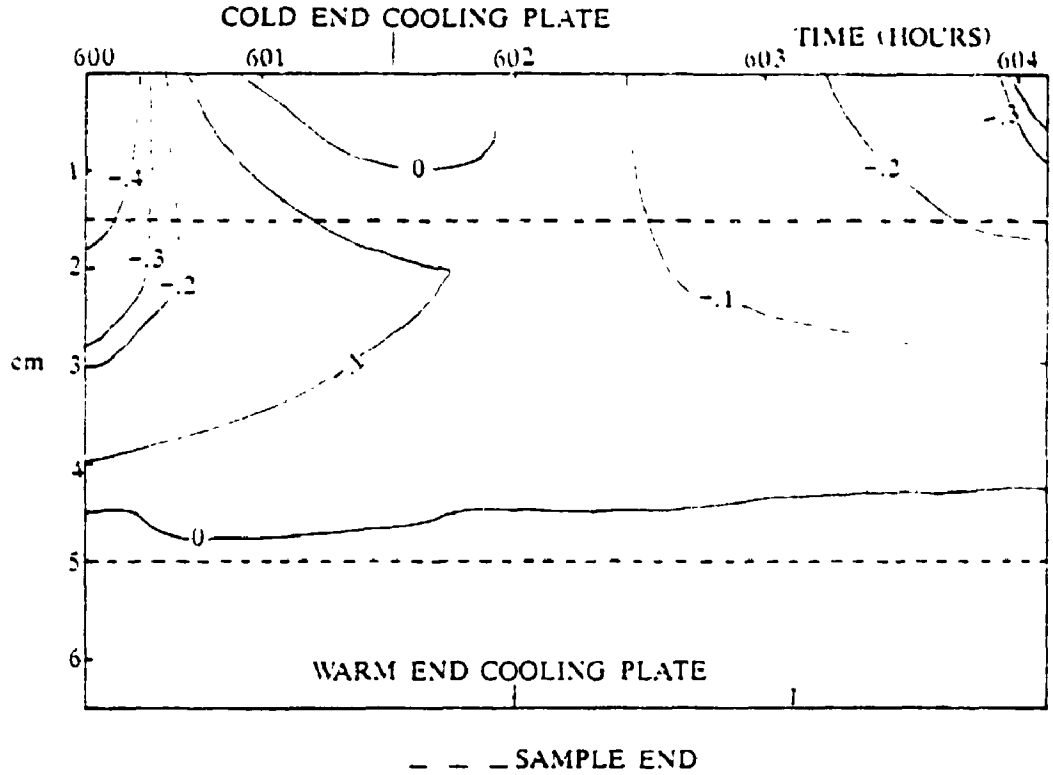

FIGURE A.2.4b. Water flow and pressure following temperature increase on day 25 of experiment 21.

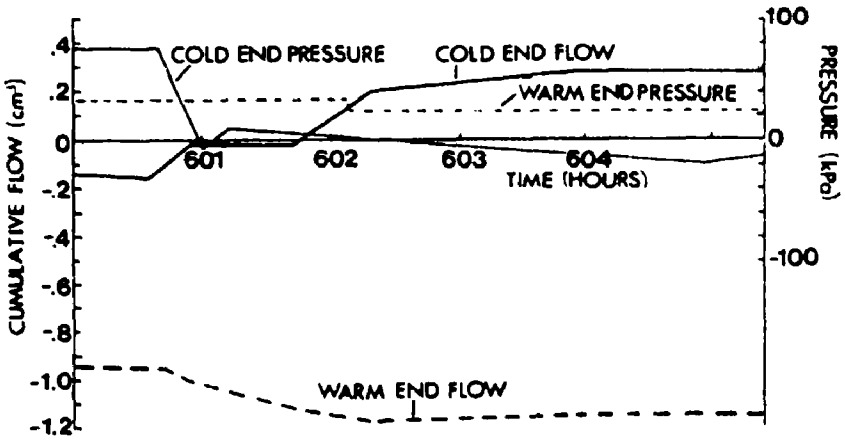

FIGURE A.2.5. Sample temperature following abrupt increase in temperature (during power failure) on day 10 of experiment 22.

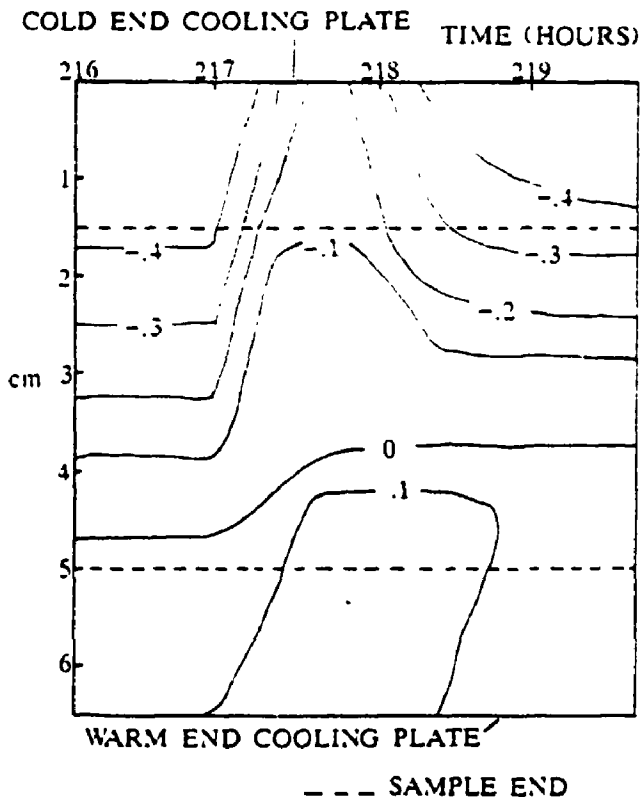

FIGURE A.2.6a. Sample temperature following temperature increase at cold end on day 21 of experiment 22.

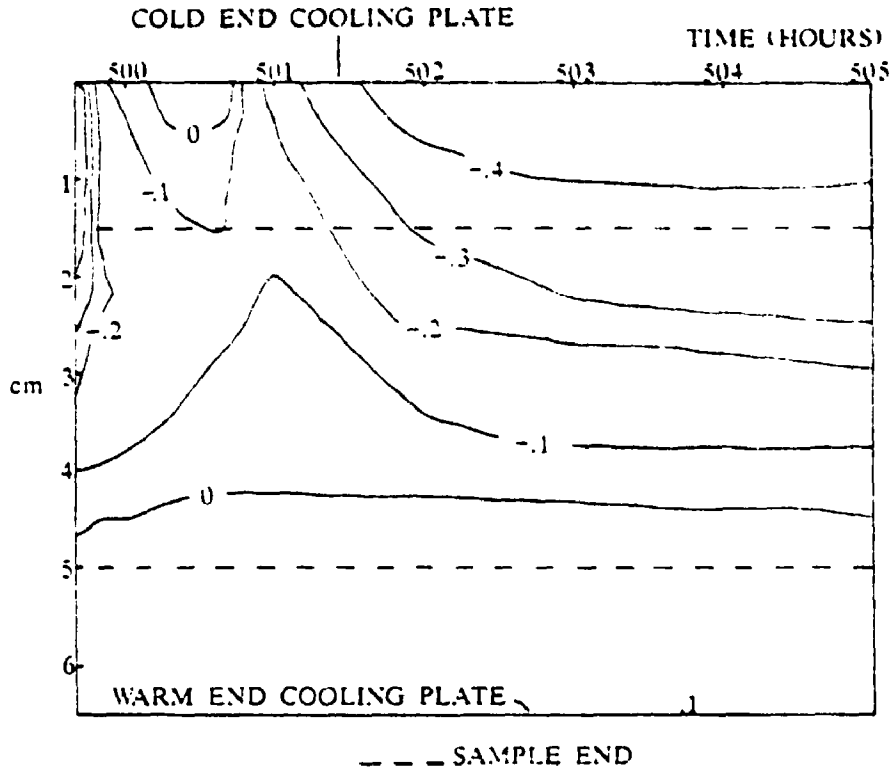

FIGURE A.2.6b. Water flow and pressure following temperature increase on day 21 of experiment 22.

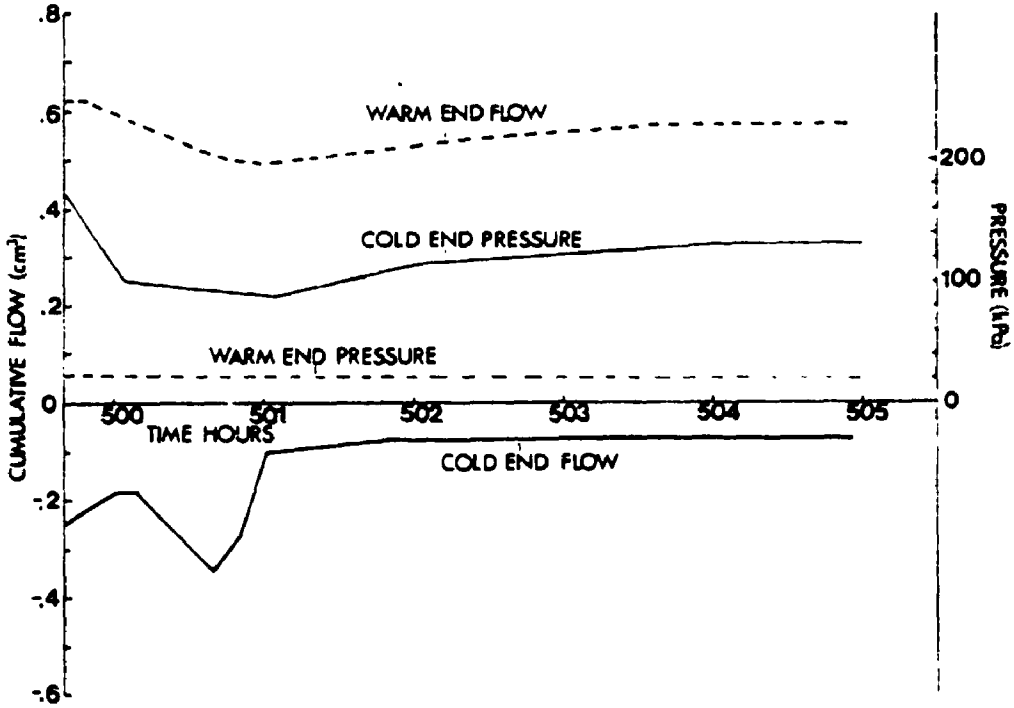

FIGURE A.2.7a. Sample temperature following temperature increase at cold end on day 28 of experiment 22.

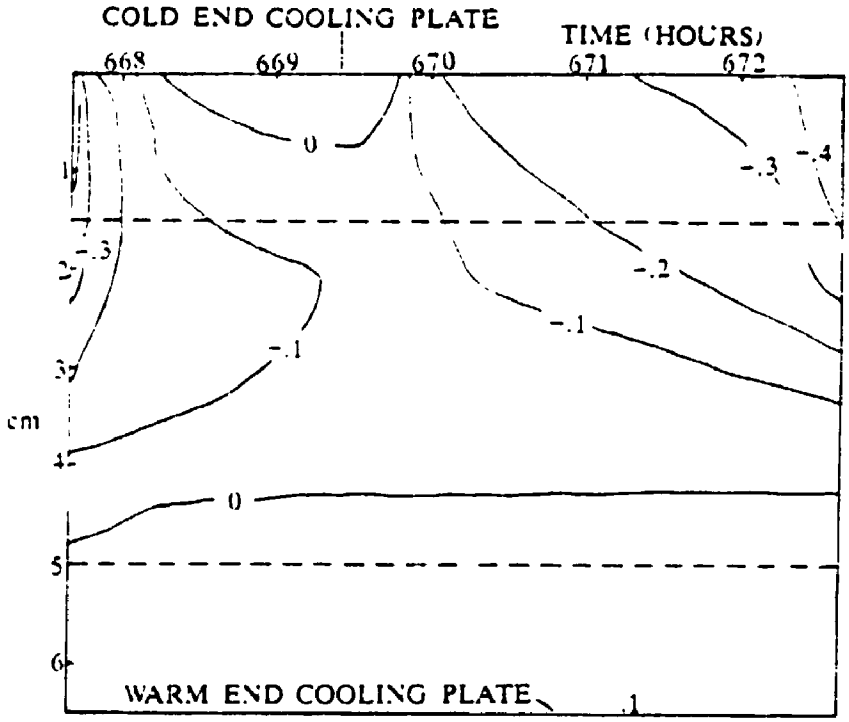

FIGURE A.2.7b. Water flow and pressure following temperature increase on day 28 of experiment 28.

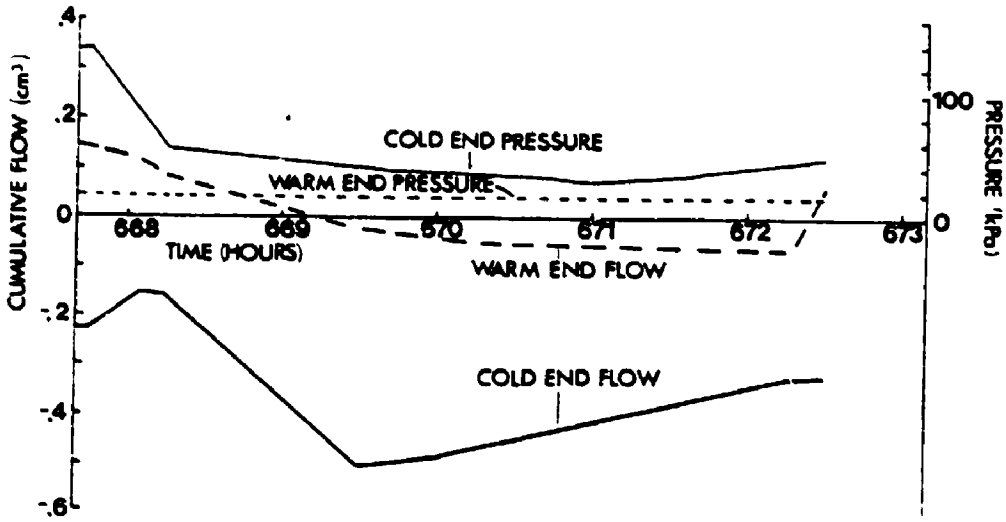

APPENDIX THREE

MOISTURE CONTENT AND DRY BULK DENSITY OF FROZEN SOIL AT CAEN SITE

FIGURE A.3.1. Gravimetric and volumetric moisture content of soil at site 1.

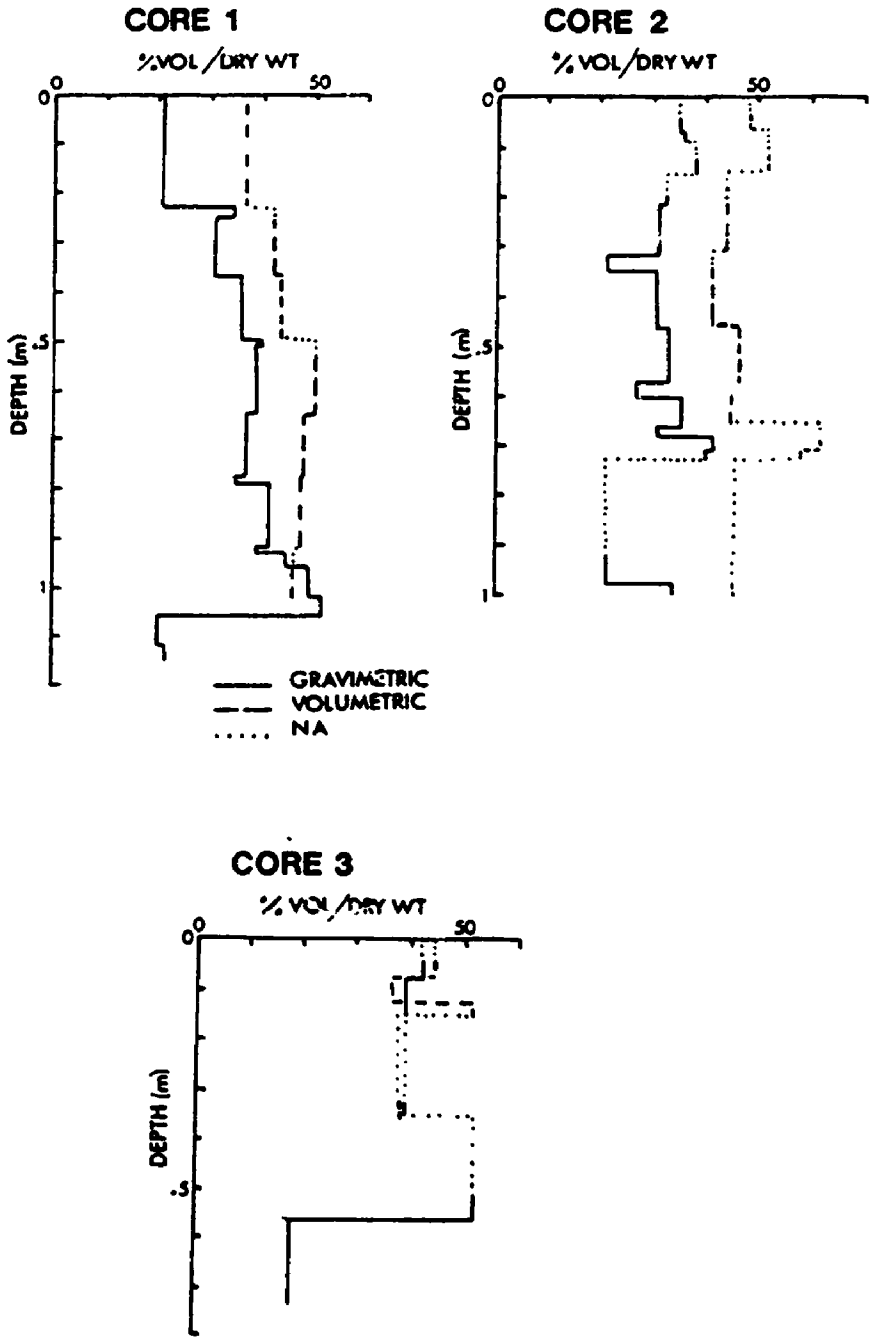

FIGURE A.3.2. Dry bulk density of soil at site 1.

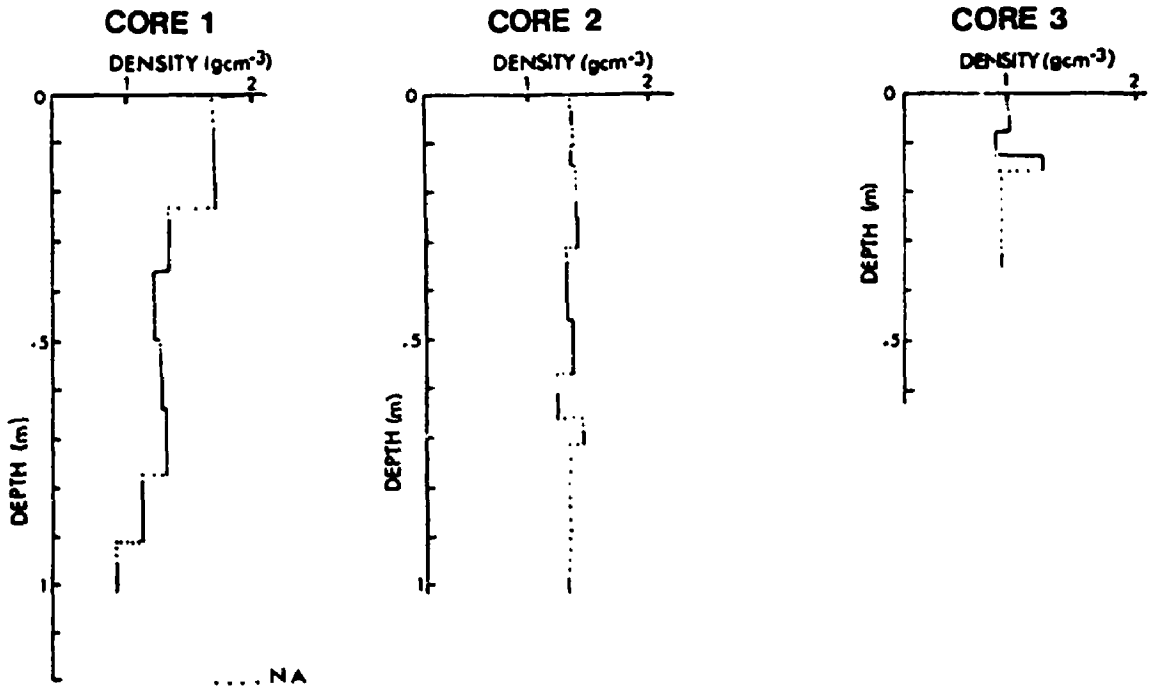

FIGURE A.3.3. Gravimetric and volumetric moisture content of soil at site 2.

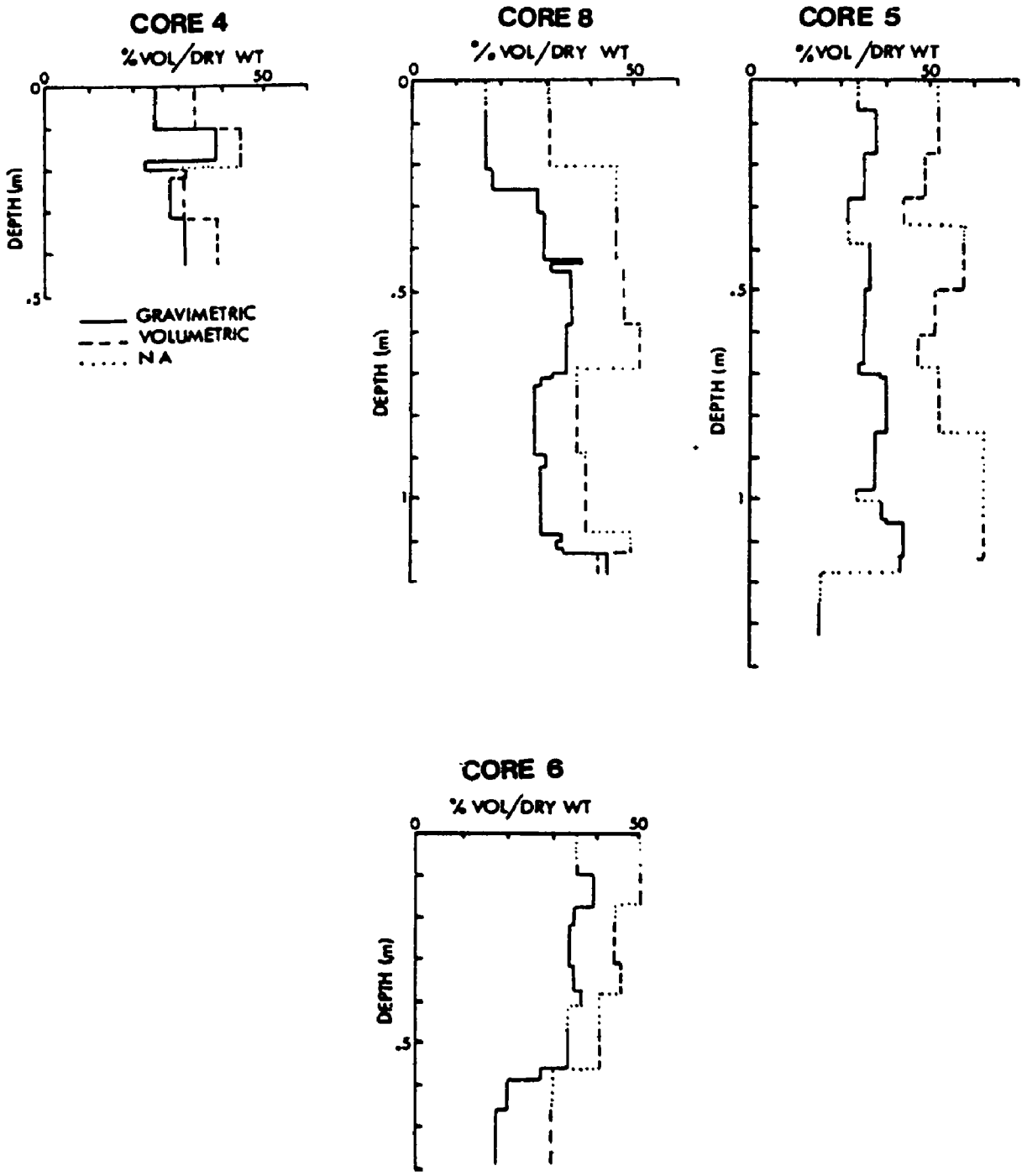

FIGURE A.3.4. Dry bulk density of soil at site 2.

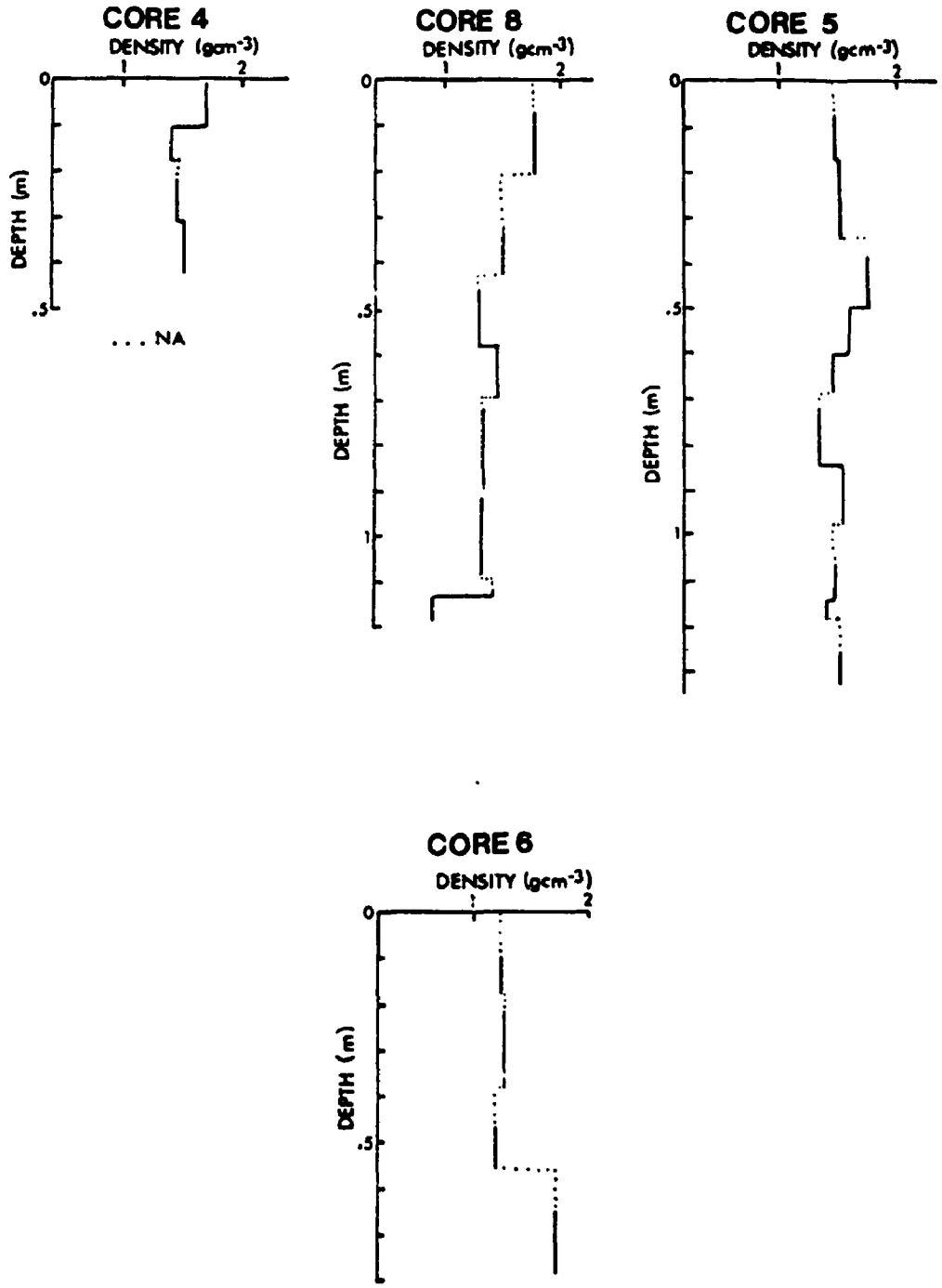

REFERENCES

Andersland, O.B, Sayles, F.H. and Ladanyi, B. 1978. Mechanical properties of frozen ground. In Geotechnical Engineering for Cold Regions. Andersland, O.B. and D.M. Anderson Ed. McGraw Hill Book Company, pg. 216-225.

Anderson, D.M. and Morgenstern, N.R. 1973. Physics, chemistry, and mechanics of frozen ground: A review. Proc. Second Int. Conf. on Permafrost, pg 257-288.

Anderson, D.M., Tice, A.R. and McKim, H.L. 1973. The unfrozen water and the apparent specific heat capacity of frozen soils. Proc. 2nd Int. Conf. on Permafrost, pg 289-294.

Berg, R.L. 1983. Status of numerical models for heat and mass transfer in frost-susceptible soils. Permafrost: Fourth International Conference Proceedings, pg. 67-71.

Black, P.B. and Miller, R.D. 1985. A continuum approach to modelling of frost heaving. Freezing and Thawing of Soil Water Systems. Technical Council on Cold Regions Engineering Monograph. D.M. Anderson and P.J. Williams Eds. ASCE, NY, pg. 36-45.

Budd, W.F. and Jacka, T.H. 1989. A review of ice rheology for ice sheet modelling. Cold Reg. Sci. and Tech. 16: 107-144.

Burn, C.R. 1990. Frost heave in lake bottom sediments, Mackenzie Delta Northwest Territories. Fifth Canadian Permafrost Conference, Centre d'études nordiques, Université Laval Collection Nordicana No. 54, pg. 103-109.

Burt, T.P. 1974. A Study of Hydraulic Conductivity in Frozen Soils. M.A. Thesis, Carleton University, Ottawa, Canada.

Carlson, L.E. and Nixon, J.F. 1988. Subsoil investigation of ice lensing at Calgary Canada, frost heave test facility. Can. Geotech. J. 25: 307-319.

Cary, J.W. 1987. A new method for calculating frost heave including solute effects. Water Resources Research 23: 1620-1624.

Cole, D.M. 1987. Strain-rate and grain size effects in ice. J. Glaciology 33: 274-280.

Dumoulin, R., Dupas, A. and Valeux, J.C. 1987. Mesures et interprétations des gonflements internes et des variations de densité des sols par double sonde gamma. 2ième Colloque, Franco-Polonais, Gel et Génie Civil, La Central des Ponts et Chaussées.

Dupas, A. and Van Vliet-Lanoe, B. 1988. Connaissances actuelles sur les phénomènes de cryosuction et de la formation des lentilles de glace dans les sols. Bull. Liaison Laboratoires des Ponts et Chaussées, Publ. Spec. XV, pg. 79-87.

Fletcher, N.H. 1970. The Chemical Physics of Ice. Cambridge 271 pgs.

Geotechnical Science Laboratories 1989. Canada-France Pipeline-Ground Freezing Experiment: Fourth Freeze Cycle. Report to Permafrost Section, Terrain Sciences Division, Geological Survey of Canada, 63p.

Geotechnical Science Laboratories 1988. The Third Freeze Cycle of the Canada-France Ground Freezing Experiment. Final Report for Permafrost Section, Terrain Sciences Division, Geological Survey of Canada, 76p.

Geotechnical Science Laboratories 1982. Feasibility Studies for Stresses in a Pipeline Buried in Freezing Soil. Report to Energy, Mines and Resources, Canada, Earth Physics Branch, 36p.

Glen, J.W. 1987. Fifty years of progress in ice physics. J. Glaciology Special Issue, pg. 52-59.

Glen, J.W. 1963. The rheology of ice. In Ice and Snow, properties, processes and applications. W.D. Kingerly Ed. MIT Press Cambridge, Mass. pg. 3-7.

Gold, L.W. 1978. Ice pressures and bearing capacity. In Geotechnical Engineering for Cold Regions. O.B. Andersland and D.M. Anderson Eds. McGraw-Hill Book Company pg. 505-542.

Gold, L.W. 1973. Activation energy for creep of columnar-grained ice. In Physics and Chemistry of Ice. E. Walley, S.J. Jones and L.W. Gold Eds. Royal Soc. of Canada, pg. 362-364.

Gold, L.W. 1963. Deformation mechanisms in ice. In Ice and Snow, properties, processes and applications. W.D. Kingerly Ed. MIT Press Cambridge, Mass. pg. 8-27.

Groenvelt, P.H. and Kay, B.D. 1977. Water and ice potentials in frozen soils. Water Resources Research 13: 445-449.

Guymon, G.L. and Luthin, J.L. 1974. A coupled heat and moisture transport model for arctic soils. Water Resources Research 10: 995-1001.

Haefeli, R. 1965. Creep and progressive failure in snow, soil, rock and ice. Proc. 6th int. Conf. on Soil Mechanics and Foundation Engineering, pg. 134-148.

Harlan, R.L. 1973. Analysis of coupled heat-fluid transport in partially frozen soil. Water Resources Research 9: 1314-1323.

Hoekstra, P. 1966. Moisture movement in soils under temperature gradients with cold-side temperature below freezing. Water Resources Research 2: 241-250.

Hoekstra, P. and Miller, R. D. 1967. On the mobility of water molecules in the transition layer between ice and a solid surface. J. Colloid and Interface Science 25: 166-173.

Hoeve, T.E. and Smith L.B. 1988. Mechanical properties of ice and frozen soil. Rept. submitted to Supply and Services Canada, DSS File No. 63ss.23233-7-1126.

Holden, J.T. 1983. Approximate solutions for Miller's theory of secondary frost heave. Permafrost: Fourth International Conference Proceedings, pg. 498-503.

Holden, J.T., Piper, D. and Jones, R.H. 1985. Some developments of a rigid-ice model of frost heave. Ground Freezing: Proc. Fourth International Symposium, pg. 93-98.

Hopke, S.W. 1980. A model for frost heave including overburden. Cold Region Science and Technology 3: 111-127.

Horiguchi, K. 1987. An osmotic model for soil freezing. Cold Reg. Sci. and Tech. 14: 13-22.

Horiguchi, K. and Miller, R.D. 1983. Hydraulic conductivity functions of frozen materials. Permafrost: Fourth International Conference Proceedings, pg. 504-508.

Horiguchi, K. and Miller, R.D. 1980. Experimental studies with frozen soil in an ice sandwich permeameter. Cold Regions Science and Technology 3: 177-183.

Johansen, O. 1973. A method for calculation of thermal conductivity of soils, Part II. Frost I Jord 10: 25-28.

Johnston, G.H., Ladanyi, B. Morgenstern, N.R. and Penner, E. 1981. Engineering characteristics of frozen and thawing soils. In Permafrost: Engineering Design and Construction. G.H. Johnston Ed. J. Wiley and Sons, pg. 73-147.

Jumikis, A.R. 1979. Cryogenic texture and strength aspects of artificially frozen soils. Ground Freezing, Proc. 1st Int. Symp. on Ground Freezing, pg. 125-135.

Jumikis, A.R. 1966. Thermal Soil Mechanics. Rutgers University Press, 267p.

Kay, B.D., Fukuda, M., Izuta, H. and Sheppard, M.I. 1981. The importance of water migration in the measurement of the thermal conductivity of unsaturated frozen soils. Cold Reg. Sci. and Tech. 5: 95-106.

Kay, B.D. and Groenvelt, P.H. 1974. On the interaction of water and heat transport in frozen soils. I Basic theory: The vapor phase. Soil Sci. Soc. Amer. Proc. 38: 395-400.

Kay, B. D. and Perfect, E. 1988. State of the art: Heat and mass transfer in freezing soils. Proc. Fifth International Symposium on Ground Freezing, Vol. 1: 3-21.

Kinosita, S. 1975. Soil-water movement and heat flux in freezing ground. Proc. Conference on Soil-water Problems in Cold Regions, Calgary, Alberta.

Konrad, J.M. and Morgenstern, N.R. 1983. Frost susceptibility of soils in terms of their segregation potential. Permafrost: Fourth International Conference Proceedings, pg. 660-665.

Konrad, J.M. and Morgenstern, N.R. 1980. A mechanistic theory of ice lens formation in fine-grained soils. Canadian Geotechnical J. 17: 473-486.

Koopmans, R.W.R. and Miller, R.D. 1966. Soil freezing and soil water characteristic curves. Soil Science Society of America Proc. 30: 680-685.

Langdon, T.G. 1973. Creep mechanisms in ice. In Physics and Chemistry of Ice. E. Walley, S.J. Jones and L.W. Gold Eds. Royal Soc. of Canada, pg. 356-361.

Loch, J.P.G. and Kay, B.D. 1978. Water redistribution in partially frozen, saturated silt under several temperature gradients and overburden loads. Soil Science Society of America J. 42: 400-406.

Lundin, L.-C. 1989. Water and Heat Flows in Frozen Soils. Basic theory and operational modeling. Acta Universitatis Upsaliensis. Comprehensive Summaries of Uppsala Dissertations from the Faculty of Science 186.

Loch, J.P.G. and Miller, R.D. 1975. Tests of the concept of secondary frost heaving. Soil Science Society of America Proc. 39: 1036-1041.

Lunardini, V.J. 1981. Heat Transfer in Cold Climates. Van Nostrand Reinhold Co. 736p.

Mackay, J.R. 1974. Reticulate ice veins in permafrost, Northern Canada. Can. Geotech. J. 11: 230-237.

Mackay, J.R. and Leslie, R.V. 1987. A simple probe for the measurement of frost heave within frozen ground in a permafrost environment. Current Research Part A, GSC Paper 87-1A, pg. 37-41.

McRoberts, E.C. and Nixon, J.F. 1975. Reticulate ice veins in permafrost, Northern Canada: Discussion. Can. Geotech. J. 12:159-162.

Mellor, M. and Testa, R. 1969. Effect of temperature on creep of ice. J. Glaciology 8: 131-145.

Michel, B. 1978. Ice Mechanics. Les Presses de L'Université Laval, 499 pgs.

Miller, R.D. 1983. Thermally induced regelation: A qualitative discussion. Permafrost: Fourth International Conference Proceedings, pg. 61-63.

Miller, R.D. 1978. Frost heaving in non-colloidal soils. Proc. Third International Conference on Permafrost, pg. 707-713.

Miller, R.D. 1977. Lens initiation in secondary heaving. Symposium on Frost Action in Soils Lulea, Sweden, Vol 2, pg. 68-74.

Miller, R.D. 1970. Ice sandwich: functional semipermeable membrane. Science 169: 584-585.

Miller, R.D., Loch, J.P.G. and Bresler, E. 1975. Transport of water and heat in a frozen permeameter. Soil Science Society of America Proc. 39: 1029-1036.

National Research Council (Washington) 1984. Ice Segregation and Frost Heaving: Report of a Study Group. 72 pgs.

Nixon, J.F. 1991. Discrete ice lens theory for frost heave in soils. Canadian Geotech. J. 28: 843-859.

Nye, J.F. 1973. The motion of ice past obstacles. In Physics and Chemistry of Ice. E. Walley, S.J. Jones and L.W. Gold Eds., Royal Soc. of Canada, pg. 387-394.

Ohrai, T. and Yamamoto, H. 1985. Growth and migration of ice lenses in partially frozen soil. Ground Freezing. Proc. Fourth International Symposium, pg 79-84.

Oke, T.R. 1978. Boundary Layer Climates. Methuen, 372p.

Oliphant, J.L., Tice, A.R. and Nakano, Y. 1983. Water migration due to a temperature gradient in frozen soil. Permafrost, Fourth International Confrerence Proc., pg. 951-956.

O'Neill, K. 1983. The physics of mathematical frost heave models: A review. Cold Regions Science and Technology 6: 275-291.

O'Neill, K. and Miller, R.D. 1985. Exploration of a rigid ice model of frost heave. Water Resources Research 21: 281-296.

Outcalt, S.I. 1969. Weather and diurral frozen soil structure at Charlottesville, Virginia. Water Resources Research 5: 1377-1382.

Patterson, D.E. 1988. Personal communication.

Penner, E. 1986a. Ice lensing in layered soils. Canadian Geotechnical J. 23:334-340.

Penner, E. 1986b. Aspects of ice lens growth in soils. Cold Reg. Sci. and Tech. 13: 91-100.

Penner, E. and Goodrich, L.E. 1980. Location of segregated ice in frost-susceptible soil. Selected papers of Second International Symposium on Ground Freezing. Developments in Geotechnical Engineering 28: 231-244.

Perfect, E. and Williams, P.J. 1980. Thermally induced water migration in frozen soils. Cold Regions Science and Technology 3: 101-109.

Philip, J.R. 1980. Thermal fields during regelation. Cold Regions Science and Technology 3: 193-203.

Prigogine, I. 1967. Thermodynamics of Irreversible Processes, 3rd ed. Interscience New York.

Romkens, M.J.M. and Miller, R.D. 1973. Migration of mineral particles in ice with a temperature gradient. J. of Colloid and Interface Science 42: 103-111.

Ryokai, K. 1985. Frost heave theory of saturated soil coupling water/heat flow and its application. Ground Freezing: Proc. Fourth International Symposium, pg 101-117.

Sayles, F.H. 1988. State of the Art: Mechanical properties of frozen soil. Ground Freezing 88 vol. 1, R.H. Jones and J.T. Holden Eds., pg 143-165.

Sayles, F.H. and Carbee, D.L. 1982. Strength of frozen silt as fuction of ice content and dry unit weight. Ground Freezing 1980, Proc, 2nd Int. Symp. on Ground Freezing, pg. 55-66.

Shen, M. and Ladanyi, B. 1987. Modelling of coupled heat, moisture and stress field in freezing soil. Cold Regions Science and Technology 14: 237-246.

Shumskii, P.A. 1964. Principles of Geocryology, Part 1, General Geocryology. NRC Technical Translation 1130.

Smith, M.W. 1985. Observations of soil freezing and frost heave at Inuvik, Northwest Territories, Canada. Canadian J. Earth Sciences 22: 283-290.

Smith, M.W. and Onysko, D. 1990. Observations and significance of internal pressures in freezing soil. Fifth Canadian Permafrost Conference. Centre d'études nordiques, Université Laval, Collection Nordicana No. 54, pg. 75-81.

Smith, M.W. and Patterson, D.E. 1989. Detailed observations on the nature of frost heaving at a field scale. Can. Geotech. J. 26: 306-312.

Smith, M.W. and Riseborough, D.W. 1985. The sensitivity of thermal predictions to assumptions in soil properties. Proc. 4th Int. Symp. on Ground Freezing, Sapporo, pg. 17-23.

Taber, S. 1930. The mechanics of frost heaving. J. Geology 38: 303-317.

Takagi, S. 1980. Summary of the adsorption force theory of frost heaving. Cold Regions Science and Technology 3: 233-2

Takagi, S. 1978. Segregation freezing as the cause of suction force for ice lens formation. Proc. First International Symposium on Ground Freezing. Developments in Geotechnical Engineering 25: 93-100.

Tsytovich, N.A. 1975. The Mechanics of Frozen Ground. G.K. Swinzow Ed. Scripta Book Co. Wash. D.C. 349p.

Van Vliet-Lanoe, B. 1989. Personal Communication.

Van Vliet-Lanoe, B. 1988. The significance of cryoturbation phenomena in environmental reconstruction. J. Quaternary Science 3: 85-96.

Van Vliet-Lanoe, B. 1985. Frost effects in soils. In Soils and Quaternary Landscape Evolution. J. Boardman Ed. J. Wiley and Sons.

Van Vliet-Lanoe, B., Dupas, A. and Coutard, J.P. 1985. Soulèvement cryogenique de petites pierres par la glace en lentilles: rôle initiateur de la cryodessiccation. Bulletin du Centre de Géomorphologie du CNRS Caen No. 30: 77-83.

Van Vliet-Lanoe, B., Dupas, A. and Dumoulin, R. 1987. L'étude de la structure des sols gelés et dégelés: a) Méthodes de carottage et de préparation des échantillons b) Applications géotechniques, 2ième Colloque Franco-Polonais, Gel et Gé Civil Laboratoire Central des Ponts de Chaussées.

Vialov, S.S 1986. Rheological Fundamentals of Soil Mechanics. Developments in Geotechnical Engineering 36, Elsevier, 564 pgs.

Vialov, S.S. 1965. The strength and creep of frozen soils and calculations for ice-soil retaining structures. CRREL Translation No. 76.

Walden, J.S. 1986. Motion of sub-freezing ice past particles with applications to wire regelation and frozen soil. J. Glaciology 32: 404-414.

Washburn, A.L. 1979. Geocryology: A survey of periglacial processes and environments. Arnold, 406p.

Weertman, J. 1973. Creep of ice. In Physics and Chemistry of Ice. E. Walley, S.J. Jones and L.W. Gold Eds., Royal Soc. Canada, pg. 320-337.

White, T.L. 1989. Personal communication.

Williams, P.J. 1991. Properties and behaviour of freezing soils. Proc. 3rd Int. Symp. on Cold Regions Heat Transfer, Fairbanks, Alaska, pg. 57-67.

Williams, P.J. 1982. The Surface of the Earth: An introduction to geotechnical science. Longman 212p.

Williams, P.J. 1977. Thermodynamic conditions for ice accumulation in freezing soils. Proc. of International Symposium on Frost Action in Soils 1: 42-53.

Williams, P.J. 1967. Properties and Behaviour of Feezing Soils. Norwegian Geotech. Inst. Publication 72.

Williams, P.J. and Burt, T.P. 1974. Measurement of hydraulic conductivity of frozen soils. Canadian Geotechnical J. 11: 647-650.

Williams, P.J. and Smith, M.W. 1989. The Frozen Earth: Fundamentals of Geocryology. Cambridge University Press, 306 pgs.

Williams, P.J. and Wood, J.A. 1985. Investigations of the internal stresses in freezing soils and their effects on longterm migration of moisture. Final rept. to Earth Physics Branch, EMR.

Williams, P.J. and Wood, J.A. 1985. Internal stresses in frozen ground. Canadian Geotechnical J. 22: 413-416.

Wood, J.A. 1990. The role of irreversible thermodynamics and rheology in the regelation flow phenomenon. Cold Reg. Sci. and Tech. 18: 133-145.

Wood, J.A. 1985. Internal pressures in freezing soils. Ph.D. Thesis, Carleton University, 261 pgs.

Wood, J.A. and Williams, P.J. 1985. Stress distribution in frost heaving soils. Ground Freezing: Proc. Fourth International Symposium, pg 165-171.

Wood, J.A. and Williams, P.J. 1985. Further experimental investigation of regelation flow with an ice sandwich permeameter. Technical Council on Cold Regions Engineering Monograph. American Society of Civil Engineers, pg 85-94.

Yuanlin, Z. and Carbee, D. 1987. Creep strength behaviour of frozen silt in uniaxial compression. CRREL report 87-10.

END

26 05 93

FIN